Chemical Geology
November 2022, Volume 610 Pages 121092 (24p.)
https://doi.org/10.1016/j.chemgeo.2022.121092
https://archimer.ifremer.fr/doc/00865/97690/

Mineralogy, geochemistry and microbiology insights into precipitation of stibnite and orpiment at the Daiyon-Yonaguni Knoll (Okinawa Trough) hydrothermal barite deposits

Dekov V. M. [1, *], Kyono K. [1], Yasukawa K. [2, 3], Gueguen Bleuenn [4, 5], Ivarsson M. [6], Kamenov G. D. [7], Yamanaka T. [1], Asael Dan [8], Ishida M. [3], Cavalcante L. L. [6], Kato Y. [2, 3, 9, 10], Toki T. [11], Ishibashi J-I [12]

[1] Department of Ocean Sciences, Tokyo University of Marine Science and Technology, 4-5-7 Konan, Minato-ku, Tokyo 108-8477, Japan
[2] Frontier Research Center for Energy and Resources, School of Engineering, The University of Tokyo, Bunkyo-ku, Tokyo 113-8656, Japan
[3] Department of Systems Innovation, School of Engineering, The University of Tokyo, 7-3-1 Hongo, Bunkyo-ku, Tokyo 113-8656, Japan
[4] CNRS, Univ Brest, UMR 6538 Laboratoire Géosciences Océan, F-29280 Plouzané, France
[5] CNRS, Univ Brest, UMS 3113, F-29280 Plouzané, France
[6] Department of Palaeobiology, Swedish Museum of Natural History, SE 104 05 Stockholm, Sweden
[7] Department of Geological Sciences, University of Florida, 241 Williamson Hall, Gainesville, FL 32611, USA
[8] Department of Geology and Geophysics, Yale University, New Haven, CT 06520, USA
[9] Ocean Resources Research Center for Next Generation, Chiba Institute of Technology, 2-17-1 Tsudanuma, Narashino, Chiba 275-0016, Japan
[10] Submarine Resources Research Center, Research Institute for Marine Resources Utilization, Japan Agency for Marine-Earth Science and Technology (JAMSTEC), 2-15 Natsushima-cho, Yokosuka, Kanagawa 237-0061, Japan
[11] Department of Chemistry, Biology and Marine Science, Faculty of Science, University of the Ryukyus, 1 Senbaru, Nishihara, Okinawa 903-0213, Japan
[12] Kobe Ocean-Bottom Exploration Center, Kobe University, 5-1-1 Fukaeminami-machi, Higashinada-ku, Kobe 658-0022, Japan

* Corresponding author : V. M. Dekov, email address : vdekov0@kaiyodai.ac.jp

Abstract :

Samples of active chimneys, chimney flanges and massive sulfides from the Daiyon-Yonaguni Knoll hydrothermal field are composed of major barite and minor stibnite and orpiment. Barite is inferred to precipitate from focused-discharge fluids composed of >40% hydrothermal end-member fluid at T = 100-240 degrees C, whereas the stibnite and orpiment are later and lower temperature precipitates. The hydrothermal fluids from this field were subject of sub-seafloor boiling and phase separation and, consequently, are brine-rich depleted in volatile and enriched in non-volatile elements. Boiling and phase

separation exerted major control on the rare earth elements (REE) partitioning in the vent fluids: high-chlorinity high-temperature fluids were enriched in light REE and low -chlorinity low-temperature fluids were enriched in heavy REE. Y/Ho molar ratio and Ce anomaly of the vent fluids suggest that the seawater has not completely reacted with the basement rocks and has not equilibrated with them. The trace element concentrations in the hydrothermal deposits suggest a complex interplay among hydrothermal, hydrogenetic and microbial processes. Sulfur isotope composition of the sulfides suggests that the sulfide S is a mixture of both basement rock and seawater S with a higher proportion of the basement rock S. The sulfate dissolved in the fluids was subjected to reduction during a slow mixing of hydrothermal fluid and seawater within the chimney walls of the Tiger and Abyss vents and this resulted in a heavy S-isotope compo-sition of the vent fluid sulfate. Lead isotope composition of the hydrothermal deposits indicates mixing re-lationships suggesting that Pb and potentially other metals with similar geochemical behavior were derived from two or three sources. The Pb isotopes in the hydrothermal deposits imply that an enriched source, either sedi-ments or extended continental lithosphere, and a depleted source, potentially back-arc mafic volcanics, are present in the area of Daiyon-Yonaguni Knoll. Filamentous orpiment found in the deposits is supposed to be either heavily mineralized fungal hyphae or pure abiogenic biomorphs. Presence of carbonaceous matter on and around the orpiment filaments suggests for microbial activity during filament formation. The filaments experi-enced temperature of 209.1 +/- 37.1 degrees C which falls within the temperature range of the Daiyon-Yonaguni Knoll vent fluids. Stability phase diagrams modeling reveals that the stability of stibnite does not depend on the vent fluid chlorinity, but depends on the vent fluid temperature: the area of stibnite stability increases with decreasing vent fluid temperature and results in stibnite precipitation at low log10a of Sb2S42-and less reduced environment (Eh still <0). Orpiment is stable in a wide range of log10a of H2AsO4-, in reduced conditions and at high S activity. Barite is stable in wide range of log10a of Ba2+ and precipitates in slightly reduced to slightly oxic conditions.

Highlights

► Stibnite and orpiment are minor minerals in Daiyon-Yonaguni Knoll hydroT deposits. ►Boiling and phase separation exert major control on REE partitioning in vent fluids. ► Heavy S-isotope composition of vent fluid sulphate implies for sulphate reduction. ►Stability phase diagrams show the stability of stibnite depends on vent fluid T.

Keywords : Daiyon-Yonaguni Knoll hydrothermal field, geomicrobiology, Okinawa Trough, orpiment, seafloor hydrothermal activity, stibnite

1. Introduction

Substantial effort has been made to elucidate the mineralogy of seafloor hydrothermal deposits since their discovery (Corliss et al., 1979; Spiess et al., 1980) and nowadays we can dare to think that we have extensive knowledge on it (e.g., Haymon and Kastner, 1981; Oudin, 1983; Koski et al., 1984; Fouquet et al., 1988; Koski et al., 1988; Hannington et al., 1991; Fouquet et al., 1993a, b; Iizasa et al., 1999; Fouquet et al., 2010; Webber et al., 2015). Although the studies of the seafloor hydrothermal deposits recognize distinct mineralogical differences among the deposits formed at mid-ocean ridges (MOR) (sedimented and unsedimented), volcanic arcs and back-arc spreading centers, they show that most seafloor hydrothermal deposits are composed of relatively simple mineral assemblages. Metal (Fe, Cu, Zn, Pb) sulfides, and Ca- and Ba-sulfates are the main constituents of these deposits, whereas silicates, oxyhydroxides, carbonates and

sulfosalts are minor minerals (Herzig and Hannington, 1995). Sulfides of metalloids (B, Si, Ge, As, Sb and Te) are rare. Therefore, seafloor hydrothermal deposits containing metalloid sulfides attract particular scientific interest because these minerals imply for uncommon conditions of precipitation (T, P, pH, Eh, ion activity and speciation).

Stibnite (Sb_2S_3) and orpiment (As_2S_3) are accessory minerals in the seafloor hydrothermal deposits according to published observations. Stibnite is mainly reported ~~from~~ at volcanic arc [Palinuro Seamount, Aeolian Arc (Dekov and Savelli, 2004); Wakamiko Crater, Kagoshima Bay, Kyushu Island (Nedachi et al., 1991; Yamanaka et al., 2013)], back-arc [Minami-Ensei Knoll (Nakashima et al., 1995), JADE (Halbach et al., 1993; Nakashima et al., 1995) and Hatoma Knoll (Okamoto et al., 2002) at Okinawa Trough] and fore-arc [Conical Seamount, New Ireland fore-arc (Petersen et al., 2002)] settings. There is only one report on stibnite occurrence at MOR setting: Ashadze-1 hydrothermal field at the Mid-Atlantic Ridge (Firstova et al., 2016). Stibnite was also observed to form in the artificially produced hydrothermal chimneys at the Iheya-North field, Okinawa Trough (Nozaki et al., 2016). Orpiment has also been reported ~~from~~ at volcanic arc [Suiyo Seamount, Izu-Bonin Arc (Marumo et al., 2008); off-shore Milos Island, Aegean Arc (Price et al., 2009)], back-arc [Lau back-arc basin (Petersen, 1992); JADE field, Okinawa Trough (Halbach et al., 1993; Dekov et al., 2013); Kaia Natai Seamount, Manus back-arc basin (Dekov et al., 2013)] and fore-arc [Conical Seamount, New Ireland fore-arc (Petersen et al., 2002; Herzig et al., 2003; Dekov et al., 2013)] settings only.

In 2000 during the YK00-06 *Yokosuka-Shinkai 6500* research cruise in the southern Okinawa Trough a new hydrothermal system was discovered and named Daiyon-Yonaguni Knoll (Matsumoto et al., 2001; Hsu et al., 2003). Along with the common barite, ~~würtzite~~wurtzite, galena, tetrahedrite, chalcopyrite, pyrite and native sulfur, minor stibnite and orpiment were detected in the Daiyon-Yonaguni Knoll hydrothermal deposit (Okamoto et al., 2002; Suzuki et al., 2005; 2008).

Motivated by the scarce knowledge on the stibnite and orpiment precipitation at seafloor hydrothermal conditions, we investigated the stibnite-orpiment containing barite deposits and hydrothermal fluids from the Daiyon-Yonaguni Knoll hydrothermal site and report the results of our study in this contribution.

2. Geologic setting

The Okinawa Trough is an intra-continental back-arc basin extending behind the Ryukyu Trench-Arc system (Fig. 1 A). The rifting of this trough located at the eastern margin of the Eurasian tectonic plate was discussed in several works (e.g., Kimura et al., 1986; Glasby and Notsu, 2003; Ishibashi et al., 2015). The lithosphere beneath the Okinawa Trough is thinned continental lithosphere with a minimum thickness of ~8 km (Nagumo et al., 1986; Hirata et al., 1991; Oshida et al., 1992; Klingelhoefer et al., 2009). Thick sediment supplied from the Yangtze and Yellow rivers covers the seafloor of the Okinawa Trough and reaches ~2 km in its southern part (Sibuet et al., 1987). The volcanic rocks sampled in the southern Okinawa Trough range from calc-alkaline andesite to rhyolite (Shinjo et al., 1999). Active hydrothermal vents were discovered close to some of the seafloor volcanic edifices and the composition of both the venting fluids and hydrothermal deposits were described in a several works (Okamoto et al., 2002; Glasby and Notsu, 2003; Gena et al., 2005).

The Daiyon-Yonaguni Knoll is one of the seamounts that delineate a volcanic belt in the southernmost part of the Okinawa Trough (Matsumoto et al., 2001) (Fig. 1 B). An active hydrothermal field, adjacent to this seamount and named after it, is located in an elongated valley (~1000 m long and ~500 m wide) covered by thick muddy sediment (Gena et al., 2005) (Fig. 1 B). Volcanic breccias were observed in the northeastern part of the hydrothermal field. Four major hydrothermal chimney–mound complexes venting hot (up to 328°C) both black and clear fluids are aligned north–south and were named Lion, Tiger, Swallow and Crystal (Konno et al., 2006; Suzuki et al., 2008; Fujiwara et al., 2015). Liquid CO_2 emissions were detected at the seafloor between the Tiger and Swallow sites (Konno et al., 2006). Diffuse venting ($T \leq 80°C$) was observed in the southern part of the hydrothermal field and named the Abyss Vent (Suzuki et al., 2008).

3. Samples

In our efforts to shed more light on the mineralogy and geochemistry of the stibnite-orpiment containing deposits at the Daiyon-Yonaguni Knoll hydrothermal field, we selected six

samples (collected during the R/V *Natsushima* cruise NT01-05 Leg2; 2001) of active chimney, and active chimney flange, and massive sulfides from the Tiger vent (Table 1; Fig. 2) from the(sample repository of the Japan Agency for Marine-Earth Science and Technology (JAMSTEC) and investigated them. Sub-samples from macroscopically different areas of the samples (Fig. 2) were collected using a mini-drill bore with diamond bit and ground to fine powders in an agate mortar for further analyses. Thin polished sections were prepared from each sample for optical microscopy and electron microprobe investigations.

Eleven vent fluid samples (recovered during the R/V *Yokosuka* cruise YK03-05; 2003) collected from the Tiger vent (8 samples from the vent and 2 from the buoyant plume above the vent) and Abyss diffuse venting site (1 sample) using water-hydrothermal *atsuryoku* tight sampler (WHATS; developed for collecting fluid samples while maintaining gas pressure; Tsunogai et al., 2003), bag sampler, and Niskin sampler (Table 2) were filtered (0.45 µm membrane filters) and acidified immediately after recovery and analyzed in onshore laboratories later.

4. Methods of investigation

4.1. Mineralogy of hydrothermal deposits

Initially, the hydrothermal deposit samples were observed with a stereomicroscope (Nikon SMZ745T) and pictures of the major minerals that constitute the samples were acquired in natural light. The mineral composition and texture of the samples were investigated in thin polished sections by optical polarizing microscope (Nikon ECLIPSE LV100N POL) in transmitted and reflected light.

Crystal habit of the minerals that compose the studied samples was studied on small (~1x1 cm) sub-samples using a Hitachi TM3030 Plus tabletop scanning electron microscope (SEM) (V=15.0 kV, I=1850 mA, electron beam diameter 0.1 µm), after mounting of the sub-samples on aluminum stubs using carbon tape and coating them with carbon. The crystal habit was documented on secondary electron images (SEI) and the chemistry (qualitative) of the imaged minerals was probed by energy dispersive X-ray spectrometry (EDS).

Mineral chemistry (point analyses) and element distribution within the minerals (X-ray maps in major elements detected: Sb *L*α, As *L*α, Ba *L*α, S *K*α lines) were analyzed on ~~the same~~ thin polished sections (those used in the optical microscope studies) after coating them with carbon and using JEOL JXA-8230 electron microprobe (EMP) (V=15 kV, I=1.2 nA, electron beam diameter 2 μm). Standards used were $CaSO_4$ (S *K*α), Sb_2S_3 (S *K*α and Sb *L*α), $CaCO_3$ (Ca *K*α), GaAs (As *L*α), As (As *L*α), $BaSO_4$ (Ba *L*α), $SrSO_4$ (Sr *L*α), and the detection limits (in wt.%) were 0.030 for Sb, 0.013 for S ($CaSO_4$ standard), 0.005 for S (Sb_2S_3 standard), 0.027 for As (As standard), 0.017 for As (GaAs standard), 0.016 for Ca, 0.047 for Ba, 0.018 for Sr.

Bulk mineral composition of the finely powdered samples was determined by X-ray diffraction (XRD) analysis of random mounts using Rigaku Ultima ⅣX-ray diffractometer with monochromatic Cu *K*α radiation with scans from 4 to 70 °2θ, with 0.05 °2θ step, and 4 s/step. XRD patterns were interpreted by using the MacDiff software.

4.2. Chemistry of hydrothermal deposits

Chemistry (elemental concentrations) of the hydrothermal deposits was determined by Inductively Coupled Plasma Quadrupole Mass Spectrometer (ICP-QMS; Thermo Fisher Scientific i-CAP Q; Department of Systems Innovation, The University of Tokyo) after total sample dissolution (Kato et al., 1998; 2002; 2005; Yasukawa et al., 2014; 2020). In short, after drying the sample powders at 110°C for ~12 h, we weighed ~50 mg from each sample and put them in Teflon beakers. The samples were dissolved with HNO_3-HF-$HClO_4$ after heating on a hot (130°C) plate in the tightly closed beakers for 2 h. The dissolved samples were progressively evaporated at 110°C for 12 h, at 160°C for 6 h, and at 190°C until dry. The residues were subsequently dissolved in 2 mL *aqua regia* on a hot (90°C) plate for 6 h. The dissolved samples were progressively evaporated at 120°C for 2 h, then at 160°C until dry. Subsequently, the residues were dissolved by 10 mL of a 2 wt.% acid mixture consisting of HNO_3:HCl:HF (20:5:1) on a hot (90°C) plate for 3 h. The remaining residues in the solutions were removed by filtration (0.45-μm mesh, polytetrafluoroethylene membrane filters; Merck Millipore Millex®), precisely weighted and investigated by XRD. Before the ICP-QMS measurements the sample solutions were diluted to 1:50, 1:250 and 1:500 (or 1:10000, 1:50000, and 1:100000 with respect to the

sample powder, respectively) by mass using the same 2 wt.% HNO_3-HCl-HF (20:5:1) acid mixture. During the ICP-QMS measurements, spectral overlaps from oxides and hydroxides ($^{44}Ca^{16}O$ on ^{60}Ni, $^{47}Ti^{16}O$ on ^{63}Cu, $^{50}Ti^{16}O$ on ^{66}Zn, $^{137}Ba^{16}O$ on ^{153}Eu, $^{141}Pr^{16}O$ and $^{140}Ce^{16}O^{1}H$ on ^{157}Gd, $^{143}Nd^{16}O$ on ^{159}Tb, $^{147}Sm^{16}O$ and $^{146}Nd^{16}O^{1}H$ on ^{163}Dy, $^{149}Sm^{16}O$ on ^{165}Ho, $^{150}Nd^{16}O$ and $^{150}Sm^{16}O$ on ^{166}Er, and $^{165}Ho^{16}O$ on ^{181}Ta) were corrected following the method described by Aries et al. (2000). Samples along with the standards and blanks were analyzed as one analytical batch. To check the analytical precision and accuracy, reference standards issued by the Geological Survey of Japan [JB-2 (basalt), JB-3 (basalt) (Imai et al., 1995; Makishima and Nakamura, 2006; Lu et al., 2007) and JMS-2 (pelagic clay) (Takaya et al., 2014)] were analyzed twice within the analytical batch. The analytical errors for the unknown samples were calculated on the basis of the relative standard deviation for each element in JMS-2.

4.3. Chemistry of vent fluids

A pre-concentration method was employed for the determination of the concentrations of a set of elements (Fe, Mn, Co, Ni, Cu, Zn, Cd, Mo, Sb, Pb, U, V, Y, La, Ce, Pr, Nd, Sm, Eu, Gd, Tb, Dy, Ho, Er, Tm, Yb, Lu) in the collected vent fluids using a separation procedure with the NOBIAS chelate-PA1 resin (Hitachi High-Technologies) following already published protocols (Sohrin et al., 2008; Minami et al., 2015). 2 mL of each fluid sample were weighted and the samples were adjusted to pH~6 with a buffer prior to column purification. Then, the columns were loaded with 0.5 mL of clean resin and the resin was washed with 30 mL 18.2 MΩ water, 0.5 mL 3*M* HNO_3, and 10 mL 18.2 MΩ water. Before the sample load, the resin was conditioned with 1 mL 2.5% HNO_3 + 120 µL of the buffer to reach a final pH~6. The sample matrix was eluted with 10 mL 18.2 MΩ water. Elements of interest (listed above) were eluted with 23 mL 3*M* HNO_3. The resin was washed with 20 mL 18.2 MΩ water and the columns stored for further separation procedures. We were not able to measure the As concentrations because of analytical challenges: (1) As is not retained on the NOBIAS resin; (2) As is difficult to be measured directly in the vent fluid because of the number of interferences it experiences during the Inductively Coupled Plasma – Mass Spectrometry (ICP-MS) measurements.

The solutions with eluted elements were evaporated to dryness and re-dissolved in 2 mL ~0.28*M* HNO_3 for High Resolution – Inductively Coupled Plasma – Mass Spectrometry (HR-ICP-MS) measurements. Concentrations of elements in these solutions were measured with a HR-ICP-MS Element XR (Thermofisher Scientific) at Pôle de Spectrométrie Océan (PSO, IUEM, Brest, France). Indium was used as an internal standard for correcting drift of the signal and concentrations were calibrated using external calibration standards. A referenced seawater standard (CASS-6; National Research Council, Canada) and one blank were also processed following the above protocol and analyzed with the same HR-ICP-MS instrument.

4.4. Sulfur isotope analysis of hydrothermal deposits and fluids

The sulfide contained in the hydrothermal deposit samples was separated through the following procedures before the analysis of its S isotope composition:

(1) About 0.5 g of each powdered sample were weighed and put in three-necked flasks. A Pasteur pipette was attached to the tip of a tube connected to the flask and the tip was placed in $Cd(CH_3CO_2)_2$ solution in a test tube. N_2 gas was introduced in the system for 2-3 minutes.

(2) Fine-grained sulfide minerals were separated using selective chemical dissolution procedures. Sphalerite, pyrrhotite, and galena were reacted with 30 mL 12*M* HCl at 80°C in the three-necked flask. The glass stopper was tightened and N_2 gas flowed for 20-30 minutes while H_2S gas was generated during the reaction between the sulfides (sphalerite, pyrrhotite, galena) and HCl. The generated H_2S gas was fixed as CdS (yellow precipitate formed in the test tubes) and oxidized to $BaSO_4$. Chalcopyrite, isocubanite, pyrite, tennantite, and native sulfur were oxidized to SO_4^{2-} in mixture solution of Br_2 and HNO_3 and precipitated as $BaSO_4$.

(3) The N_2 gas flow was stopped, 1 mL H_2O_2 solution was added in the test tube, the tube was plugged with a rubber stopper, stirred, and left overnight.

(4) The solution was transferred from the test tube to a beaker and heated on a hot (140°C) plate until the solution amount was reduced by ~20%. If a white precipitate formed, 2 mL 6*M* HCl were added and the precipitate was collected by filtration.

(5) The sample solution was heated to 140°C, 10 mL $BaCl_2$ solution was added to it and it was left overnight. Precipitated $BaSO_4$ was collected through suction filtration and dried at 110°C.

$BaSO_4$ recovered through the above procedures was used for measuring the S-isotope composition of the sulfide in the hydrothermal deposit samples.

Sulfur isotope composition of sulfate in the vent fluids was analyzed according to the following protocol. 2 mL of each fluid sample was diluted with 10 mL 18.2 MΩ water, acidified with 1 mL 6*M* HCl and heated at 150℃ for 5 minutes. 1 mL $BaCl_2$ solution was added to each sample solution to precipitate dissolved sulfate as $BaSO_4$, which was collected by filtration and dried at 110℃. Recovered $BaSO_4$ was used for measuring the S-isotope composition of the vent fluid sulfate.

0.15-0.20 mg $BaSO_4$ precipitate from all samples (deposits and vent fluids) were mixed with 1.0-3.0 mg V_2O_5 and wrapped in Sn capsules. In a similar way, MSS-2 and MSS-3 standards were mixed with V_2O_5 and wrapped in Sn capsules as work standards for measurement. The S isotopes were measured by EA-IRMS, the data are reported against the Canyon Diablo Troilite (CDT) and expressed in per mil (‰). The analytical error of the measurements was ± 0.3‰.

4.5. Lead isotope analysis of hydrothermal deposits

All reagents used for sample preparation for Pb isotope analyses were Optima-grade. The sample preparation was performed under a clean lab environment at the Department of Geological Sciences at the University of Florida. Around 30 mg of sample powder was transferred in pre-cleaned Teflon beaker and dissolved in 3 mL aqua regia on a hot (100°C) plate overnight. After digestion, the solutions were evaporated to dryness and the dry residue was dissolved in 1*M* HBr and loaded on columns packed with clean Dowex 1X-8 resin to separate Pb for isotope analysis. After 3x1 mL of 1*M* HBr washes the purified Pb fraction was collected in 1 mL of 3*M* HNO_3. Pb isotopes were determined with Tl-normalization on a "Nu Plasma" Multi-Collector – Inductively Coupled Plasma – Mass Spectrometer (MC-ICP-MS), following methods described in Kamenov et al. (2004). The reported Pb isotope data for the samples are relative to

NBS 981 values of $^{206}Pb/^{204}Pb$=16.937 (±0.004, 2σ), $^{207}Pb/^{204}Pb$=15.490 (±0.004, 2σ), $^{208}Pb/^{204}Pb$=36.695 (±0.009, 2σ).

4.6. Stability phase diagrams modeling

In order to get insight into the conditions of abiogenic precipitation of the stibnite, orpiment and barite in the studied hydrothermal chimneys we modeled Eh *vs* $\log_{10}a$ phase diagrams at the physical-chemical conditions of three selected vent fluids (Daiyon-Yonaguni Knoll hydrothermal field) using the Geochemist's Workbench 8.0 (GWB) software (based on the "thermo_minteq" database) (Bethke, 2008).

4.7. Investigations of filamentous structures

Raman spectra of selected sub-samples (light orange filamentous structures and surrounding dark red colloform mineral) from sample 2K1267 L1 were acquired using a Horiba LabRAM HR 800 Raman spectrometer (Department of Materials and Environmental Chemistry, Stockholm University), equipped with an air cooled double-frequency Nd:YAG laser operating at 532 nm. The selected sub-samples were exposed to a laser power of 5 mW through an objective lens with 50× magnification (NA 0.42). A diffraction grating with 600 grooves mm^{-1} was used to resolve the spectra. Acquisition time was set at 2 s, with 20 scans accumulated from 0 to 4000 cm^{-1} with a spectral resolution of 2 cm^{-1}.

The filamentous structures were further studied using a stereomicroscope (Olympus SZX2-ILLT) and an Olympus BX51 microscope with an X-cite Series 120 Q fluorescence light source. The filaments were stained by CalcoFlourwhite (BioTium), a dye that binds to chitin. Before staining, the samples were treated with sterile gloves and forceps to reduce the introduction of exotic fluorescent particles.

An XL30 environmental scanning electron microscope (ESEM) with a field emission gun (XL30 ESEM-FEG) was also used to analyze the filamentous structures. The ESEM was equipped with an Oxford x-act energy dispersive spectrometer (EDS), backscatter electron (BSE) detector and a secondary electron (SE) detector. The acceleration voltage was 20 kV. The

instrument was calibrated with a cobalt standard. Peak and element analyses were recorded using the accompanying AZTEC software.

5. Results

5.1. Mineralogy of hydrothermal deposits

The hand specimens of the studied deposits were porous, fragile, greyish-black (Fig. 2 A) to blackish-grey (Fig. 2 B, E, F) with orange to white stains (Fig. 2 B-F).

The XRD studies of bulk samples (active chimney~~,~~ and active chimney flange~~, and massive sulfide~~) showed that the major mineral that composes them is barite (Table 3). Only one sample of ~~massive sulfide~~active chimney is composed of pyrite and isocubanite (Table 3). However, our stereomicroscope, optical polarizing microscope, SEM and EMP studies showed regular presence of two other minerals (stibnite and orpiment) and traces of several others (native sulfur, pyrite, gypsum, and clays). Obviously, these minerals are in quantities below the XRD detection limits: i.e., <4 wt.%. We will focus our attention on the stibnite and orpiment in the following description.

Long (0.3 mm), needle-like, black to grey with metallic lustre stibnite forms rosettes of radiating crystals, which fill cavities and cover the surface of greyish-white to white barite (Fig. 3 A). The optical microscope (thin polished sections) and SEM observations revealed that the studied samples were composed of bunches and stacks of prismatic and tabular transparent (in transmitted light) crystals of barite overgrown by long prismatic crystals of stibnite forming rosettes (Fig. 3 B, C). The average empirical formula of stibnite is $Sb_{1.93}As_{0.08}S_{3.00}$ (average of 10 point analyses; Table 4), which suggests that its chemistry is close to the stoichiometry with a little excess in cations. Mapping of the concentration distributions of the elements (in characteristic lines) present in the studied samples showed that Sb, As and S are homogenously distributed within the stibnite crystals (Fig. 4 A, B, D, E) and the stibnite always grows on barite (Fig. 4 A-D).

Orange filaments (Fig. 5 A) and dark red colloform aggregates (Fig. 5 B) of orpiment stain the surface of the samples and fill cracks in them. At places, yellow fine precipitates and yellow

thin filaments of orpiment occur along with the orange orpiment filaments and overgrow transparent to white barite crystals (Fig. 5 F). Orpiment mostly occurs as colloform masses (Fig. 5 D) composed of fine (<1 μm) crystals deposited on barite. Rarely, it occurs as stacks of branching filaments ~300 μm long and 20 μm wide (Fig. 5 C, E) with clear axis and two concentric zones in cross section (Fig. 5 E). Orpiment rarely contains traces of Sb and has an average empirical formula $As_{1.98}Sb_{0.01}S_{3.01}$ (average of 19 point analyses; Table 4). The chemistry of orpiment slightly deviates from the stoichiometry with a slight deficiency in cations and slight excess in S. Orpiment and barite show homogenous distribution of the major elements that compose them (As and S, and Ba and S, respectively; Fig. 6 A-E) and only the traces of Sb in the orpiment show slight enrichment in some zones (Fig. 6 B).

The most common morphology of barite in the studied samples is tabular (match box-like; Fig. 3 D), but radial barite crystals forming rosettes (dendritic barite) among the sulfides can rarely be observed (Fig. 3 E). The average empirical formula of barite $(Ba_{0.95}Ca_{0.03}Sr_{0.02})SO_4$ (average of 5 point analyses; Table 4) is close to the stoichiometry with traces of Ca and Sr as isomorphic replacements for Ba. Whitish-yellow to yellow native sulfur (as closely packed rhombic crystals; Fig. 3 F), fine-grained greenish-yellow pyrite, white gypsum, and flake-like alumino-silicates (presumably clays) filling the open space among the barite crystals are rare minerals.

5.2. Geochemistry of hydrothermal deposits

Logically, the chemistry of the stibnite and orpiment separates (expected to be monomineralic according to stereomicroscope observations) ~~separates of stibnite and orpiment~~ differ from that of the bulk samples (Table 5). Orpiment samples along with that of stibnite are rich in As, Ca, Mg, K, Al, Ti, Fe, Mn, Zn, Pb, Bi, Hf, Ta, U, and Au (Table 5). The bulk samples as well as the stibnite sample are rich in Sb, and P (Table 5). The stibnite separate is highly enriched in Tl (Table 5). The ~~monomineralic~~ stibnite and orpiment separates ~~of stibnite and orpiment~~ are richer in REE than the bulk deposit samples (ΣREE; Table 6). The bulk samples exhibit well-pronounced negative Ce anomaly (Ce/Ce*<1) when normalized to chondrite REE concentrations whereas the stibnite and orpiment samples show either less-pronounced negative

or weak positive Ce anomaly (Ce/Ce*>1) (Table 6; Fig. 7 A). Bulk deposit samples show stronger both positive Eu anomaly (Eu/Eu*>1) and light REE enrichment relative to the heavy REE (La_{CN}/Lu_{CN}>1) than the ~~monomineralic~~ stibnite and orpiment ~~samples~~ separates (Table 6; Fig. 7 A).

5.3. Geochemistry of vent fluids

Previous works investigated the major ion chemistry of the Daiyon-Yonaguni Knoll hydrothermal fluids (Suzuki et al., 2008) and in order to complete our knowledge on them, we focused our attention on the trace elements chemistry of these fluids (Table 7). Although the REE were studied in the Daiyon-Yonaguni Knoll fluids (Hongo et al., 2007), we extended this exploration with more detailed analysis of the Tiger vent fluids and analyzed for the first time the REE in the Abyss vent fluids (Table 8). In order to facilitate the interpretations of the vent fluid chemistry from the point of view of possible phase separation and to consider the potential vent fluid mixing with seawater, we also cite Cl and Mg concentrations in the same fluids from previous work (Suzuki et al., 2008) ~~in our data tables~~ (Tables 7, 8). Chlorine and Mg concentrations in the seawater from the vicinity of the Tiger vent (Suzuki et al., 2008) are given as background values (Table 7). The ~~Chemistry~~ chemistry of the Tiger vent end-member fluid was calculated by extrapolating the data points in Mg *vs.* Element diagrams to 0 mmol/kg Mg, considering that Mg is quantitatively removed from seawater during its interaction with hot magmatic rocks of the basement (Von Damm, 1990).

Vent fluid with the highest chlorinity (D762 W1 F, [Cl] = 606 mmol/kg) and lowest Mg concentration ([Mg] = 18.4 mmol/kg) has the highest concentrations of Fe, La, Ce, Pr, Nd, Sm, Eu, Tb, ΣREE, second high concentrations of Mn, Ni and Y, and the lowest concentrations of Sb (Tables 7, 8). Two other vent fluids with high chlorinity and low Mg content (D763 W2 F, D763 W4 F) have the highest concentrations of Zn, Pb, Cu and Cd, high contents of Fe, Mn, Ni and Sb, high Eu anomalies, low concentration of V, and the lowest content of U (along with sample D762 W1 F) (Tables 7, 8). The chemistry of the Tiger vent end-member fluid is close to that of the three vent fluids with the lowest Mg content and highest chlorinity (D762 W1 F, D763 W2 F, D763 W4 F). Iron, Mn, Y and REE concentrations of the Tiger end-member fluid are close to

those of the vent fluid with the highest chlorinity (D762 W1 F), whereas the concentrations of Zn, Pb, Cu, Ni and Cd in the end-member fluid are similar to those in the other two high-chlorinity and low-Mg vent fluids (D763 W2 F, D763 W4 F) (Tables 7, 8). The Tiger end-member fluid has very low Mo and V concentrations, and U content calculated to be negative (Table 7).

The fluid of the buoyant plume above the Tiger vent has the lowest concentrations of Fe, Mn, Ni, Y and REE, and the highest content of V (Tables 7, 8).

The low-temperature Abyss vent fluid (T = 80°C; Table 2) has a chlorinity ([Cl] = 547 mmol/kg) close to that of the local seawater ([Cl] = 544 mmol/kg), the highest Mn, Y, Dy, Ho, Er, Tm, Yb and Lu concentrations, the lowest Pb and Cd concentrations, among the lowest Zn, Mo, Sb and Co concentrations, and the lowest positive Eu anomaly (Tables 7, 8).

Chondrite-normalized REE distribution patterns of the Tiger venting and end-member fluids show weak negative Ce anomalies, weak to strong positive Eu anomalies and enrichment in the light relative to heavy REE (Fig. 7 B, Table 8). The REE distribution pattern of the Tiger end-member fluid closely resembles that of the venting fluid with the highest chlorinity (D762 W1 F; Fig. 7 B). Chondrite-normalized REE distribution pattern of the low-temperature Abyss vent fluid shows weak both negative Ce and positive Eu anomalies, and flat distribution of the heavy REE (Fig. 7 B, Table 8). Y/Ho ratio of all venting fluids and of the Tiger end-member fluid is between 50 and 100, and is lower than that of the previously published data for the Tiger hydrothermal fluids (Y/Ho > 100, Table 8; Hongo et al., 2007).

5.4. Sulfur isotope compositions of hydrothermal deposits and vent fluids

The S-isotope composition of the sulfides from the studied Daiyon-Yonaguni Knoll hydrothermal deposits varies in a narrow range ($\delta^{34}S_{sulfide}$ = 4.0 - 5.3‰; Table 5), falling within the range of the S-isotope composition of the Okinawa Trough hydrothermal deposits (Fig. 8).

The S-isotope composition of the Daiyon-Yonaguni Knoll vent fluid sulfate ($\delta^{34}S_{sulfate}$ = 20.3 - 21.6‰; Table 7) clusters around the average seawater value ($\delta^{34}S_{sulfate}$ = 20.97 ± 0.10‰; Paris et al., 2013) with some scattering to slightly lighter (2 samples) and slightly heavier (2 samples) isotope compositions relative to that of seawater (Table 7, Fig. 8).

441

442 *5.5. Lead isotope composition of hydrothermal deposits*

443

444 Lead isotope data for the analyzed hydrothermal deposits are presented in Table 9. The
445 samples show relatively limited variations in $^{206}Pb/^{204}Pb$ (18.491 to 18.545), but wider spread in
446 $^{207}Pb/^{204}Pb$ (15.575 to 15.652) and $^{208}Pb/^{204}Pb$ (38.564 to 38.951). As a result the data form a
447 relatively steep linear trend in Pb isotope space (Fig. 9).

448

449 *5.6. Stability phase diagrams modeling*

450

451 In the modeling of Eh *vs* $\log_{10}a$ phase diagrams for the stability of the stibnite, orpiment,
452 barite and the most possible Sb-, As- and Ba-ions at the conditions of Daiyon-Yonaguni Knoll
453 hydrothermal system, we used the physical and chemical parameters of three vent fluids. We
454 chose the vent fluids with: the highest temperature (sample D759 W1 F, Tiger vent), the lowest
455 temperature (sample D762 B F, Abyss vent), and the highest both chlorinity and metal
456 concentrations (sample D763 W2 F, Tiger vent) (Tables 2, 7). For the modeling we used our data
457 for vent fluid temperature, pH, hydrostatic pressure (calculated from the depth of sampling), and
458 trace element concentrations (Tables 2, 7). Major ion concentrations, which we used, were the
459 unpublished vent fluid chemistry on the basis of which Suzuki et al. (2008) calculated the
460 Daiyon-Yonaguni Knoll end-member hydrothermal fluid. They were as follows:

461 -(1) sample D759 W1 F: [Cl] = 550 mmol/kg, [SO_4] = 28.8 mmol/kg, [NH_4] = 0.14
462 mmol/kg, [Na] = 450 mmol/kg, [K] = 9.9 mmol/kg, [Mg] = 49.2 mmol/kg, [Ca] = 9.4 mmol/kg,
463 [B] = 0.40 mmol/kg, [SiO_2] = 0.18 mmol/kg, [Sr] = 81.6 µmol/kg;

464 -(2) sample D763 W2 F: [Cl] = 600 mmol/kg, [SO_4] = 13.1 mmol/kg, [NH_4] = 4.96
465 mmol/kg, [Na] = 454 mmol/kg, [K] = 58.0 mmol/kg, [Mg] = 22.0 mmol/kg, [Ca] = 17.8
466 mmol/kg, [Li] = 2.53 mmol/kg, [B] = 2.49 mmol/kg, [SiO_2] = 7.33 mmol/kg, [Sr] = 98.8
467 µmol/kg;

468 -(3) sample D762 B F: [Cl] = 547 mmol/kg, [SO_4] = 23.9 mmol/kg, [NH_4] = 1.04 mmol/kg,
469 [Na] = 456 mmol/kg, [K] = 14.4 mmol/kg, [Mg] = 45.9 mmol/kg, [Ca] = 9.6 mmol/kg, [B] = 0.72
470 mmol/kg, [SiO_2] = 2.65 mmol/kg, [Sr] = 84. 1 µmol/kg.

5.7. Carbonaceous matter in the orpiment filaments

The Raman spectra of orpiment filaments (sample 2K1267 L1) are characterized by bands between 1000 and 1800 cm^{-1}, and between 2700 and 3000 cm^{-1}, denoted as first and second order regions, respectively (Fig. 10 B). These bands are typical of carbonaceous matter (Kouketsu et al., 2014; Qu et al., 2015) that suggests the orpiment filaments contain carbonaceous matter.

The two main bands occurring at approximately 1350 and 1600 cm^{-1} in the first order region are commonly identified as disordered carbon (D) and ordered graphite (G) bands, respectively. These bands have previously been attributed as ring breathing modes of disordered carbonaceous matter, and in-plane vibrations of sp^2 carbon atoms (Ferrari and Robertson, 2000). Moreover, the intensity ratio between the D and G bands (I(1350)/I(1600)) has ~~been~~ previously been used to indicate the structure order of the carbonaceous matter (Kouketsu et al., 2014; Qu et al., 2015), and the calculated value of 0.765±0.08 was obtained for the analyzed filaments.

Additionally, a deconvolution of the region between 1000 and 1800 cm^{-1} was done. Using the FWHM-D1 value calculated, and applying the relationship determined by Kouketsu et al. (2014), the maximum temperature experienced by the filaments was calculated to be between 190-230°C.

The Raman spectra of both light orange filamentous (Fig. 10 B) and dark red colloform (Fig. 10 C) structures showed a weak band at 230 cm^{-1}, and a broad strong band at 339 cm^{-1}, which supported the electron microprobe analyses that both types of sub-samples are composed of an arsenic sulfide mineral phase. Previously, in analogous deposits from hydrothermal vents off Milos Island, similar Raman spectra were attributed to poorly to non-crystalline forms of orpiment (Godelitsas et al., 2015).

Staining with ChalcoFlourWhite under fluorescence microscopy turned out to be unsuccessful, thus suggesting that chitin is not present in the filaments.

The ESEM analyses (sample 2K1267 L1) are in support of the Raman data indicating a carbonaceous phase associated with the filaments. The carbonaceous matter occurs rather as a film coating the filaments than incorporated in them (Fig. 11).

6. Discussion

6.1. Sequence of mineral precipitation at the Daiyon-Yonaguni Knoll hydrothermal field

The chemistry of the major mineral in the studied deposits, barite (Table 3), is close to its stoichiometry with negligible isomorphic replacement of Ca and Sr for Ba (Table 4). The isomorphic replacements of As for Sb and of Sb for As in stibnite and orpiment, respectively, are also insignificant and the chemistries of the studied stibnite and orpiment (Table 4) practically match their stoichiometric empirical formulae. The textural relations between the major barite and minor stibnite and orpiment (Figs 3 B, C; 4 A-E; 5 F; 6 A-E) suggest that the stibnite and orpiment have precipitated after barite.

Barite is an abundant mineral in the back-arc basin hydrothermal deposits (Shikazono and Kusakabe, 1999) and a number of studies have been focused on it (e.g., Shikazono, 1994; Shikazono et al., 2012; Jamieson et al., 2016). These studies showed that tabular large-crystal barite with smooth crystal faces precipitates from solutions with low degrees of supersaturation (saturation index below ~100) and dominates the barite deposited at the back-arc basin hydrothermal systems (Shikazono, 1994). Dendritic barite with rough crystal faces is rare (or lacking) in these deposits and forms from solutions with high degrees of supersaturation (Shikazono, 1994). It was found that dendritic barite at seafloor hydrothermal systems precipitates from fluids composed of less than 40% hydrothermal end-member fluid (and more than 60% seawater), whereas the tabular barite forms from fluids containing greater proportion of hydrothermal end-member fluid (Jamieson et al., 2016). In general, the seafloor hydrothermal barite precipitates from solutions with high flow rates (i.e., focused discharge) (Shikazono et al., 2012) and at temperatures of between 100°C and 240°C (Tokunaga and Honma, 1974; Jamieson et al., 2016).

Our studies of the Daiyon-Yonaguni Knoll hydrothermal deposits confirm the previous observations that the tabular barite is the dominant barite morphology at the back-arc basin hydrothermal systems (Shikazono, 1994). On the basis of the knowledge gained up to now we may infer that the Daiyon-Yonaguni Knoll barite precipitated from focused-discharge fluids composed of high proportion (>40%) of hydrothermal end-member fluid and at temperatures

100-240°C. The minor minerals, stibnite and orpiment, have precipitated after barite and seem to be later lower temperature precipitates.

6.2. Phase separation and trace element chemistry of the Daiyon-Yonaguni Knoll vent fluids

The chlorinities of all studied fluids from the Tiger and Abyss vents vary and are higher than that of the local ambient seawater (Table 7). The richest in chloride vent fluid (D762 W1 F) has a chlorinity ~11% higher than that of the seawater. Deviations (positive and negative) from seawater chlorinity have long been measured in seafloor hydrothermal fluids (Edmond et al., 1979; Michard et al., 1984; Von Damm et al., 1985a; Von Damm and Bischoff, 1987; Bowers et al., 1988; Butterfield et al., 1990; Von Damm, 1990; Butterfield et al., 1994; Von Damm et al., 2005) and explained with sub-seafloor boiling and phase separation (Von Damm, 1990). Analyzing the major ion chemistry of the Daiyon-Yonaguni Knoll vent fluids Suzuki et al. (2008) also ascribed their enhanced chlorinity relative to the ambient seawater to sub-seafloor phase separation.

Sub-seafloor boiling, phase separation and emission of brine-rich (chloride-rich) fluids from the Daiyon-Yonaguni Knoll vents explain the enrichment in non-volatile elements (Fe, Mn, Zn, Pb, Cu, Cd, Ni, Y, La, Ce, Pr, Nd, Sm, Eu and Tb) and depletion in volatile elements (Sb) of the three Tiger vent fluids with the highest chlorinity and lowest Mg content as well as of the Tiger vent end-member fluid (Tables 7, 8). The lowest concentrations of Mo, V and U in the lowest-Mg (highest chlorinity) vent fluids and in the end-member fluid ([Mg] = 0 mmol/kg) (Table 7) support the knowledge that these elements are nearly quantitatively removed from the seawater during its interaction with the hot basement rocks (German and Von Damm, 2003) and their contents in a vent fluid depend on the seawater proportion in it. The calculated negative U concentration in the end-member fluid (Table 7) implies that U is not only 0 nmol/kg in this fluid, but that the end-member fluid is a sink for U from the seawater and entrains it upon fluid-seawater mixing.

The lowest concentrations of Fe, Mn, Ni, Y and REE, and the highest content of V in the fluid of the buoyant plume above the Tiger vent (Tables 7, 8) are likely a result of removal of dissolved Fe, Mn, Ni, Y and REE from the vent fluid to plume particles (Feely et al., 1990;

561 Ludford et al., 1996; Edmonds and German, 2004; Klevenz et al., 2011; Findlay et al., 2015) and
562 entrainment of seawater V (Trefry and Metz, 1989), respectively.

563 Although the chlorinity of the Abyss vent fluid is close to that of the ambient seawater it is
564 yet slightly higher than it (Table 7). This implies that the Abyss low-temperature vent fluid must
565 contain a proportion of high-temperature brine-rich vent fluid that has undergone phase
566 separation (Von Damm and Lilley, 2004). The low Pb, Cd, Zn and Sb concentrations in the
567 Abyss vent fluid (Table 7) are likely a result of sub-seafloor element-sulfide precipitation during
568 fluid cooling and dilution with seawater that are typical for low-temperature diffuse venting at the
569 seafloor (Koschinsky et al., 2002). As the most ubiquitous metal in the seafloor hydrothermal
570 fluids, Fe, preferentially precipitates relative to the other common metal Mn on cooling (Seyfried
571 and Ding, 1993) the low-temperature vent fluids usually appear to be enriched in Mn over Fe
572 (Thompson et al., 1985) and this explains the highest Mn concentration in the Abyss vent fluids
573 (Table 7).

574 The highest concentrations of La, Ce, Pr, Nd, Sm, Eu and Tb in the highest chlorinity (and
575 high-temperature) vent fluid (Tiger vent, D762 W1 F) and the highest concentrations of Y, Dy,
576 Ho, Er, Tm, Yb and Lu in the lowest chlorinity (and low-temperature) vent fluid (Abyss vent,
577 D762 B F) ~~(Table 8; Fig. 7 B)~~ are directly related to the chlorinity and temperature control on the
578 distribution of the REE in the vent fluids (Table 8; Fig. 7 B). Previous studies revealed (1) that in
579 a chloride-rich hydrothermal fluid, the REE transport is facilitated by formation of chloride
580 complexes at acidic conditions and (2) that the light REE (La-Sm) are complexed more strongly
581 by chloride, than the heavy REE (Gd-Lu) (Haas et al., 1995). At elevated temperatures this
582 relation (2) becomes more pronounced. The REE speciation calculations (Douville et al., 1999a)
583 confirmed that in the hot acidic fluids of the seafloor hydrothermal systems the REE were mainly
584 complexed by Cl^- ions. Because the Cl complexing tends to be stronger for the light REE, an
585 increased aqueous chloride content will tend to favor these lighter elements. Therefore, the high-
586 chlorinity high-temperature Tiger vent fluids have the highest contents of La, Ce, Pr, Nd, Sm, Eu
587 and Tb, whereas the low-chlorinity low-temperature Abyss vent fluids have the highest contents
588 of Y, Dy, Ho, Er, Tm, Yb and Lu within the Daiyon-Yonaguni Knoll vent field.

589 Compared to the end-member hydrothermal fluids from three other sedimented seafloor
590 hydrothermal systems (Escanaba Trough, Guaymas Basin and Middle Valley), the Daiyon-

Yonaguni Knoll end-member hydrothermal fluid shows the highest Pb, La, Ce, Pr, Nd, Sm, Eu, Tb, Dy, Ho and Er concentrations, and the lowest Mn concentration (Table 10). These differences deserve particular scientific attention involving the chemistry of the source rocks (volcanic and sedimentary) that is beyond the scope of this work.

6.3. Yttrium and REE insights into fluid-rock equilibrium

In most seafloor hydrothermal fluids, Y is trivalent and behaves like Ho, and it is supposed that the Y/Ho molar ratio can give important clues for the origin of the hydrothermal fluids (Douville et al., 1999a). The Y/Ho molar ratio of the studied Daiyon-Yonaguni Knoll vent fluids (50.5 - 76.4; Table 8) is between that of the southern Okinawa Trough lavas [27.6 - 31.8, basalts, andesites, dacites and rhyolites; Shinjo et al. (1999), Shu et al. (2017), Guo et al. (2018)] and North Pacific deep water (101; Nozaki et al., 1999). It seems likely that the seawater-based hydrothermal fluids of the Daiyon-Yonaguni Knoll field have not completely lost their original high seawater Y/Ho molar ratio (Bau and Dulski, 1999; Nozaki et al., 1999). This suggests that the seawater has not completely reacted with the basement rocks and has not equilibrated with them.

The REE distribution pattern of the Daiyon-Yonaguni Knoll end-member fluid (Fig. 7 B) implies the same conclusion. It not only closely matches the REE distribution pattern of the highest chlorinity Tiger vent fluid (D762 W1 F) thus, suggesting that this fluid is close to the end-member, but still shows a weak negative Ce anomaly (Fig. 7 B). This supports the assumption that the mother fluid, seawater, has not completely reacted with the basement rocks and has not completely lost its original negative Ce anomaly.

The origin of the positive Eu anomaly and the enrichment of light REE over the heavy REE when the REE concentrations are normalized to those of chondrite are discussed elsewhere (Michard et al., 1983; Michard and Albarède, 1986; Michard, 1989; Klinkhammer et al., 1994; Bau and Dulski, 1999; Douville et al., 1999a) and we will not repeat this discussion here.

6.4. Trace elements in the Daiyon-Yonaguni Knoll hydrothermal deposits: hydrothermal – microbial – hydrogenetic interplay

The studied Daiyon-Yonaguni Knoll hydrothermal deposits (bulk samples and mineral separates) are rich in Sb and As (Table 5). Previous works (Douville et al., 1999b; Breuer and Pichler, 2013) found that these two volatile elements are particularly enriched in the hydrothermal fluids discharged at back-arc and volcanic arc settings. Their high concentrations in these fluids are inferred to be primarily controlled by phase separation processes and source rock types: felsic volcanic rocks and sedimentary blanket. Thus, the fluid phase separation at the Daiyon-Yonaguni Knoll vents (see *6.2*) and the source rock types, felsic volcanics [calc-alkaline andesite to rhyolite; Shinjo et al. (1999)] and sediment cover (Sibuet et al., 1987) explain the high Sb and As concentrations in the hydrothermal deposits. Antimony and As are highly volatile elements and most probably separate in the vapor (low-chlorinity) during the boiling and phase separation. As the chlorinities of all studied vent fluids are higher than that of the local ambient seawater (Table 7), it seems reasonable to assume that Sb and As minerals in the Daiyon-Yonaguni Knoll deposits had precipitated in the past when the vapor phase (rich in volatiles) had dominated in the vent fluids.

Thallium is also a volatile element and its high concentration in the stibnite precipitates (Table 5) may also be explained with vent fluid phase separation and source rock types.

Gold concentrations in the bulk Daiyon-Yonaguni Knoll hydrothermal deposits (0.50 - 1.00 ppm; Table 5) fall within the range of Au content in the Okinawa Trough hydrothermal deposits (0.05 - 4.5 ppm; Fuchs et al., 2019) whereas the Daiyon-Yonaguni Knoll stibnite and orpiment samples are richer in Au (1.00 - 11.0 ppm; Table 5) than the Okinawa Trough hydrothermal deposits. However, the Au concentrations of the Daiyon-Yonaguni Knoll hydrothermal deposits (0.50 - 11.0 ppm; Table 5) are within the lower end of the Au content range of the global seafloor hydrothermal deposits (0.01 - 43.0 ppm; Fuchs et al., 2019). Almost linear correlation between Au and As concentrations (diagram available on request) suggests that (1) Au (like As) is hydrothermally derived in these deposits, (2) Au (like As) may also be contributed by direct magmatic degassing (e.g., Fuchs et al., 2019), and (3) As plays an essential role in Au intake in the As-containing sulfides (Pokrovski et al., 2021).

Higher concentrations of Fe, Mn, Zn, Pb and Bi in the orpiment samples than in the bulk samples can be explained with high hydrothermal input.

In addition to the high Au concentrations, the stibnite and orpiment samples have also enhanced U concentrations relative to those of the bulk deposit samples (Table 5). This seems controversial because unlike Au, the U is quantitatively removed (~98%) from seawater during hydrothermal circulation through the oceanic crust (Michard and Albarede, 1985; Chen et al., 1986) and, as a result, the seafloor end-member hydrothermal fluids are depleted in U. Therefore, hydrothermal contribution of U to the Daiyon-Yonaguni Knoll hydrothermal deposits had likely been negligible and the low U concentrations of the bulk samples (0.03-0.07 ppm; Table 5) seem to show that. The enhanced U concentrations in the stibnite and orpiment samples (0.12-3.96 ppm; Table 5) relative to the bulk deposits suggest that a factor other than the hydrothermal fluid controlled U concentration in the stibnite and orpiment. Previous work (Lovley et al., 1991; Mills et al., 1994) suggested that U enrichment within the TAG seafloor hydrothermal deposits is microbially mediated. The presence of carbonaceous matter associated with the filamentous orpiment and inferred microbial activity (see *6.6*) imply that the elevated U content in this type of orpiment is a result of bacterial concentration of U from a seawater-dominated fluid. Thus, the enrichments of the stibnite and orpiment in two elements with different mechanisms of mobilization and fixation, Au and U, likely happened at different stages of the mineral deposition. Gold seems to have been deposited within stibnite and orpiment, and during their hydrothermal precipitation, while U has mostly likely been deposited within bacterial biofilms on stibnite and orpiment after their deposition.

Chondrite-normalized REE distribution patterns of the Daiyon-Yonaguni Knoll (bulk) deposits and one stibnite and one orpiment samples show negative Ce anomalies, positive Eu anomalies and enrichment of light relative to the heavy REE (Fig. 7 A; Table 6). These patterns resemble that of the Daiyon-Yonaguni Knoll end-member hydrothermal fluid, which slightly differs from those of the end-member fluids from other seafloor hydrothermal fields (Michard et al., 1983; Michard and Albarède, 1986; Michard, 1989; Klinkhammer et al., 1994; Bau and Dulski, 1999; Douville et al., 1999a) in possessing of a weak negative Ce anomaly (Fig. 7 B). We interpreted this feature as a result of incomplete reaction of seawater with the basement rocks and partial preservation of its original negative Ce anomaly (see *6.3*). Thus, the REE distribution patterns of the discussed deposits (bulk, one stibnite and one orpiment) seem to be inherited from the end-member hydrothermal fluid (mixed or not with ambient seawater). However, two of the

orpiment samples (2K1271 L1 flange, outer bottom, Op and 2K1267 L1, Op-1) have positive Ce anomalies, highest Nd concentrations, the smallest positive Eu anomalies, and the smallest fractionation between the light and heavy REE (La_{CN}/Lu_{CN}) (Table 6; Fig. 7 A). Previous studies showed that positive Ce anomalies and high Nd concentrations (>100 ppm) are typical for the seafloor hydrogenetic Fe-Mn deposits (Bau et al., 2014). The origin of the positive Ce anomaly in the seafloor Fe-Mn deposits is discussed elsewhere (Bau and Koschinsky, 2009). Although we are not aware of any particular study of the REE in the seafloor hydrothermal orpiment we may assume that the observed positive Ce anomalies, high Nd concentrations, little positive Eu anomalies, and little fractionation between the light and heavy REE in the two orpiment samples (Table 6) are results of hydrogenetic influence.

Hence, the trace element contents in the Daiyon-Yonaguni Knoll hydrothermal deposits suggest a complex interplay among hydrothermal (hydrothermal input), microbial (preferential concentration) and hydrogenetic (preferential scavenging from seawater) processes.

6.5. Origin of S in the sulfide precipitates and sulfate reduction in the vent fluids of the Daiyon-Yonaguni Knoll hydrothermal field

The S-isotope systematics in the seafloor hydrothermal systems at arc/back-arc settings show substantial variability in $\delta^{34}S$ (Fig. 8). The wide variation in $\delta^{34}S$ is a result of S-isotope fractionation due to three processes contributing to the S budget of the hydrothermal system: (1) basement rock sulfide supplied by interaction of hydrothermal fluid with basement rocks (Shanks and Seyfried, 1987; Shanks, 2001), (2) thermochemical reduction of sulfate supplied by seawater (Shanks and Seyfried, 1987; Shanks, 2001), (3) disproportionation of SO_2 supplied by magma vapors (Kusakabe et al., 2000; Peters et al., 2021).

Sulfide S of the Daiyon-Yonaguni Knoll hydrothermal deposits has isotope composition ($\delta^{34}S$) between those of the terrestrial mantle (basement rocks) sulfide and seawater sulfate, but being closer to the former (Table 5; Fig. 8). This suggests that the Daiyon-Yonaguni Knoll S bound in sulfides is a mixture of both basement rock and seawater S with a higher proportion of the basement rock S. The S-isotope composition of the Daiyon-Yonaguni Knoll sulfides supports the origin of sulfide S in the overall Okinawa Trough hydrothermal deposits being generally

dominated by basement rock S (Fig. 8). There are no clear indications for magmatic S supply to the Daiyon-Yonaguni Knoll hydrothermal deposits.

The slightly heavier S-isotope composition of sulfate in one Tiger vent and one Abyss vent fluids (21.2 and 21.6‰, respectively; Table 7) than that of the seawater ($\delta^{34}S_{sulfate}$ = 20.97 ± 0.10‰; Paris et al., 2013) is similar to the heavy S-isotope composition of sulfate of the CLAM hydrothermal fluids ($\delta^{34}S_{sulfate}$ > 21.0‰; Gamo et al., 1991) and deserves some consideration. We know that sulfate reduction in a closed system causes an increase of $\delta^{34}S$ of the residual sulfate (removal of the isotopically light sulfide during sulfate reduction) with decreasing sulfate concentration (Ohmoto and Rye, 1979; Shanks et al., 1981). Thus, the S-isotope composition of the sulfate from these two Daiyon-Yonaguni Knoll vent fluids can be interpreted as a result of sulfate reduction. Sulfate reduction or sulfide oxidation depends on the rate of mixing between the hydrothermal fluid and seawater (Peter and Shanks, 1992). Slow mixing of the hydrothermal fluid and seawater in the chimney walls or within a mound favors sulfate reduction. This sulfate reduction results in S isotope fractionation approaching equilibrium values and ^{34}S-enriched sulfate resulting from a reservoir effect, as ^{32}S is removed to the sulfide reservoir (Peter and Shanks, 1992). Overall, it appears that the hydrothermal fluid mixed slowly with seawater within the chimney walls of the Tiger and Abyss vents that favored reduction of the sulfate dissolved in the fluids and resulted in a heavy S-isotope composition of the vent fluids.

6.6. Sources of Pb to the Daiyon-Yonaguni Knoll hydrothermal deposits

The Pb isotope data for the Daiyon-Yonaguni Knoll hydrothermal deposits form a steep array indicating mixing of two Pb end-members (Fig. 9). At the low end of the array is sample 2K1271 L1 flange, outer bottom, Op. This sample plots below regional sedimentary and volcanic rocks, towards the NHRL indicating more primitive, mantle-like source of Pb. This in turn suggests presence of more depleted Pb isotopic source, possibly back-arc mafic volcanic rocks, in the area of Daiyon-Yonaguni Knoll. Three of the samples (2K1271 L1 flange, center upper; 2K1271 L1 flange, outer bottom, Stb; and 2K1271 L1, Op) plot close to the regional lavas. This suggests that Pb and other metals in these three hydrothermal samples can be derived from the local lavas. Alternatively, the Pb isotopic compositions of these three samples can be explained

by mixing between the more primitive source, responsible for the isotopic composition of 2K1271 L1 flange, outer bottom, Op and more enriched source reflected in the rest of the hydrothermal deposit samples. The enriched samples are very similar to laser ablation Pb isotope data for galena and anglesite from the Daiyon-Yonaguni Knoll (Zeng et al., 2022) and plot above the regional lavas indicating Pb derivation from more evolved source, potentially continental lithosphere and/or sedimentary rocks. This is consistent with Pb isotope studies of other hydrothermal deposits in the Okinawa Trough that also found evidence for significant involvement of sedimentary Pb in the hydrothermal systems (e.g., Ma et al., 2021; Zeng et al., 2022~~; Dekov et al. submitted~~). However, it is interesting to note that the Pb isotope data for the closest hydrothermal fields [southern Okinawa Trough (SOT) sulfides] are very distinct from the Daiyon-Yonaguni Knoll hydrothermal deposits (Fig. 9). As can be seen on the Figure 9, the SOT sulfides are close to the regional sediment Pb data, thus providing direct evidence for a significant sedimentary component in the hydrothermal system (Ma et al., 2021). In contrast, the Daiyon-Yonaguni Knoll hydrothermal deposits are isotopically distinct from the SOT sulfides. Furthermore, the hydrothermal deposits are not close isotopically to any of the available sediment samples (Fig. 9). However, based on their position above the regional volcanic rocks it is most likely that another enriched source, either sediments or extended continental lithosphere, is present in the area of Daiyon-Yonaguni Knoll.

6.7. Filamentous orpiment: biogenic or abiogenic?

The morphology of the light orange filaments (Fig. 5 A, C, E) resembles microbial fossils (especially, fossilized fungi) previously described at the seafloor (Ivarsson et al., 2020). The longitudinal, branching filaments forming a network-like framework (Fig. 5 A, C) can be compared to fossilized fungal mycelium. The consistent and distinct center of the filaments (Fig. 5 C, E) corresponds size-wise to known sizes for fungal hyphae. The empty core (Fig. 5 E) can be the remains or cast of an initial microbial/fungal filament/hyphae. However, the concentric layering in cross sections of the filaments (Fig. 5 E) implies this morphology can be a result of repeated mineral deposition. Additionally, the overall features of the filaments with the rather straight appearance, the 90° branching and interconnections between filaments, the distinct

tapering and variation in diameter could be explained by abiotic biomorphs, or heavily encrusted fungal hyphae. Based on morphology alone we can neither rule out nor support a biological or an abiotic origin of the filaments at this point. The staining for chitin was unsuccessful, thus there ~~are~~ is no solid evidence for fungal (biogenic) origin of the filaments.

The Raman data, on the other hand, supports the presence of carbonaceous matter associated with the orpiment filaments. Thus, even though a fungal origin of the orpiment filaments cannot be unambiguously supported, the presence of microbial activity can be. The filaments and their close proximity appear coated by a thin carbonaceous film that may represent the remains of a biofilm. The I(1350)/I(1600) value indicates that the carbonaceous matter associated with the filaments present medium structural order. The calculated maximum temperature experienced by the filaments (209.1±37.1°C) falls within the temperature range of the vent fluids (Table 2) and indicates that the carbonaceous matter reached low to medium-grade thermal maturity. This excludes the possibility of recent contamination by carbonaceous matter and supports the idea that the carbonaceous matter associated with the orpiment filaments is indigenous to the primary hydrothermal environment.

6.8. Stibnite, orpiment and barite hydrothermal precipitation: implications from stability phase diagrams

The maximum temperature, which the GWB can consider in the modeling is 300°C. Therefore, we used this temperature when modeling the stability diagrams for vent fluid sample D759 W1 F (T = 323°C) (Fig. 12 A, D, G).

In view of the chemistry of the Daiyon-Yonaguni Knoll vent fluids (Tables 7, 8; Suzuki et al., 2008), it seems plausible to assume that the major Sb- and As-ions in these fluids will be chloride and sulfide. We could not obtain any stability diagrams when using Sb-chloride and As-chloride ions as major Sb- and As-ions, respectively, in the vent fluid. This may mean that the incorporation of these species in the GWB data base may not be correct. Therefore, we used Sb-sulfide ions as main Sb-ions in the vent fluids. Using the measured Sb concentrations in the Daiyon-Yonaguni Knoll vent fluids (Table 7) in the modeling, we did not get any stability field of stibnite. This suggests that stibnite does not precipitate from the current vent fluids: Sb content

is lower than that necessary for stibnite precipitation. Therefore, we put as a variable $\log_{10}a$ of the main Sb-ion suggested by the GWB, $Sb_2S_4^{2-}$, along one of the axes of the diagrams (Fig. 12 A, B, C).

On the basis of the vent fluid chemistry of the three vent fluids the GWB suggested only one As-sulfide ion, but it did not yield any diagram with stability field of orpiment. The main As-ion suggested by the GWB was $H_2AsO_4^-$ and we used it in the modeling. As we were not able to measure the As concentrations in the vent fluids (see sub-section *4.3*) we put as a variable $\log_{10}a$ of $H_2AsO_4^-$ along one of the axes of the diagrams and investigated a wide range of $\log_{10}a$: from -10 to +5 (Fig. 12 D, E, F).

We assumed that Ba^{2+} will be the major Ba ion in the studied vent fluids and therefore, we used Ba^{2+} in the modeling of barite stability (Fig. 12 G, H, I).

Modeling suggests that the stibnite has a limited area of stability within the physic~~al~~ochemical conditions of the selected vent fluids (Fig. 12 A, B, C). Its area of stability does not seem to depend on the vent fluid chlorinity: ~~the~~ The area of stability of stibnite in the most chloride-rich fluid, D763 W2 F, does not differ substantially from those in the other fluids (Fig. 12 A, B, C). Obviously, the ~~area of~~ stability of stibnite increases with decreasing temperature of the vent fluid and results in ~~stibnite stability (i.e.,~~ precipitation~~)~~ at lower $\log_{10}a$ of $Sb_2S_4^{2-}$ (i.e., lower Sb concentrations) and less reduced environment (i.e., higher Eh, but still <0) (Fig. 12 A, B, C). In other words, the lowest temperature Daiyon-Yonaguni Knoll vent fluid (D762 B F; T = 80°C) is the most probable environment for stibnite precipitation.

Orpiment is stable (i.e., precipitates) in a wide range of $\log_{10}a$ of $H_2AsO_4^-$ (i.e., As concentrations) and in ~~reduced~~ reducing conditions (Eh<0) (Fig. 12 D, E, F). With decreasing vent fluid temperature (from 300°C to 80°C), ~~the~~ orpiment is stable (precipitates) at slightly less reduced conditions (higher Eh, but still <0) (Fig. 12 D, E, F). The differences in vent fluid chlorinity and vent fluid trace metal concentrations do not seem to affect the stability of orpiment (Fig. 12 D, E, F). Previous studies (Rytuba, 1984) add an additional constraint for orpiment precipitation. According to them, under conditions of constant temperature and pressure, the relative stability of As-sulfides is a function of S activity. Orpiment appears to be the stable As-sulfide at high S activity, which suggests high S activity during the orpiment precipitation at the Daiyon-Yonaguni Knoll hydrothermal site.

Modeling showed that in the high-temperature vent fluids D759 W1 F (T = 300°C) and D763 W2 F (T = 210°C), the major Ba-ion is $BaCl^+$ (Fig. 12 G, H), whereas in the low-temperature vent fluid D762 B F (T = 80°C) dissolved Ba ~~is~~ appears as Ba^{2+} (Fig. 12 I). Barite is stable in wide range of $\log_{10}a$ of Ba^{2+} (i.e., Ba concentrations) in all the three vent fluids and precipitates from slightly reduced to slightly oxic conditions (Fig. 12 G, H, I). With decreasing temperature of the vent fluid (from 300°C to 80°C), the stability field of barite slightly shifts to less reduced (more oxic) conditions (Fig. 12 G, H, I). Modeling of barite precipitation from the Daiyon-Yonaguni Knoll vent fluids shows large stability field of barite in wide temperature range (80-300°C) and extends previous knowledge that hydrothermal barite precipitates at temperatures 100-240°C (see *6.1*).

7. Summary

The ~~Major~~ major mineral in the Daiyon-Yonaguni Knoll hydrothermal deposits is barite, which likely precipitated from focused-discharge fluids composed of a high proportion (>40%) of hydrothermal end-member fluid at T = 100-240°C. Stibnite and orpiment are minor minerals, which seem to be later lower temperature precipitates.

The Daiyon-Yonaguni Knoll vent fluids were subjected to sub-seafloor boiling and phase separation and are brine-rich (chloride-rich) enriched in non-volatile and depleted in volatile elements. Sub-seafloor boiling and phase separation exerted major control on the REE partitioning in the vent fluids, with the high-chlorinity high-temperature fluids enriched in light REE and low-chlorinity low-temperature fluids enriched in heavy REE. The Y/Ho molar ratio and Ce anomaly of the Daiyon-Yonaguni Knoll vent fluids suggest that the seawater ~~has~~ had not completely reacted with the basement rocks and ~~has~~ had not equilibrated with them.

The trace element contents in the Daiyon-Yonaguni Knoll hydrothermal deposits suggest a complex interplay among hydrothermal, microbial and hydrogenetic processes.

Sulfur isotope composition of the Daiyon-Yonaguni Knoll sulfides suggests that the sulfide S is a mixture of both basement rock and seawater S, with a higher proportion of the basement rock S. The hydrothermal fluid mixed slowly with seawater within the chimney walls of the Tiger

and Abyss vents ~~that~~ which favored reduction of the sulfate dissolved in the fluids and resulted in a heavy S-isotope composition of the vent fluid sulfate.

The Pb isotope data for the Daiyon-Yonaguni Knoll hydrothermal deposits indicate involvement of two or even three sources of metals in the hydrothermal system. One of the sources can be local volcanic rocks, as three of the samples show Pb isotopes close to the latter. However, the Pb isotope data form a steep array that potentially can be explained by only two end-members, one enriched (continental lithosphere and/or sediments) and one depleted (possibly back-arc basalts). It is interesting to note that both of these end-members are discrete, not identifiable in the available Pb isotope data for southern Okinawa sedimentary and volcanic rocks.

The morphology details of the filamentous orpiment suggest that these filaments are either heavily mineralized fungal hyphae or pure abiogenic biomorphs. Although a fungal origin of the orpiment filaments cannot be unambiguously inferred, microbial activity (presence of carbonaceous matter) is detected at/around them. The filaments experienced temperature of 209.1±37.1°C which falls within the temperature range of the Daiyon-Yonaguni Knoll vent fluids and indicates that the carbonaceous matter on/within the filaments reached low to medium-grade thermal maturity.

Modeling of stability phase diagrams suggests that the stability of stibnite does not seem to depend on the vent fluid chlorinity, but ~~depends~~ rather on the vent fluid temperature: the area of stibnite stability increases with decreasing temperature of the vent fluid and results in stibnite precipitation at lower $\log_{10}a$ of $Sb_2S_4^{2-}$ and less reduced environment (i.e., high Eh, but still <0). Orpiment is stable in a wide range of $\log_{10}a$ of $H_2AsO_4^-$, in reduced conditions and at high S activity. The variations in vent fluid chlorinity and trace metal concentrations do not seem to affect the stability of orpiment. Barite is stable ~~in~~ over a wide range of $\log_{10}a$ of Ba^{2+} and precipitates in slightly reduced to slightly oxic conditions.

Declaration of Competing Interest

The authors declare that they have no known competing financial interests or personal relationships that could have appeared to influence the work reported in this paper.

Acknowledgements

The successful completion of this work would not be possible without the valuable support of Dr. T. Tomiyama (JAMSTEC), who generously provided the hydrothermal deposit samples, Prof. Y. Takahashi (University of Tokyo), who gave us the possibility to perform the SEM studies in his lab, and Mrs. M. Otsuki (TUMSAT), who helped with the EMP analyses. We greatly appreciate their help. The suggestions and comments by two anonymous reviewers improved the paper significantly and are highly appreciated.

Supplementary data

Supplementary data to this article can be found online at Mendeley Data, V2, doi: 10.17632/r5twp9ftyy.2~~V1, doi: 10.17632/r5twp9ftyy.1~~

References

Alibo, D.S., Nozaki, Y., 1999. Rare earth elements in seawater: particle association, shale-normalization, and Ce oxidation. Geochim. Cosmochim. Acta 63, 363-372.

Alt, J.C., Teagle, D.A.H., Brewer, T.S., Shanks, W.C. III, Halliday, A.N., 1998. Alteration and mineralization of an oceanic forearc and the ophiolite-ocean crust analogy. J. Geophys. Res. 103, 12,365-12,380.

Aries, S., Valladon, M., Polvé, M., Dupré, B., 2000. A routine method for oxide and hydroxide interference corrections in ICP-MS chemical analysis of environmental and geological samples. Geostand. Newsl. 24, 19-31.

Arnold, M., Sheppard, S.M.F., 1981. East Pacific Rise at latitude 21°N: isotopic composition and origin of the hydrothermal sulfur. Earth Planet. Sci. Lett. 56, 148-156.

Bau, M., Dulski, P., 1999. Comparing yttrium and rare earths in hydrothermal fluids from the Mid-Atlantic Ridge: Implications for Y and REE fractionation during near-vent mixing and for the Y/Ho ratio of Proterozoic seawater. Chem. Geol. 155, 77-90.

Bau, M., Koschinsky, A., 2009. Oxidative scavenging of cerium on hydrous Fe oxide: evidence from the distribution of rare earth elements and yttrium between Fe oxides and Mn oxides in hydrogenetic ferromanganese crusts. Geochem. J. 43, 37-47.

922 Bau, M., Schmidt, K., Koschinsky, A., Hein, J., Kuhn, T., Usui, A., 2014. Discriminating between different genetic
923 types of marine ferro-manganese crusts and nodules based on rare earth elements and yttrium. Chem. Geol.
924 381, 1-9.
925 Bentahila, Y., Ben Othman, D., Luck, J.-M., 2008. Strontium, lead and zinc isotopes in marine cores as tracers of
926 sedimentary provenance: A case study around Taiwan orogen. Chem. Geol. 248, 62-82.
927 Bethke, C.M., 2008. Geochemical and Biogeochemical Reaction Modeling. Cambridge University Press, New York,
928 547 p.
929 Bluth, G.J., Ohmoto, H., 1988. Sulfide-sulfate chimneys on the East Pacific Rise, 11° and 13°N latitudes. Part II:
930 Sulfur isotopes. Can. Mineral. 26, 505-515.
931 Bowers, T.S., Campbell, A.C., Measures, C.I., Spivack, A.J., Khadem, M., Edmond, J., 1988. Chemical controls on
932 the composition of vent fluids at 13°-11°N and 21°N, East Pacific Rise. J. Geophys. Res. 93, 4522-4536.
933 Breuer, C., Pichler, T., 2013. Arsenic in marine hydrothermal fluids. Chem. Geol. 348, 2-14.
934 Butler, I.B., Fallick, A.E., Nesbitt, R.W., 1998. Mineralogy, sulphur isotope geochemistry and the development of
935 sulphide structures at the Broken Spur hydrothermal vent site, 29°10´N, Mid-Atlantic Ridge. J. Geol. Soc.
936 London 155, 773-785.
937 Butterfield, D.A., Massoth, G.J., McDuff, R.E., Lupton, J.E., Lilley, M.D., 1990. Geochemistry of hydrothermal
938 fluids from Axial Seamount Hydrothermal Emissions Study vent field, Juan de Fuca Ridge: Subseafloor
939 boiling and subsequent fluid-rock interaction. J. Geophys. Res. 95, B8, 12895-12921.
940 Butterfield, D.A., McDuff, R.E., Franklin, J., Wheat, C.G., 1994. Geochemistry of hydrothermal vent fluids from
941 Middle Valley, Juan de Fuca Ridge. In: Mottl, M.J., Davis, E.E., Fisher, A.T., and Slack, J.F. (Eds.),
942 Proceedings of the Ocean Drilling Program, Scientific Results 139, 395-410.
943 Campbell, A.C., Bowers, T.S., Measures, C.I., Falkner, K.K., Khadem, M., Edmond, J.M., 1988. A time series of
944 vent fluid compositions from 21°N East Pacific Rise (1979, 1981, 1985) and the Guaymas Basin, Gulf of
945 California (1982, 1985). J. Geophys. Res. 93, 4537-4549.
946 Chen, J.H., Wasserburg, G.J., Von Damm, K.L., Edmond, J.M., 1986. The U-Th-Pb systematics in hot springs on the
947 East Pacific Rise at 21°N and in the Guaymas Basin. Geochim. Cosmochim. Acta 50, 2467-2479.
948 Chen, Z., Zeng, Z., Yin, X., Wang, X., Zhang, Y., Chen, S., Shu, Y., Guo, K., Li, X., 2019. Petrogenesis of highly
949 fractionated rhyolites in the southwestern Okinawa Trough: Constraints from whole-rock geochemistry data
950 and Sr-Nd-Pb-O isotopes. Geol. J. 54, 316-332.
951 Corliss, J.B., Dymond, J., Gordon, L.I., Edmon, J.M., Von Herzen, R.P., Ballard, R.D., Green, K., Williams, D.,
952 Bainbridge, A., Crane, K., Van Andell, T.H., 1979. Submarine thermal springs on the Galapagos Rift. Science
953 203, 1073-1083.
954 Dekov, V.M., Savelli, C., 2004. Hydrothermal activity in the SE Tyrrhenian Sea: An overview of 30 years of
955 research. Mar. Geol. 204, 161-185.
956 Dekov, V.M., Bindi, L., Burgaud, G., Petersen, S., Asael, D., Rédou, V., Fouquet, Y., Pracejus, B., 2013. Inorganic
957 and biogenic As-sulfide precipitation at seafloor hydrothermal fields. Mar. Geol. 342, 28-38.

~~Dekov, V.M., Yasuda, K., Kamenov, G., Yasukawa, K., Guéguen, B., Kano, A., Yoshimura, T., Yamanaka, T., Bindi, L., Okumura, T., Asael, D., Araoka, D., Kato, Y., 2022. Mn-carbonate deposition in a seafloor hydrothermal system (CLAM field, Iheya Ridge, Okinawa Trough): Insights from mineralogy, geochemistry and isotope studies. Geochim. Cosmochim. Acta (submitted).~~

de Ronde, C.E.J., Hannington, M.D., Stoffers, P., Wright, I.C., Ditchburn, R.G., Reyes, A.G., Baker, E.T., Massoth, G.J., Lupton, J.E., Walker, S.L., Greene, R.R., Soong, C.W.R., Ishibashi, J., Lebon, G.T., Bray, C.J., Resing, J.A., 2005. Evolution of a submarine magmatic-hydrothermal system: Brothers volcano, southern Kermadec Arc, New Zealand. Econ. Geol. 100, 1097-1133.

de Ronde, C.E.J., Massoth, G.J., Butterfield, D.A., Christenson, B.W., Ishibashi, J., Ditchburn, R.G., Hannington, M.D., Brathwaite, R.L., Lupton, J.E., Kamenetsky, V.S., Graham, I.J., Zellmer, G.F., Dziak, R.P., Embley, R.W., Dekov, V.M., Munnik, F., Lahr, J., Evans, L.J., Takai, K., 2011. Submarine hydrothermal activity and gold-rich mineralization at Brothers Volcano, Kermadec Arc, New Zealand. Miner. Deposita 46, 541-584.

Douville, E., Bienvenu, P., Charlou, J.L., Donval, J.P., Fouquet, Y., Appriou, P., Gamo, T., 1999a. Yttrium and rare earth elements in fluids from various deep-sea hydrothermal systems. Geochim. Cosmochim. Acta 63, 627-643.

Douville, E., Charlou, J.L., Donval, J.P., Hureau, D., Appriou, P., 1999b. As and Sb behaviour in fluids from various deep-sea hydrothermal systems. C. R. Acad. Sci. Paris, Sciences de la terre et des planètes 328, 97-104.

Duckworth, R.C., Knott, R., Fallick, A.E., Rickard, D., Murton, B.J., van Dover, C., 1995. Mineralogy and sulphur isotope geochemistry of the Broken Spur sulphides, 29°N, Mid-Atlantic Ridge. In: Parson, L.M., Walker, C.L., Dixon, D.R. (Eds.), Hydrothermal Vents and Processes. Geol. Soc. Spec. Publ. 87, 175-189.

Edmond, J.M., Measures, C.I., McDuff, R.E., Chan, L.H., Collier, R., Grant, B., Gordon, L.I., Corliss, J.B., 1979. Ridge crest hydrothermal activity and the balance of the major and minor elements in the ocean: The Galapagos data. Earth Planet. Sci. Lett. 46, 1-18.

Edmonds, H.N., German, C.R., 2004. Particle geochemistry in the Rainbow hydrothermal plume, Mid-Atlantic Ridge. Geochim. Cosmochim. Acta 68, 759-772.

Feely, R.A., Geiselman, T.L., Baker, E.T., Massoth, G.J., Hammond, S.R., 1990. Distribution and composition of hydrothermal plume particles from the ASHES Vent Field at Axial Volcano, Juan de Fuca Ridge. J. Geophys. Res. Solid Earth 95, 12855-12873.

Ferrari, A.C., Robertson, J., 2000. Interpretation of Raman spectra of disordered and amorphous carbon. Phys. Rev. B 61, 14095.

Findlay, A.J., Gartman, A., Shaw, T.J., Luther, G.W., 2015. Trace metal concentration and partitioning in the first 1.5 m of hydrothermal vent plumes along the Mid-Atlantic Ridge: TAG, Snakepit, and Rainbow. Chem. Geol. 412, 117-131.

Firstova, A., Stepanova, T., Cherkashov, G., Goncharov, A., Babaeva, S., 2016. Composition and formation of gabbro-peridotite hosted seafloor massive sulfide deposits from the Ashadze-1 hydrothermal field, Mid-Atlantic Ridge. Minerals 6, 19.

Fouquet, Y., Auclair, G., Cambon, P., Etoubleau, J., 1988. Geological setting, mineralogical, and geochemical investigations on sulfide deposits near 13°N on the East Pacific Rise. Mar. Geol. 84, 145-178.

Fouquet, Y., Von Stackelberg, U., Charlou, J.-L., Erzinger, J., Herzig, P.M., Mühe, R., Wiedicke, M., 1993a. Metallogenesis in back-arc environments: The Lau Basin example. Econ. Geol. 88, 2154-2181.

Fouquet, Y., Wafik, A., Cambon, P., Mevel, C., Meyer, G., Gente, P., 1993b. Tectonic setting and mineralogical and geochemical zonation in the Snake Pit sulfide deposit (Mid-Atlantic Ridge at 23° N). Econ. Geol. 88, 2018-2036.

Fouquet, Y., Knott, R., Cambon, P., Fallick, A., Rickard, D., Desbruyeres, D., 1996. Formation of large sulfide mineral deposits along fast spreading ridges. Example from off-axial deposits at 12°43´N on the East Pacific Rise. Earth Planet. Sci. Lett. 144, 147-162.

Fouquet, Y., Cambon, P., Etoubleau, J., Charlou, J.L., Ondréas, H., Barriga, F.J.A.S., Cherkashov, G., Semkova, T., Poroshina, I., Bohn, M., Donval, J.P., Henry, K., Murphy, P., Rouxel, O., 2010. Geodiversity of hydrothermal processes along the Mid-Atlantic Ridge and ultramafic-hosted mineralization: A new type of oceanic Cu-Zn-Co-Au volcanogenic massive sulfide deposit. In: Rona, P.A., Devey, C.W., Dyment, J., Murton, B.J. (Eds.), Diversity of Hydrothermal Systems on Slow Spreading Ocean Ridges. Geophysical Monograph 188, 321-367.

Fuchs, S., Hannington, M.D., Petersen, S., 2019. Divining gold in seafloor polymetallic massive sulfide systems. Miner. Deposita 54, 789-820.

Fujiwara, T., Toyoda, S., Uchida, A., Ishibashi, J., Nakai, S., Takamasa, A., 2015. ESR dating of barite in sea-floor hydrothermal sulfide deposits in the Okinawa Trough. In: Ishibashi, J., et al. (Eds), Subseafloor Biosphere Linked to Hydrothermal Systems: TAIGA Concept, pp. 369-386.

Gamo, T., Sakai, H., Kim, E-S., Shitashima, K., Ishibashi, J.-I., 1991. High alkalinity due to sulfate reduction in the CLAM hydrothermal field, Okinawa Trough. Earth Planet. Sci. Lett. 107, 328-338.

Gemmell, J.B., Sharpe, R., 1998. Detailed sulfur-isotope investigation of the TAG hydrothermal mound and stockwork zone, 26°N, Mid-Atlantic Ridge. In: Herzig, P.M., Humphris, S.E., Miller, D.J., Zierenberg, R.A. (Eds.), Proc. ODP, Sci. Results, College Station, TX, 158, pp. 71-84.

Gena, K., Chiba, H., Kase, K., 2005. Tin-bearing chalcopyrite and platinum-bearing bismuthinite in the active Tiger chimney, Yonaguni Knoll IV seafloor hydrothermal system, South Okinawa Trough, Japan. Earth Science Reports, Okayama University 12, 1-5.

German, C.R., Von Damm, K.L., 2003. Hydrothermal processes. In: Turekian, K.K., Holland, H.D. (Eds), *Treatise on Geochemistry*, Vol. 6 The Oceans and Marine Geochemistry, Elsevier, Oxford, pp. 181-222.

Glasby, G.P., Notsu, K., 2003. Submarine hydrothermal mineralization in the Okinawa Trough, SW of Japan: an overview. Ore Geol. Rev. 23, 299-339.

Godelitsas, A., Price, R.E., Pichler, T., Amend, J., Gamaletsos, P., Göttlicher, J., 2015. Amorphous As-sulfide precipitates from the shallow-water hydrothermal vents off Milos Island (Greece). Mar. Chem. 177, 687-696.

Guo, K., Zhai, S., Yu, Z., Wang, S., Zhang, X., Wang, X., 2018. Geochemical and Sr-Nd-Pb-Li isotopic characteristics of volcanic rocks from the Okinawa Trough: Implications for the influence of subduction components and the contamination of crustal materials. J. Mar. Syst. 180, 140-151.

1031 Haas, J.R., Shock, E.L., Sassani, D.C., 1995. Rare earth elements in hydrothermal systems: Estimates of standard
1032 partial molal thermodynamic properties of aqueous complexes of the rare earth elements at high pressures and
1033 temperatures. Geochim. Cosmochim. Acta 59, 4329-4350.
1034 Halbach, P., Pracejus, B., Märten, A., 1993. Geology and mineralogy of massive sulfide ores from the central
1035 Okinawa Trough, Japan. Econ. Geol. 88, 2210-2225.
1036 Hannington, M.D., Scott, S.D., 1988. Mineralogy and geochemistry of an hydrothermal silica-sulfide-sulfate spire in
1037 the caldera of Axial-Seamount, Juan de Fuca Ridge. Can. Mineral. 26, 603-625.
1038 Hannington, M., Herzig, P., Scott, S., Thompson, G., Rona, P., 1991. Comparative mineralogy and geochemistry of
1039 gold-bearing sulfide deposits on the mid-ocean ridges. Mar. Geol. 101, 217-248.
1040 Hart, S.R., 1984. A large-scale isotope anomaly in the Southern Hemisphere mantle. Nature 309, 753-757.
1041 Haymon, R.M., Kastner, M., 1981. Hot spring deposits on the East Pacific Rise at 21°N: Preliminary descriptions of
1042 mineralogy and genesis. Earth Planet. Sci. Lett. 53, 363-381.
1043 Hekinian, R., Fevrier, H., Bischoff, J.L., Picot, P., Shanks, W.C., 1980. Sulfide deposits from the East Pacific Rise
1044 near 21°N. Science 207, 1433-1444.
1045 Herzig, P.M., Hannington, M.D., 1995. Polymetallic massive sulfides at the modern seafloor: A review. Ore Geol.
1046 Rev. 10, 95-115.
1047 Herzig, P.M., Petersen, S., Hannington, M.D., 1998. Geochemistry and sulfur-isotopic composition of the TAG
1048 hydrothermal mound, Mid-Atlantic Ridge, 26°N. In: Herzig, P.M., Humphris, S.E., Miller, D.J., Zierenberg,
1049 R.A. (Eds.), Proc. ODP, Sci. Results, College Station, TX, 158, pp. 47-70.
1050 Herzig, P.M., Petersen, S., Kuhn, T., Hannington, M.D., Gemmell, J.B., Skinner, A.C., 2003. Shallow drilling of
1051 seafloor hydrothermal systems: The missing link. In: Eliopoulos, D., et al. (Eds), Mineral Exploration and
1052 Sustainable Development, Millpress, Rotterdam. pp. 103-105.
1053 Hirata, N., Kinoshita, H., Katao, H., Baba, H., Kaiho, Y., Koresawa, S., Ono, Y., Hayashi, K., 1991. Report on
1054 DELP 1988 cruises in the Okinawa Trough part 3. Crustal structure of the southern Okinawa Trough. Bull.
1055 ERI Univ. Tokyo 66, 37-70.
1056 Hongo, Y., Obata, H., Gamo, T., Nakaseama, M., Ishibashi, J., Konno, U., Saegusa, S., Ohkubo, S., Tsunogai, U.,
1057 2007. Rare earth elements in the hydrothermall system at Okinawa Trough back-arc basin. Geochem. J. 41, 1-
1058 15.
1059 Hsu, S.-C., Lin, F.-J., Jeng, W.-L., Chung, Y.-C., Shaw, L.-M., 2003. Hydrothermal signatures in the southern
1060 Okinawa Trough detected by the sequential extraction of settling particles. Mar. Chem. 84, 49-66.
1061 Iizasa, K., Fiske, R.S., Ishizuka, O., Yuasa, M., Hashimoto, J., Ishibashi, J., Naka, J., Horii, Y., Fujiwara, Y., Imai,
1062 A., Koyama, S., 1999. A Kuroko-type polymetallic sulfide deposit in a submarine silicic caldera. Science 283,
1063 975-977.
1064 Imai, N., Terashima, S., Itoh, S., Ando, A., 1995. 1994 compilation of analytical data for minor and trace elements in
1065 seventeen GSJ geochemical reference samples, "igneous rock series". Geostandard Newslett. 19, 135-213.

1066 Ishibashi, J., Ikegami, F., Tsuji, T., Urabe, T., 2015. Hydrothermal activity in the Okinawa Trough Back-Arc Basin:
1067 geological background and hydrothermal mineralization. In: Ishibashi, J. (Ed.), Subseafloor Biosphere Linked
1068 to Hydrothermal Systems: TAIGA Concept. Springer, New York, pp. 337-359.
1069 Jamieson, J.W., Hannington, M.D., Tivey, M.K., Hansteen, T., Williamson, N.M.-B., Stewart, M., Fietzke, J.,
1070 Butterfield, D., Frische, M., Allen, L., Cousens, B., Langer, J., 2016. Precipitation and growth of barite within
1071 hydrothermal vent deposits from the Endeavour Segment, Juan de Fuca Ridge. Geochim. Cosmochim. Acta
1072 173, 64-85.
1073 Kamenov, G.D., Mueller, P., Perfit, M., 2004. Optimization of mixed Pb-Tl solutions for high precision isotopic
1074 analyses by MC-ICP-MS. J. Anal. At. Spectrom 19, 1262-1267.
1075 Kase, K., Yamamoto, M., Shibata, T., 1990. Copper-rich sulfide deposit near 23°N, Mid-Atlantic Ridge: chemical
1076 composition, mineral chemistry, and sulfur isotopes. In: Detrick, R., Honnorez, J., Bryan, W.B., Juteau, T., et
1077 al. (Eds.), Proc. ODP, Sci. Results, College Station, TX, 106/109, pp. 163-177.
1078 Kato, Y., Ohta, I., Tsunematsu, T., Watanabe, Y., Isozaki, Y., Maruyama, S., Imai, N., 1998. Rare earth element
1079 variations in mid-Archean banded iron formations: Implications for the chemistry of ocean and continent and
1080 plate tectonics. Geochim. Cosmochim. Acta 62, 3475-3497.
1081 Kato, Y., Nakao, K., Isozaki, Y., 2002. Geochemistry of Late Permian to Early Triassic pelagic cherts from
1082 southwest Japan: implications for an oceanic redox change. Chem. Geol. 182, 15-34.
1083 Kato, Y., Fujinaga, K., Suzuki, K., 2005. Major and trace element geochemistry and Os isotopic composition of
1084 metalliferous umbers from the Late Cretaceous Japanese accretionary complex. Geochem. Geophys. Geosyst.
1085 6, Q07004.
1086 Kawasumi, S., Chiba, H., Ishibashi, J., 2016. Sulfur systematics in the Izena Hole seafloor hydrothermal
1087 systems, Okinawa Trough: Stable isotope, mineralogy and redox equilibria. Japan Geoscience
1088 Union meeting 2016, May 22-26, Makuhari Messe.
1089 Kerridge, J.F., Haymon, R.M., Kastner, M., 1983. Sulfur isotope systematics at the 21°N site, East Pacific Rise.
1090 Earth Planet. Sci. Lett. 66, 91-100.
1091 Kim, J., Lee, I., Lee, K.-Y., 2004. S, Sr, and Pb isotopic systematic of hydrothermal chimney precipitates from the
1092 Eastern Manus Basin, western Pacific: Evaluation of magmatic contribution to hydrothermal system. J.
1093 Geophys. Res. 109, B12210, doi:10.1029/2003JB002912.
1094 Kim, J., Lee, K.-Y., Kim, J.-H., 2011. Metal-bearing molten sulfur collected from a submarine volcano: Implications
1095 for vapor transport of metals in seafloor hydrothermal systems. Geology 39, 351-354.
1096 Kimura, M., Kaneoka, I., Kato, Y., Yamamoto, S., Kushiro, I., Tokuyama, H., Kinoshita, H., Isezaki, N., Masaki, H.,
1097 Ishida, A., Uyeda, S., Hilde, T.W.C., 1986. Report on DELP 1984 Cruise in the Middle Okinawa Trough-5:
1098 topography and geology of the central grabens and their vicinity. Bull. Earth. Res. Inst. Univ. Tokyo 61, 269-
1099 310.
1100 Klevenz, V., Bach, W., Schmidt, K., Hentscher, M., Koschinsky, A., Petersen, S., 2011. Geochemistry of vent fluid
1101 particles formed during initial hydrothermal fluid–seawater mixing along the Mid-Atlantic Ridge. Geochem.
1102 Geophys. Geosyst. 12, Q0AE05.

1103 Klingelhoefer, F., Lee, C.-S., Lin, J.-Y., Sibuet, J.-C., 2009. Structure of the southernmost Okinawa Trough from
1104 reflection and wide-angle seismic data. Tectonophysics 446, 281-288.
1105 Klinkhammer, G.P., Elderfield, H., Edmond, J.M., Mitra, A., 1994. Geochemical implications of rare earth element
1106 patterns in hydrothermal fluids from mid-ocean ridges. Geochim. Cosmochim. Acta 58, 5105-5113.
1107 Knott, R., Fallick, A.E., Rickard, D., Bäcker, H., 1995. Mineralogy and sulphur isotope characteristics of a massive
1108 sulphide boulder, Galapagos Rift, 85°55´W. In: Parson, L.M., Walker, C.L., Dixon, D.R. (Eds.),
1109 Hydrothermal Vents and Processes. Geol. Soc. Spec. Pub. 87, 207-222.
1110 Konno, U., Tsunogai, U., Nakagawa, F., Nakaseama, M., Ishibashi, J.-I., Nunoura, T., Nakamura, K., 2006. Liquid
1111 CO_2 venting on the seafloor: Yonaguni Knoll IV hydrothermal system, Okinawa Trough. Geophys. Res. Lett.
1112 33, L16607.
1113 Koschinsky, A., Seifert, R., Halbach, P., Bau, M., Brasse, S., de Carvalho, L.M., Fonseca, N.M., 2002. Geochemistry
1114 of diffuse low-temperature hydrothermal fluids in the North Fiji basin. Geochim. Cosmochim. Acta 66, 1409-
1115 1427.
1116 Koski, R.A., Clague, D.A., Oudin, Ë., 1984. Mineralogy and chemistry of massive sulfide deposits from the Juan de
1117 Fuca Ridge. Geol. Soc. Am. Bull. 95, 930-945.
1118 Koski, R.A., Shanks, W.C. III, Bohrson, W.A., Oscarson, R.L., 1988. The composition of massive sulfide deposits
1119 from the sediment-covered floor of Escanaba Trough, Gorda Ridge: Implications for depositional processes.
1120 Can. Mineral. 26, 655-674.
1121 Kouketsu, Y., Mizukami, T., Mori, H., Endo, S., Aoya, M., Hara, H., Nakamura, D., Wallis, S., 2014. A new
1122 approach to develop the Raman carbonaceous material geothermometer for low-grade metamorphism using
1123 peak width. Island Arc 23, 33-50.
1124 Kusakabe, M., Mayeda, S., Nakamura, E., 1990. S, O and Sr isotope systematics of active vent materials from the
1125 Mariana backarc basin spreading axis at 18°N. Earth Planet. Sci. Lett. 100, 275-282.
1126 Kusakabe, M., Komoda, Y., Takano, B., Abiko, T., 2000. Sulfur isotopic effects in the disproportionation reaction of
1127 sulfur dioxide in hydrothermal fluids: implications for the $\delta^{34}S$ variations of dissolved bisulfate and elemental
1128 sulfur from active crater lakes. J. Volcanol. Geotherm. Res. 97, 287-307.
1129 Labidi, J., Cartigny, P., Birck, J.L., Assayag, N., Bourrand, J.J., 2012. Determination of multiple sulfur isotopes in
1130 glasses: A reappraisal of the MORB $\delta^{34}S$. Chem. Geol. 334, 189-198.
1131 Lovley, D.R., Phillips, E.J.P., Gorby, Y.A., Landa, E.R., 1991. Microbial reduction of uranium. Nature 350, 413-
1132 416.
1133 Lu, Y., Makishima, A., Nakamura, E., 2007. Coprecipitation of Ti, Mo, Sn and Sb with fluorides and application to
1134 determination of B, Ti, Zr, Nb, Mo, Sn, Sb, Hf and Ta by ICP-MS. Chem. Geol. 236, 13-26.
1135 Lüders, V., Pracejus, B., Halbach, P., 2001. Fluid inclusion and sulfur isotope studies in probable modern analogue
1136 Kuroko-type ores from the JADE hydrothermal field (Central Okinawa Trough, Japan). Chem. Geol. 173, 45-
1137 58.
1138 Ludford, E.M., Palmer, M.R., German, C.R., Klinkhammer, G.P., 1996. The geochemistry of Atlantic hydrothermal
1139 particles. Geophys. Res. Lett. 23, 3503-3506.

Ma, L., Xi, S., Zhang, X., Luan, Z., Du, Z., Li, L., Yan, J., 2021. Influence of vapor-phase fluids on the geochemical characterization of hydrothermal sulfides in the shimmering waters of the southern Okinawa Trough. Ore Geol. Rev. 139, 104496.

Makishima, A., Nakamura, E., 2006. Determination of major/minor and trace elements in silicate samples by ICP-QMS and ICP-SFMS applying isotope dilution-internal standardization (ID-IS) and multi-stage internal standardisation. Geostand. Geoanalytical Res. 30, 245-271.

Marchig, V., Puchelt, H., Rösch, H., Blum, N., 1990. Massive sulfides from ultra-fast spreading ridge, East Pacific Rise at 18-21°S: A geochemical stock report. Mar. Mining 9, 459-493.

Marumo, K., Urabe, T., Goto, A., Takano, Y., Nakaseama, M., 2008. Mineralogy and isotope geochemistry of active submarine hydrothermal field at Suiyo Seamount, Izu-Bonin Arc, West Pacific Ocean. Resource Geology 58, 220-248.

Matsumoto, T., Kinoshita, M., Nakamura, M., Sibuet, J.-C., Lee, C.-S., Hsu, S.-K., Oomori, T., Shinjo, R., Hashimoto, Y., Hosoya, S., Imamura, M., Ito, M., Tukuda, K., Yagi, H., Tatekawa, K., Kagaya, I., Hokakubo, S., Okada, T., Kimura, M., 2001. Volcanic and hydrothermal activities and possible "segmentation" of the axial rifting in the westernmost part of the Okinawa Trough – preliminary results from the YOKOSUKA/SHINKAI 6500 Lequios Cruise, JAMSTEC Journal of Deep-Sea Research 19, 95-107. (in Japanese with English abstract).

McDonough, W.F., Sun, S.-s., 1995. The composition of the Earth. Chem. Geol. 120, 223-253.

Melekestseva, I.Yu., 2010. Sulfur isotopic composition of massive sulfides from the Semenov hydrothermal cluster, 13°31´N, MAR. Minerals of the Ocean-5 and Deep-Sea Minerals and Mining-2 Joint International Conference, St. Petersburg, Russia, 28 June – 01 July 2010, Abstract Volume, pp. 70-73.

Michard, A., 1989. Rare earth element systematics in hydrothermal fluids. Geochim. Cosmochim. Acta 53, 745-750.

Michard, A., Albarède, F., 1985. Hydrothermal uranium uptake at ridge crests. Nature 317, 244-246.

Michard, A., Albarède, F., 1986. The REE content of some hydrothermal fluids. Chem. Geol. 55, 51-60.

Michard, G., Albarède, F., Michard, A., Minster, J.F., Charlou, J.L., 1983. Rare-earth elements and uranium in high-temperature solutions from East Pacific Rise hydrothermal vent field (13 °N). Nature 303, 795-797.

Michard, G., Albarède, F., Michard, A., Minster, J.-F., Charlou, J.-L., Tan, N., 1984. Chemistry of solutions from the 13°N East Pacific Rise hydrothermal site. Earth Planet. Sci. Lett. 67, 297-307.

Mills, R.A., Thomson, J., Elderfield, H., Hinton, R.W., Hyslop, E., 1994. Uranium enrichment in metalliferous sediments from the Mid-Atlantic Ridge. Earth Planet. Sci. Lett. 124, 35-47.

Minami, T., Konagaya, W., Zheng, L., Takano, S., Sasaki, M., Murata, R., Nakaguchi, Y., Sohrin, Y., 2015. An off-line automated preconcentration system with ethylenediaminetriacetate chelating resin for the determination of trace metals in seawater by high-resolution inductively coupled plasma mass spectrometry. Anal. Chim. Acta 854, 183-190.

Nagumo, S., Kinoshita, H., Kasahara, J., Ouchi, T., Tokuyama, H., Asanuma, T., Koresawa, S., Akiyoshi, H., 1986. Report on DELP 1984 cruises in the middle Okinawa Trough part 2: seismic structural studies. Bull. ERI Univ. Tokyo 61, 167-202.

Nakashima, K., Sakai, H., Yoshida, H., Chiba, H., Tanaka, Y., Gamo, T., Ishibashi, J.-I., Tsunogai, U., 1995. Hydrothermal mineralization in the Mid-Okinawa Trough. In: Sakai, H., Nozaki, Y. (Eds), Biogeochemical Processes and Ocean Flux in the Western Pacific. Terra Scientific Publishing Company, Tokyo, pp. 487-508.

Nedachi, M., Ueno, H., Oki, K., Shiga, Y., Hayasaka, S., Ossaka, J., Nogami, K., Ito, N., Hashimoto, J., 1991. Sulfide veinlets and the surrounding marine sediments in the fumarole area in the Wakamiko Caldera, northern Kagoshima Bay. JAMSTEC Journal of Deep-Sea Research 7, 235-243.

Nishio, R., Chiba, H., 2012. Mineralogical and sulfur stable isotopic study of mineralization at the No.4 Yonaguni Knoll seafloor hydrothermal system, Okinawa Trough. Annual Meeting of the Geochemical Society of Japan, Abstracts, Geochemical Society of Japan, 59.

Nozaki, Y., Alibo, D.S., Amakawa, H., Gamo, T., Hasumoto, H., 1999. Dissolved rare earth elements and hydrography in the Sulu Sea. Geochim. Cosmochim. Acta 63, 2171-2181.

Nozaki, T., Ishibashi, J.-I., Shimada, K., Nagase, T., Takaya, Y., Kato, Y., Kawagucci, S., Watsuji, T., Shibuya, T., Yamada, R., Saruhashi, T., Kyo, M., Takai, K., 2016. Rapid growth of mineral deposits at artificial seafloor hydrothermal vents. Scientific Reports 6, 22163.

Ohmoto, H., Rye, R.O., 1979. Isotopes of sulfur and carbon. In: Barnes, H.L. (Ed.), Geochemistry of Hydrothermal Ore Deposits, Wiley, New York, pp. 509-567.

Okamoto, K., Ishibashi, J.-I., Motomura, Y., Yamanaka, T., Fujikura, K., 2002. Mineralogical studies of hydrothermal deposits collected from the Daiyon-Yonaguni Knoll and the Hatoma Knoll in the Okinawa Trough. JAMSTEC Journal of Deep-Sea Research 21, 75-81. (in Japanese with English abstract).

Ono, S., Shanks III, W.C., Rouxel, O.J., Rumble, D., 2007. S-33 constraints on the seawater sulfate contribution in modern seafloor hydrothermal vent sulfides. Geochim. Cosmochim. Acta 71, 1170-1182.

Oshida, A., Tamaki, K., Kimura, M., 1992. Origin of the magnetic anomalies in the southern Okinawa Trough. J. Geomagn. Geoelectr. 44, 345-359.

Oudin, Ë., 1983. Hydrothermal sulfide deposits of the East Pacific Rise (21° N). Part I: Descriptive mineralogy. Mar. Mining 4, 39-72.

Paris, G., Sessions, A.L., Subhas, A.V., Adkins, J.F., 2013. MC-ICP-MS measurement of $\delta^{34}S$ and $\Delta^{33}S$ in small amounts of dissolved sulfate. Chem. Geol. 345, 50-61.

Peter, J.M., Shanks, W.C. III, 1992. Sulfur, carbon, and oxygen isotope variations in submarine hydrothermal deposits of Guaymas Basin, Gulf of California, USA. Geochim. Cosmochim. Acta 56, 2025-2040.

Peters, C., Strauss, H., Haase, K., Bach, W., de Ronde, C.E.J., Kleint, C., Stucker, V., Diehl, A., 2021. SO_2 disproportionation impacting hydrothermal sulfur cycling: Insights from multiple sulfur isotopes for hydrothermal fluids from the Tonga-Kermadec intraoceanic arc and the NE Lau Basin. Chem. Geol. 586, 120586.

Peters, M., Strauss, H., Farquhar, J., Ockert, C., Eickmann, B., Jost, C.L., 2010. Sulfur cycling at the Mid-Atlantic Ridge: A multiple sulfur isotope approach. Chem. Geol. 269, 180-196.

Peters, M., Strauss, H., Petersen, S., Kummer, N.-A., Thomazo, C., 2011. Hydrothermalism in the Tyrrhenian Sea: Inorganic and microbial sulfur cycling as revealed by geochemical and multiple sulfur isotope data. Chem. Geol. 280, 217-231.

Petersen, S., 1992. Mineralogie und Geochemie goldführender Massivsulfide des Lau Back-Arc (Südwest-Pazifik). M.Sc. thesis, Aachen University of Technology, Aachen, Germany, 92 pp.

Petersen, S., Herzig, P.M., Hannington, M.D., Jonasson, I.R., Arribas, JR. A., 2002. Submarine gold mineralization near Lihir Island, New Ireland fore-arc, Papua New Guinea. Econ. Geol. 97, 1795-1813.

Petersen, S., Monecke, T., Westhues, A., Hannington, M.D., Gemmell, J.B., Sharpe, R., Peters, M., Strauss, H., Lackschewitz, K., Augustin, N., Gibson, H., Kleeberg, R., 2014. Drilling shallow-water massive sulfides at the Palinuro Volcanic Complex, Aeolian Island Arc, Italy. Econ. Geol. 109, 2129-2158.

Pokrovski, G.S., Escoda, C., Blanchard, M., Testemale, D., Hazemann, J.-L., Gouy, S., Kokh, M.A., Boiron, M.-C., de Parseval, F., Aigouy, T., Menjot, L., de Parseval, P., Proux, O., Rovezzi, M., Béziat, D., Salvi, S., Kouzmanov, K., Bartsch, T., Pöttgen, R., Doert, T., 2021. An arsenic-driven pump for invisible gold in hydrothermal systems. Geochem. Persp. Let. 17, 39-44.

Price, R.E., Planer-Friedrich, B., Savov, I.P., Pichler, T., 2009. Elevated concentrations of arsenic, predominance of thioarsenates, and orpiment precipitation on the seafloor at the marine shallow-water hydrothermal system off Milos Island, Greece. American Geophysical Union, Fall Meeting, abstract #B23E-0416.

Qu, Y., Engdahl, A., Zhu, S., Vajda, V., McLoughlin, N., 2015. Ultrastructural heterogeneity of carbonaceous material in ancient cherts: Investigating biosignature origin and preservation. Astrobiology 15, 825-842.

Rouxel, O., Fouquet, Y., Ludden, J.N., 2004. Copper isotope systematics of the Lucky Strike, Rainbow, and Logatchev sea-floor hydrothermal fields on the Mid-Atlantic Ridge. Econ. Geol. 99, 585-600.

Rytuba, J.J., 1984. Arsenic minerals as indicators of conditions of gold deposition in Carlin-type gold deposits. J. Geochem. Explor. 25, 237-238.

Seyfried, W.E., Ding, K., 1993. The effect of redox on the relative solubilities of copper and iron in Cl-bearing aqueous fluids at elevated temperatures and pressures: An experimental study with application to subseafloor hydrothermal systems. Geochim. Cosmochim. Acta 57, 1905-1917.

Shanks, W.C., 2001. Stable isotopes in seafloor hydrothermal systems: Vent fluids, hydrothermal deposits, hydrothermal alteration, and microbial processes. In: Valley, J.W., Cole, D.R. (Eds), Stable Isotope Geochemistry. Rev. Mineral. Geochem. 43, pp. 469-525.

Shanks, W.C. III, Bischoff, J.L., Rosenbauer, R.J., 1981. Seawater sulfate reduction and sulfur isotope fractionation in basaltic systems: Interaction of seawater with fayalite and magnetite at 200-350°C. Geochim. Cosmochim. Acta 45, 1977-1995.

Shanks, W.C. III, Koski, R.A., Woodruff, L.G., 1984. Mineralogy and stable isotope systematics of sulfide deposits from the Juan de Fuca Ridge. EOS 65, 1113.

Shanks, W.C. III, Seyfried, W.E. Jr., 1987. Stable isotope studies of vent fluids and chimney minerals, southern Juan de Fuca Ridge. Sodium metasomatism and seawater sulfate reduction. J. Geophys. Res. 92, 11387-11399.

1248 Shikazono, N., 1994. Precipitation mechanisms of barite in sulfate-sulfide deposits in back-arc basins. Geochim.
1249 Cosmochim. Acta 58, 2203-2213.
1250 Shikazono, N., Kusakabe, M., 1999. Mineralogical characteristics and formation mechanism of sulfate-sulfide
1251 chimneys from Kuroko area, Mariana Trough and mid-ocean ridges. Resour. Geol., Spec. Issue, 20, 1-12.
1252 Shikazono, N., Kawabe, H., Ogawa, Y., 2012. Interpretation of mineral zoning in submarine hydrothermal ore
1253 deposits in terms of coupled fluid flow-precipitation kinetics model. Resour. Geol. 62, 352-368.
1254 Shinjo, R., Chung, S.-L., Kato, Y., Kimura, M., 1999. Geochemical and Sr-Nd isotopic characteristics of volcanic
1255 rocks from the Okinawa Trough and Ryukyu Arc: Implications for the evolution of a young intracontinental
1256 back arc basin. J. Geophys. Res. 104, 10591-10608.
1257 Shu, Y., Nielsen, S.G., Zeng, Z., Shinjo, R., Blusztajn, J., Wang, X., Chen, S., 2017. Tracing subducted sediment
1258 inputs to the Ryukyu arc-Okinawa Trough system: Evidence from thallium isotopes. Geochim. Cosmochim.
1259 Acta 217, 462-491.
1260 Sibuet, J.-C., Letouzey, J., Barbier, F., Charvet, J., Foucher, J.-P., Hilde, T., Kimura, M., Ling-Yun, C., Marsset, B.,
1261 Muller, C., Stephan, J.-F., 1987. Back arc extension in the Okinawa Trough. J. Geophys. Res. 92, 14041-
1262 14063.
1263 Skirrow, R., Coleman, M.L., 1982. Origin of sulfur and geothermometry of hydrothermal sulfides from the
1264 Galapagos Rift, 86°N. Nature 299, 142-144.
1265 Sohrin, Y., Urushihara, S., Nakatsuka, S., Kono, T., Higo, E., Minami, T., Norisuye, K., Umetani, S., 2008.
1266 Multielemental determination of GEOTRACES key trace metals in seawater by ICPMS after
1267 preconcentration using an ethylenediaminetriacetic acid chelating resin. Anal. Chem. 80, 6267-6273.
1268 Spiess, F.N., Macdonald, K.C., Atwater, T., Ballard, R., Carranza, A., Cordoba, D., Cox, C., Diaz Garcia, V.M.,
1269 Francheteau, J., Guerrero, J., Hawkins, J., Haymon, R., Hessler, R., Juteau, T., Kastner, M., Larson, R.,
1270 Luyendyk, B., Macdougall, J.D., Miller, S., Normark, W., Orcutt, J., Rangin, C., 1980. East Pacific Rise: hot
1271 springs and geophysical experiments. Science 207, 1421-1433.
1272 Stuart, F.M., Turner, G., Duckworth, R.C., Fallick, A.E., 1994. Helium isotopes as tracers of trapped hydrothermal
1273 fluids in ocean-floor sulfides. Geology 22, 823-826.
1274 Stuart, F.M., Harrop, P.J., Knott, R., Fallick, A.E., Turner, G., Fouquet, Y., Rickard, D., 1995. Noble gas isotopes in
1275 25 000 years of hydrothermal fluids from 13°N on the East Pacific Rise. In: Parson, L.M., Walker, C.L.,
1276 Dixon, D.R. (Eds.), Hydrothermal Vents and Processes. Geol. Soc. Spec. Publ. 87, 133-143.
1277 Styrt, M.M., Brackmann, A.J., Holland, H.D., Clark, B.C., Pisutha-Arnold, V., Eldridge, C.S., Ohmoto, H., 1981.
1278 The mineralogy and the isotopic composition of sulfur in hydrothermal sulfide/sulfate deposits on the East
1279 Pacific Rise, 21°N latitude. Earth Planet. Sci. Lett. 53, 382-390.
1280 Suzuki, R., Chiba, H., Ishibashi, J., Gena, K., 2005. Mineralogy and geochemistry of submarine hydrothermal
1281 deposits at the Dai-yon Yonaguni Knoll. Society of Resource Geology, 55th Annual Conference, Abstract
1282 with Program, P26.

Suzuki, R., Ishibashi, J., Nakaseama, M., Konno, U., Tsunogai, U., Gena, K., Chiba, H., 2008. Diverse range of mineralization induced by phase separation of hydrothermal fluid: Case study of the Yonaguni Knoll IV hydrothermal field in the Okinawa Trough back-arc basin. Resour. Geol. 58, 267-288.

Takaya, Y., Hiraide, T., Fujinaga, K., Nakamura, K., Kato, Y., 2014. A study on the recovery method of rare-earth elements from REY-rich mud toward the development and the utilization of REY-rich mud. J. MMIJ 130, 104-114 (in Japanese with English abstract).

Thompson, G., Mottl, M.J., Rona, P.A., 1985. Morphology, mineralogy and chemistry of hydrothermal deposits from the TAG area, 26°N Mid-Atlantic Ridge. Chem. Geol. 49, 243-257.

Tokunaga, M., Honma, H., 1974. Fluid inclusions in the minerals from some Kuroko deposits. Soc. Mining Geol. Jpn., Spec. Issue, 6, 385-388.

Trefry, J.H., Metz, S., 1989. Role of hydrothermal precipitates in the geochemical cycling of vanadium. Nature 342, 531-533.

Tsunogai, U., Toki, T., Nakayama, N., Gamo, T., Kato, H., Kaneko, S., 2003. WHATS: a new multi-bottle gas-tight sampler for seafloor vent fluids. Chikyukagaku (Geochemistry) 37, 101-109 (in Japanese).

Ueno, H., Hamasaki, H., Murakawa, Y., Kitazono, S., Takeda, T., 2003. Ore and gangue minerals of sulfide chimneys from the North Knoll, Iheya Ridge, Okinawa Trough, Japan. JAMSTEC J. Deep Sea Res. 22, 49-62.

Von Damm, K.L., 1990. Seafloor hydrothermal activity: Black smoker chemistry and chimneys. Annu. Rev. Earth Planet. Sci. 18, 173-204.

Von Damm, K.L., Bischoff, J.L., 1987. Chemistry of hydrothermal solutions from the Southern Juan de Fuca Ridge. J. Geophys. Res. 92, 11334-11346.

Von Damm, K.L., Lilley, M.D., 2004. Diffuse flow hydrothermal fluids from 9°50'N East Pacific Rise: Origin, evolution and biogeochemical controls. In: Wilcock, W.S.D., DeLong, E.F., Kelley, D.S., Baross, J.A., Cary, S.C. (Eds), The Subseafloor Biosphere at Mid-Ocean Ridges. Geophysical Monograph Series 144, American Geophysical Union, Washington, DC. pp. 245-268.

Von Damm, K.L., Edmond, J.M., Grant, B., Measures, C.I., Walden, B., Weiss, R.F., 1985a. Chemistry of submarine hydrothermal solutions at 21°N, East Pacific Rise. Geochim. Cosmochim. Acta 49, 2197-2220.

Von Damm, K.L., Edmond, J.M., Measures, C.I., Grant, B., 1985b. Chemistry of submarine hydrothermal solutions at Guaymas Basin, Gulf of California. Geochim. Cosmochim. Acta 49, 2221-2237.

Von Damm, K.L., Parker, C.M., Zierenberg, R.A., Lilley, M.D., Olson, E.J., Clague, D.A., McClain, J.S., 2005. The Escanaba Trough, Gorda Ridge hydrothermal system: Temporal stability and subseafloor complexity. Geochim. Cosmochim. Acta 69, 21, 4971-4984.

Webber, A.P., Roberts, S., Murton, B.J., Hodgkinson, M.R.S., 2015. Geology, sulfide geochemistry and supercritical venting at the Beebe Hydrothermal Vent Field, Cayman Trough. Geochem. Geophys. Geosyst. 16, 2661-2678.

Woodruff, L.G., Shanks, W.C., III., 1988. Sulfur isotope study of chimney minerals and vent fluids from 21°N, East Pacific Rise: Hydrothermal sulfur sources and disequilibrium sulfate reduction. J. Geophys. Res. 93, 4562-4572.

Yamanaka, T., Maeto, K., Akashi, H., Ishibashi, J.-I., Miyoshi, Y., Okamura, K., Noguchi, T., Kuwahara, Y., Toki, T., Tsunogai, U., Ura, T., Nakatani, T., Maki, T., Kubokawa, K., Chiba, H., 2013. Shallow submarine hydrothermal activity with significant contribution of magmatic water producing talc chimneys in the Wakamiko Crater of Kagoshima Bay, southern Kyushu, Japan. J. Volcanol. Geotherm. Res. 258, 74-84.

Yang, B., Liu, J., Shi, X., Zhang, H., Wang, X., Wu, Y., Fang, X., 2020. Mineralogy and sulfur isotope characteristics of metalliferous sediments from the Tangyin hydrothermal field in the southern Okinawa Trough. Ore Geol. Rev. 120, 103464.

Yasukawa, K., Liu, H., Fujinaga, K., Machida, S., Haraguchi, S., Ishii, T., Nakamura, K., Kato, Y., 2014. Geochemistry and mineralogy of REY-rich mud in the eastern Indian Ocean. J. Asian Earth Sci. 93, 25-36.

Yasukawa, K., Kino, S., Azami, K., Tanaka, E., Mimura, K., Ohta, J., Fujinaga, K., Nakamura, K., Kato, Y., 2020. Geochemical features of Fe-Mn micronodules in deep-sea sediments of the western North Pacific Ocean: Potential for co-product metal extraction from REY-rich mud. Ore Geol. Rev. 127, 103805.

Zeng, Z., Chen, Z., Qi, H., 2022. Two processes of anglesite formation and a model of secondary supergene enrichment of Bi and Ag in seafloor hydrothermal sulfide deposits. J. Mar. Sci. Eng. 10, 35.

Zierenberg, R.A., Shanks, W.C., III., Bischoff, J.L., 1984. Massive sulfide deposits at 21°N, East Pacific Rise: chemical composition, stable isotopes, and phase equilibria. Geol. Soc. Am. Bull. 95, 922-929.

Figure captions

Fig. 1. (A) Map of Ryukyu Trench-Arc system and Okinawa Trough with location of Daiyon-Yonaguni Knoll hydrothermal field (red solid square); (B) Detail map of the Daiyon-Yonaguni Knoll hydrothermal field with location of sample site (red solid dot).

Fig. 2. Studied samples from the Daiyon-Yonaguni Knoll hydrothermal field: (A) active hydrothermal chimney, sample 2K1271 L1 lower outer; (B) active hydrothermal chimney flange, sample 2K1271 L1 flange, outer top; (C) active hydrothermal chimney flange, sample 2K1271 L1 flange, center upper; (D) active hydrothermal chimney flange, sample 2K1271 L1 flange, outer bottom; (E) massive sulfide, sample 2K1267 L1; (F) massive sulfide, sample 2K1267 L2.

Fig. 3. Photomicrographs of stibnite, barite, and native sulfur from the Daiyon-Yonaguni Knoll hydrothermal deposits: (A) needle-like crystals of stibnite (Stb) (stereomicroscope, sample 2K1271 L1 flange, center upper); (B) thin, needle-like, radial crystals of stibnite (Stb) over prismatic, transparent crystals of barite (Bt) (thin polished section, optical microscope, transmitted plain polarized light, sample 2K1271 L1 flange, outer top); (C) rosettes of stibnite (Stb) radial crystals (SEM, SEI, sample 2K1271 L1 flange, outer top); (D) match box-like crystals of barite (Bt) (SEM, SEI, sample 2K1267 L1); (E) radial barite (Bt) crystals (dendritic barite) among coated by amorphous silica pyrite (Py) (SEM, SEI, sample 2K1267 L2); (F) rhombic crystals of native sulfur (SEM, SEI, sample 2K1267 L1).

Fig. 4. X-ray maps and BSE image of stibnite (Stb) within barite (Bt) matrix in the Daiyon-Yonaguni Knoll hydrothermal deposit (sample 2K1271 L1 flange, outer top): (A) X-ray scan in Sb *Lα*; (B) X-ray scan in As *Lα*; (C) X-ray scan in Ba *Lα*; (D) X-ray scan in S *Kα*; (E) BSE image. Color scales (right-hand side), elemental concentrations.

Fig. 5. Photomicrographs of orpiment from the Daiyon-Yonaguni Knoll hydrothermal deposits: (A) fillaments of orpiment (orange) (stereomicroscope, sample 2K1271 L1 flange, outer top); (B) colloform orpiment (red) (stereomicroscope, sample 2K1267 L1); (C) fillaments of orpiment among thin tabular crystals of barite (Bt) (SEM, SEI, sample 2K1267 L1); (D) colloform orpiment (SEM, SEI, sample 2K1267 L1); (E) cross-section of the filament-like orpiment shown at (C), note the concentric internal structure of the filaments (SEM, SEI, sample 2K1267 L1); (F) bunches of reddish-white barite (Bt) crystals partly covered by fine yellow orpiment (Op) crystals (thin polished section, optical microscope, reflected plain polarized light, sample 2K1271 L1 flange, outer top).

Fig. 6. X-ray maps and BSE image of orpiment (Op) over barite (Bt) crystals in the Daiyon-Yonaguni Knoll hydrothermal deposit (sample 2K1271 L1 flange, outer top): (A) X-ray scan in As *Lα*; (B) X-ray scan in Sb *Lα*; (C) X-ray scan in Ba *Lα*; (D) X-ray scan in S *Kα*; (E) BSE image. Color scales (right-hand side), elemental concentrations.

Fig. 7. CI chondrite-normalized (McDonough and Sun, 1995) REE distribution patterns of the studied hydrothermal deposits (A) and vent fluids (B) from the Daiyon-Yonaguni Knoll hydrothermal field (Okinawa Trough). NPDW = North Pacific Deep Water (Alibo and Nozaki, 1999).

Fig. 8. Sulfur-isotope composition (range) of selected hydrothermal deposits from mid-ocean ridges [unsedimented (mafic- and ultramafic-hosted) and sedimented], volcanic arcs and back-arc basins compared to those of studied stibnite-orpiment-containing deposits and vent fluids (sulfate S) from the Daiyon-Yonaguni Knoll hydrothermal field, Okinawa Trough. References: terrestrial mantle (Labidi et al., 2012), seawater (Paris et al., 2013), Galapagos Rift (Skirrow and Coleman, 1982; Knott et al., 1995), 21°N EPR (Hekinian et al., 1980; Arnold and Sheppard, 1981; Styrt et al., 1981; Kerridge et al., 1983; Zierenberg et al., 1984; Woodruff and Shanks, 1988; Stuart et al., 1994), 11-13°N EPR (Bluth and Ohmoto, 1988; Stuart et al., 1995; Fouquet et al., 1996; Ono et al., 2007), 9-10°N EPR (Ono et al., 2007), 18-21°S EPR (Marchig et al., 1990; Ono et al., 2007), Lucky Strike (Rouxel et al., 2004; Ono et al., 2007), Broken Spur (Duckworth et al., 1995; Butler et al., 1998), TAG (Stuart et al., 1994; Gemmell and Sharpe, 1998; Herzig et al., 1998; Shanks, 2001), Snakepit (Kase et al., 1990; Stuart et al., 1994), Southern MAR (Peters et al., 2010), Rainbow (Rouxel et al., 2004), Logatchev (Rouxel et al., 2004; Peters et al., 2010), Semenov (Melekestseva, 2010), Red Sea (Shanks, 2001), Juan de Fuca (Shanks et al., 1984; Shanks and Seyfried, 1987; Hannington and Scott, 1988; Stuart et al., 1994), Escanaba Trough (Shanks, 2001), Guaymas Basin (Shanks, 2001), Okinawa Trough (Lüders et al., 2001; Ueno et al., 2003; Nishio and Chiba, 2012; Kawasumi et al., 2016; Yang et al., 2020), Izu-Bonin Arc (Alt et al., 1998), Mariana Trough (Kusakabe et al., 1990), Manus Basin (Kim et al., 2004), Lau Basin (Kim et al., 2011), Kermadec Arc (de Ronde et al., 2005; 2011), Aeolian Arc (Peters et al., 2011; Petersen et al., 2014).

Fig. 9. Pb isotope data for the studied Daiyon-Yonaguni Knoll (DYK) hydrothermal (hydroT) deposits compared to DYK hydrothermal Pb minerals (galena and anglesite) (Zeng et al., 2022), southern Okinawa Trough (SOT) sulfides (Ma et al., 2021), and southern (S) Okinawa and Ryukyu sediments and lavas (Bentahila et al., 2008; Shu et al., 2017; Chen et al., 2019). Dotted

line is the Northern Hemisphere Reference Line (NHRL), after Hart (1984). Note that the studied DYK hydrothermal deposits form a trend from the DYK Pb hydrothermal minerals to the regional lavas and one sample extending to much lower $^{207}Pb/^{204}Pb$ and $^{208}Pb/^{204}Pb$ toward the NHRL, for more discussion see the text.

Fig. 10. (A) Photomicrograph (stereomicroscope) of orpiment from the Daiyon-Yonaguni Knoll hydrothermal deposits (sample 2K1267 L1) with positions (B, C) of the sub-samples analyzed by Raman spectroscopy (see Raman spectra at panels B and C); (B) Raman spectrum of light orange filamentous orpiment containing carbonaceous matter with characteristic D and G bands in the first-order region, and bands in the second-order region; (C) Raman spectrum of dark red colloform orpiment surrounding the filamentous orpiment. Raman intensity in arbitrary units (a.u.).

Fig. 11. ESEM image (A) and EDS spectra (B: spectrum 136) and (C: spectrum 137) showing the distribution of carbon as indicative of carbonaceous matter associated with the orpiment filaments (note, the major elements are As and S). ~~Carbon concentrations shown at the upper right corners of (B) and (C).~~

Fig. 12. Stability phase diagrams for the chemical species (dissolved and solid) in the three selected vent fluids from the Daiyon-Yonaguni Knoll hydrothermal field: (A), (B) and (C) - Eh-$\log_{10}a$ diagrams calculated for $Sb_2S_4^{2-}$; (D), (E) and (F) - Eh-$\log_{10}a$ diagrams calculated for $H_2AsO_4^-$; (G), (H) and (I) - Eh-$\log_{10}a$ diagrams calculated for Ba^{2+}.

Mineralogy, geochemistry and microbiology insights into precipitation of stibnite and orpiment at the Daiyon-Yonaguni Knoll (Okinawa Trough) hydrothermal barite deposits

V.M. Dekov[a,*], K. Kyono[a], K. Yasukawa[b,c], B. Guéguen[d,e], M. Ivarsson[f], G.D. Kamenov[g], T. Yamanaka[a], D. Asael[h], M. Ishida[c], L.L. Cavalcante[f], Y. Kato[b,c,i,j], T. Toki[k], J.-I. Ishibashi[l]

[a] *Department of Ocean Sciences, Tokyo University of Marine Science and Technology, 4-5-7 Konan, Minato-ku, Tokyo 108-8477, Japan*

[b] *Frontier Research Center for Energy and Resources, School of Engineering, The University of Tokyo, Bunkyo-ku, Tokyo 113-8656, Japan*

[c] *Department of Systems Innovation, School of Engineering, The University of Tokyo, 7-3-1 Hongo, Bunkyo-ku, Tokyo 113-8656, Japan*

[d] *CNRS, Univ Brest, UMR 6538 Laboratoire Géosciences Océan, F-29280 Plouzané, France*

[e] *CNRS, Univ Brest, UMS 3113, F-29280 Plouzané, France*

[f] *Department of Palaeobiology, Swedish Museum of Natural History, SE 104 05 Stockholm, Sweden*

[g] *Department of Geological Sciences, University of Florida, 241 Williamson Hall, Gainesville, FL 32611, USA*

[h] *Department of Geology and Geophysics, Yale University, New Haven, CT 06520, USA*

[i] *Ocean Resources Research Center for Next Generation, Chiba Institute of Technology, 2-17-1 Tsudanuma, Narashino, Chiba 275-0016, Japan*

[*] Corresponding author.

E-mail address: vdekov0@kaiyodai.ac.jp (V.M. Dekov)

[j] *Submarine Resources Research Center, Research Institute for Marine Resources Utilization, Japan Agency for Marine-Earth Science and Technology (JAMSTEC), 2-15 Natsushima-cho, Yokosuka, Kanagawa 237-0061, Japan*

[k] *Department of Chemistry, Biology and Marine Science, Faculty of Science, University of the Ryukyus, 1 Senbaru, Nishihara, Okinawa 903-0213, Japan*

[l] *Kobe Ocean-Bottom Exploration Center, Kobe University, 5-1-1 Fukaeminami-machi, Higashinada-ku, Kobe 658-0022, Japan*

A B S T R A C T

Samples of active chimneys, chimney flanges and massive sulfides from the Daiyon-Yonaguni Knoll hydrothermal field are composed of major barite and minor stibnite and orpiment. Barite is inferred to precipitate from focused-discharge fluids composed of >40% hydrothermal end-member fluid at T = 100-240°C, whereas the stibnite and orpiment are later and lower temperature precipitates. The hydrothermal fluids from this field were subject of sub-seafloor boiling and phase separation and, consequently, are brine-rich depleted in volatile and enriched in non-volatile elements. Boiling and phase separation exerted major control on the rare earth elements (REE) partitioning in the vent fluids: high-chlorinity high-temperature fluids were enriched in light REE and low-chlorinity low-temperature fluids were enriched in heavy REE. Y/Ho molar ratio and Ce anomaly of the vent fluids suggest that the seawater has not completely reacted with the basement rocks and has not equilibrated with them. The trace element concentrations in the hydrothermal deposits suggest a complex interplay among hydrothermal, hydrogenetic and microbial processes. Sulfur isotope composition of the sulfides suggests that the sulfide S is a mixture of both basement rock and seawater S with a higher proportion of the basement rock S. The sulfate dissolved in the fluids was subjected to reduction during a slow mixing of hydrothermal fluid and seawater within the chimney walls of the Tiger and Abyss vents and this resulted in a heavy S-isotope composition of the vent fluid sulfate. Lead isotope composition of the hydrothermal deposits indicates mixing relationships suggesting that Pb and potentially other metals with similar geochemical behavior were derived from two or three

sources. The Pb isotopes in the hydrothermal deposits imply that an enriched source, either sediments or extended continental lithosphere, and a depleted source, potentially back-arc mafic volcanics, are present in the area of Daiyon-Yonaguni Knoll. Filamentous orpiment found in the deposits is supposed to be either heavily mineralized fungal hyphae or pure abiogenic biomorphs. Presence of carbonaceous matter on and around the orpiment filaments suggests for microbial activity during filament formation. The filaments experienced temperature of 209.1±37.1°C which falls within the temperature range of the Daiyon-Yonaguni Knoll vent fluids. Stability phase diagrams modeling reveals that the stability of stibnite does not depend on the vent fluid chlorinity, but depends on the vent fluid temperature: the area of stibnite stability increases with decreasing vent fluid temperature and results in stibnite precipitation at low $\log_{10}a$ of $Sb_2S_4^{2-}$ and less reduced environment (Eh still <0). Orpiment is stable in a wide range of $\log_{10}a$ of $H_2AsO_4^-$, in reduced conditions and at high S activity. Barite is stable in wide range of $\log_{10}a$ of Ba^{2+} and precipitates in slightly reduced to slightly oxic conditions.

Keywords: Daiyon-Yonaguni Knoll hydrothermal field; geomicrobiology; Okinawa Trough; orpiment; seafloor hydrothermal activity; stibnite

1. Introduction

Substantial effort has been made to elucidate the mineralogy of seafloor hydrothermal deposits since their discovery (Corliss et al., 1979; Spiess et al., 1980) and nowadays we can dare to think that we have extensive knowledge on it (e.g., Haymon and Kastner, 1981; Oudin, 1983; Koski et al., 1984; Fouquet et al., 1988; Koski et al., 1988; Hannington et al., 1991; Fouquet et al., 1993a, b; Iizasa et al., 1999; Fouquet et al., 2010; Webber et al., 2015). Although the studies of the seafloor hydrothermal deposits recognize distinct mineralogical differences among the deposits formed at mid-ocean ridges (MOR) (sedimented and unsedimented), volcanic arcs and back-arc spreading centers, they show that most seafloor hydrothermal deposits are composed of relatively simple mineral assemblages. Metal (Fe, Cu, Zn, Pb) sulfides, and Ca- and Ba-sulfates are the main constituents of these deposits, whereas silicates, oxyhydroxides, carbonates and

sulfosalts are minor minerals (Herzig and Hannington, 1995). Sulfides of metalloids (B, Si, Ge, As, Sb and Te) are rare. Therefore, seafloor hydrothermal deposits containing metalloid sulfides attract particular scientific interest because these minerals imply for uncommon conditions of precipitation (T, P, pH, Eh, ion activity and speciation).

Stibnite (Sb_2S_3) and orpiment (As_2S_3) are accessory minerals in the seafloor hydrothermal deposits according to published observations. Stibnite is mainly reported at volcanic arc [Palinuro Seamount, Aeolian Arc (Dekov and Savelli, 2004); Wakamiko Crater, Kagoshima Bay, Kyushu Island (Nedachi et al., 1991; Yamanaka et al., 2013)], back-arc [Minami-Ensei Knoll (Nakashima et al., 1995), JADE (Halbach et al., 1993; Nakashima et al., 1995) and Hatoma Knoll (Okamoto et al., 2002) at Okinawa Trough] and fore-arc [Conical Seamount, New Ireland fore-arc (Petersen et al., 2002)] settings. There is only one report on stibnite occurrence at MOR setting: Ashadze-1 hydrothermal field at the Mid-Atlantic Ridge (Firstova et al., 2016). Stibnite was also observed to form in the artificially produced hydrothermal chimneys at the Iheya-North field, Okinawa Trough (Nozaki et al., 2016). Orpiment has also been reported at volcanic arc [Suiyo Seamount, Izu-Bonin Arc (Marumo et al., 2008); off-shore Milos Island, Aegean Arc (Price et al., 2009)], back-arc [Lau back-arc basin (Petersen, 1992); JADE field, Okinawa Trough (Halbach et al., 1993; Dekov et al., 2013); Kaia Natai Seamount, Manus back-arc basin (Dekov et al., 2013)] and fore-arc [Conical Seamount, New Ireland fore-arc (Petersen et al., 2002; Herzig et al., 2003; Dekov et al., 2013)] settings only.

In 2000 during the YK00-06 *Yokosuka-Shinkai 6500* research cruise in the southern Okinawa Trough a new hydrothermal system was discovered and named Daiyon-Yonaguni Knoll (Matsumoto et al., 2001; Hsu et al., 2003). Along with the common barite, wurtzite, galena, tetrahedrite, chalcopyrite, pyrite and native sulfur, minor stibnite and orpiment were detected in the Daiyon-Yonaguni Knoll hydrothermal deposit (Okamoto et al., 2002; Suzuki et al., 2005; 2008).

Motivated by the scarce knowledge on the stibnite and orpiment precipitation at seafloor hydrothermal conditions, we investigated the stibnite-orpiment containing barite deposits and hydrothermal fluids from the Daiyon-Yonaguni Knoll hydrothermal site and report the results of our study in this contribution.

2. Geologic setting

The Okinawa Trough is an intra-continental back-arc basin extending behind the Ryukyu Trench-Arc system (Fig. 1 A). The rifting of this trough located at the eastern margin of the Eurasian tectonic plate was discussed in several works (e.g., Kimura et al., 1986; Glasby and Notsu, 2003; Ishibashi et al., 2015). The lithosphere beneath the Okinawa Trough is thinned continental lithosphere with a minimum thickness of ~8 km (Nagumo et al., 1986; Hirata et al., 1991; Oshida et al., 1992; Klingelhoefer et al., 2009). Thick sediment supplied from the Yangtze and Yellow rivers covers the seafloor of the Okinawa Trough and reaches ~2 km in its southern part (Sibuet et al., 1987). The volcanic rocks sampled in the southern Okinawa Trough range from calc-alkaline andesite to rhyolite (Shinjo et al., 1999). Active hydrothermal vents were discovered close to some of the seafloor volcanic edifices and the composition of both the venting fluids and hydrothermal deposits were described in a several works (Okamoto et al., 2002; Glasby and Notsu, 2003; Gena et al., 2005).

The Daiyon-Yonaguni Knoll is one of the seamounts that delineate a volcanic belt in the southernmost part of the Okinawa Trough (Matsumoto et al., 2001) (Fig. 1 B). An active hydrothermal field, adjacent to this seamount and named after it, is located in an elongated valley (~1000 m long and ~500 m wide) covered by thick muddy sediment (Gena et al., 2005) (Fig. 1 B). Volcanic breccias were observed in the northeastern part of the hydrothermal field. Four major hydrothermal chimney–mound complexes venting hot (up to 328°C) both black and clear fluids are aligned north–south and were named Lion, Tiger, Swallow and Crystal (Konno et al., 2006; Suzuki et al., 2008; Fujiwara et al., 2015). Liquid CO_2 emissions were detected at the seafloor between the Tiger and Swallow sites (Konno et al., 2006). Diffuse venting ($T \leq 80°C$) was observed in the southern part of the hydrothermal field and named the Abyss Vent (Suzuki et al., 2008).

3. Samples

In our efforts to shed more light on the mineralogy and geochemistry of the stibnite-orpiment containing deposits at the Daiyon-Yonaguni Knoll hydrothermal field, we selected six

samples (collected during the R/V *Natsushima* cruise NT01-05 Leg2; 2001) of active chimney and active chimney flange from the Tiger vent (Table 1; Fig. 2) (sample repository of the JAMSTEC) and investigated them. Sub-samples from macroscopically different areas of the samples (Fig. 2) were collected using a mini-drill bore with diamond bit and ground to fine powders in an agate mortar for further analyses. Thin polished sections were prepared from each sample for optical microscopy and electron microprobe investigations.

Eleven vent fluid samples (recovered during the R/V *Yokosuka* cruise YK03-05; 2003) collected from the Tiger vent (8 samples from the vent and 2 from the buoyant plume above the vent) and Abyss diffuse venting site (1 sample) using water-hydrothermal *atsuryoku* tight sampler (WHATS; developed for collecting fluid samples while maintaining gas pressure; Tsunogai et al., 2003), bag sampler, and Niskin sampler (Table 2) were filtered (0.45 µm membrane filters) and acidified immediately after recovery and analyzed in onshore laboratories later.

4. Methods of investigation

4.1. Mineralogy of hydrothermal deposits

Initially, the hydrothermal deposit samples were observed with a stereomicroscope (Nikon SMZ745T) and pictures of the major minerals that constitute the samples were acquired in natural light. The mineral composition and texture of the samples were investigated in thin polished sections by optical polarizing microscope (Nikon ECLIPSE LV100N POL) in transmitted and reflected light.

Crystal habit of the minerals that compose the studied samples was studied on small (~1x1 cm) sub-samples using a Hitachi TM3030 Plus tabletop scanning electron microscope (SEM) (V=15.0 kV, I=1850 mA, electron beam diameter 0.1 µm), after mounting of the sub-samples on aluminum stubs using carbon tape and coating them with carbon. The crystal habit was documented on secondary electron images (SEI) and the chemistry (qualitative) of the imaged minerals was probed by energy dispersive X-ray spectrometry (EDS).

Mineral chemistry (point analyses) and element distribution within the minerals (X-ray maps in major elements detected: Sb *L*α, As *L*α, Ba *L*α, S *K*α lines) were analyzed on thin polished sections (those used in the optical microscope studies) after coating them with carbon and using JEOL JXA-8230 electron microprobe (EMP) (V=15 kV, I=1.2 nA, electron beam diameter 2 μm). Standards used were $CaSO_4$ (S *K*α), Sb_2S_3 (S *K*α and Sb *L*α), $CaCO_3$ (Ca *K*α), GaAs (As *L*α), As (As *L*α), $BaSO_4$ (Ba *L*α), $SrSO_4$ (Sr *L*α), and the detection limits (in wt.%) were 0.030 for Sb, 0.013 for S ($CaSO_4$ standard), 0.005 for S (Sb_2S_3 standard), 0.027 for As (As standard), 0.017 for As (GaAs standard), 0.016 for Ca, 0.047 for Ba, 0.018 for Sr.

Bulk mineral composition of the finely powdered samples was determined by X-ray diffraction (XRD) analysis of random mounts using Rigaku Ultima Ⅳ X-ray diffractometer with monochromatic Cu *K*α radiation with scans from 4 to 70 °2θ, with 0.05 °2θ step, and 4 s/step. XRD patterns were interpreted by using the MacDiff software.

4.2. Chemistry of hydrothermal deposits

Chemistry (elemental concentrations) of the hydrothermal deposits was determined by Inductively Coupled Plasma Quadrupole Mass Spectrometer (ICP-QMS; Thermo Fisher Scientific i-CAP Q; Department of Systems Innovation, The University of Tokyo) after total sample dissolution (Kato et al., 1998; 2002; 2005; Yasukawa et al., 2014; 2020). In short, after drying the sample powders at 110°C for ~12 h, we weighed ~50 mg from each sample and put them in Teflon beakers. The samples were dissolved with HNO_3-HF-$HClO_4$ after heating on a hot (130°C) plate in the tightly closed beakers for 2 h. The dissolved samples were progressively evaporated at 110°C for 12 h, at 160°C for 6 h, and at 190°C until dry. The residues were subsequently dissolved in 2 mL *aqua regia* on a hot (90°C) plate for 6 h. The dissolved samples were progressively evaporated at 120°C for 2 h, then at 160°C until dry. Subsequently, the residues were dissolved by 10 mL of a 2 wt.% acid mixture consisting of HNO_3:HCl:HF (20:5:1) on a hot (90°C) plate for 3 h. The remaining residues in the solutions were removed by filtration (0.45-μm mesh, polytetrafluoroethylene membrane filters; Merck Millipore Millex®), precisely weighted and investigated by XRD. Before the ICP-QMS measurements the sample solutions were diluted to 1:50, 1:250 and 1:500 (or 1:10000, 1:50000, and 1:100000 with respect to the

sample powder, respectively) by mass using the same 2 wt.% HNO_3-HCl-HF (20:5:1) acid mixture. During the ICP-QMS measurements, spectral overlaps from oxides and hydroxides ($^{44}Ca^{16}O$ on ^{60}Ni, $^{47}Ti^{16}O$ on ^{63}Cu, $^{50}Ti^{16}O$ on ^{66}Zn, $^{137}Ba^{16}O$ on ^{153}Eu, $^{141}Pr^{16}O$ and $^{140}Ce^{16}O^{1}H$ on ^{157}Gd, $^{143}Nd^{16}O$ on ^{159}Tb, $^{147}Sm^{16}O$ and $^{146}Nd^{16}O^{1}H$ on ^{163}Dy, $^{149}Sm^{16}O$ on ^{165}Ho, $^{150}Nd^{16}O$ and $^{150}Sm^{16}O$ on ^{166}Er, and $^{165}Ho^{16}O$ on ^{181}Ta) were corrected following the method described by Aries et al. (2000). Samples along with the standards and blanks were analyzed as one analytical batch. To check the analytical precision and accuracy, reference standards issued by the Geological Survey of Japan [JB-2 (basalt), JB-3 (basalt) (Imai et al., 1995; Makishima and Nakamura, 2006; Lu et al., 2007) and JMS-2 (pelagic clay) (Takaya et al., 2014)] were analyzed twice within the analytical batch. The analytical errors for the unknown samples were calculated on the basis of the relative standard deviation for each element in JMS-2.

4.3. Chemistry of vent fluids

A pre-concentration method was employed for the determination of the concentrations of a set of elements (Fe, Mn, Co, Ni, Cu, Zn, Cd, Mo, Sb, Pb, U, V, Y, La, Ce, Pr, Nd, Sm, Eu, Gd, Tb, Dy, Ho, Er, Tm, Yb, Lu) in the collected vent fluids using a separation procedure with the NOBIAS chelate-PA1 resin (Hitachi High-Technologies) following already published protocols (Sohrin et al., 2008; Minami et al., 2015). 2 mL of each fluid sample were weighted and the samples were adjusted to pH~6 with a buffer prior to column purification. Then, the columns were loaded with 0.5 mL of clean resin and the resin was washed with 30 mL 18.2 MΩ water, 0.5 mL 3*M* HNO_3, and 10 mL 18.2 MΩ water. Before the sample load, the resin was conditioned with 1 mL 2.5% HNO_3 + 120 µL of the buffer to reach a final pH~6. The sample matrix was eluted with 10 mL 18.2 MΩ water. Elements of interest (listed above) were eluted with 23 mL 3*M* HNO_3. The resin was washed with 20 mL 18.2 MΩ water and the columns stored for further separation procedures. We were not able to measure the As concentrations because of analytical challenges: (1) As is not retained on the NOBIAS resin; (2) As is difficult to be measured directly in the vent fluid because of the number of interferences it experiences during the Inductively Coupled Plasma – Mass Spectrometry (ICP-MS) measurements.

The solutions with eluted elements were evaporated to dryness and re-dissolved in 2 mL ~0.28*M* HNO_3 for High Resolution – Inductively Coupled Plasma – Mass Spectrometry (HR-ICP-MS) measurements. Concentrations of elements in these solutions were measured with a HR-ICP-MS Element XR (Thermofisher Scientific) at Pôle de Spectrométrie Océan (PSO, IUEM, Brest, France). Indium was used as an internal standard for correcting drift of the signal and concentrations were calibrated using external calibration standards. A referenced seawater standard (CASS-6; National Research Council, Canada) and one blank were also processed following the above protocol and analyzed with the same HR-ICP-MS instrument.

4.4. Sulfur isotope analysis of hydrothermal deposits and fluids

The sulfide contained in the hydrothermal deposit samples was separated through the following procedures before the analysis of its S isotope composition:

(1) About 0.5 g of each powdered sample were weighed and put in three-necked flasks. A Pasteur pipette was attached to the tip of a tube connected to the flask and the tip was placed in $Cd(CH_3CO_2)_2$ solution in a test tube. N_2 gas was introduced in the system for 2-3 minutes.

(2) Fine-grained sulfide minerals were separated using selective chemical dissolution procedures. Sphalerite, pyrrhotite, and galena were reacted with 30 mL 12*M* HCl at 80°C in the three-necked flask. The glass stopper was tightened and N_2 gas flowed for 20-30 minutes while H_2S gas was generated during the reaction between the sulfides (sphalerite, pyrrhotite, galena) and HCl. The generated H_2S gas was fixed as CdS (yellow precipitate formed in the test tubes) and oxidized to $BaSO_4$. Chalcopyrite, isocubanite, pyrite, tennantite, and native sulfur were oxidized to SO_4^{2-} in mixture solution of Br_2 and HNO_3 and precipitated as $BaSO_4$.

(3) The N_2 gas flow was stopped, 1 mL H_2O_2 solution was added in the test tube, the tube was plugged with a rubber stopper, stirred, and left overnight.

(4) The solution was transferred from the test tube to a beaker and heated on a hot (140°C) plate until the solution amount was reduced by ~20%. If a white precipitate formed, 2 mL 6*M* HCl were added and the precipitate was collected by filtration.

(5) The sample solution was heated to 140°C, 10 mL $BaCl_2$ solution was added to it and it was left overnight. Precipitated $BaSO_4$ was collected through suction filtration and dried at 110°C.

$BaSO_4$ recovered through the above procedures was used for measuring the S-isotope composition of the sulfide in the hydrothermal deposit samples.

Sulfur isotope composition of sulfate in the vent fluids was analyzed according to the following protocol. 2 mL of each fluid sample was diluted with 10 mL 18.2 MΩ water, acidified with 1 mL 6*M* HCl and heated at 150℃ for 5 minutes. 1 mL $BaCl_2$ solution was added to each sample solution to precipitate dissolved sulfate as $BaSO_4$, which was collected by filtration and dried at 110℃. Recovered $BaSO_4$ was used for measuring the S-isotope composition of the vent fluid sulfate.

0.15-0.20 mg $BaSO_4$ precipitate from all samples (deposits and vent fluids) were mixed with 1.0-3.0 mg V_2O_5 and wrapped in Sn capsules. In a similar way, MSS-2 and MSS-3 standards were mixed with V_2O_5 and wrapped in Sn capsules as work standards for measurement. The S isotopes were measured by EA-IRMS, the data are reported against the Canyon Diablo Troilite (CDT) and expressed in per mil (‰). The analytical error of the measurements was ± 0.3‰.

4.5. Lead isotope analysis of hydrothermal deposits

All reagents used for sample preparation for Pb isotope analyses were Optima-grade. The sample preparation was performed under a clean lab environment at the Department of Geological Sciences at the University of Florida. Around 30 mg of sample powder was transferred in pre-cleaned Teflon beaker and dissolved in 3 mL aqua regia on a hot (100°C) plate overnight. After digestion, the solutions were evaporated to dryness and the dry residue was dissolved in 1*M* HBr and loaded on columns packed with clean Dowex 1X-8 resin to separate Pb for isotope analysis. After 3x1 mL of 1*M* HBr washes the purified Pb fraction was collected in 1 mL of 3*M* HNO_3. Pb isotopes were determined with Tl-normalization on a "Nu Plasma" Multi-Collector – Inductively Coupled Plasma – Mass Spectrometer (MC-ICP-MS), following methods described in Kamenov et al. (2004). The reported Pb isotope data for the samples are relative to

NBS 981 values of $^{206}Pb/^{204}Pb$=16.937 (±0.004, 2σ), $^{207}Pb/^{204}Pb$=15.490 (±0.004, 2σ), $^{208}Pb/^{204}Pb$=36.695 (±0.009, 2σ).

4.6. Stability phase diagrams modeling

In order to get insight into the conditions of abiogenic precipitation of the stibnite, orpiment and barite in the studied hydrothermal chimneys we modeled Eh *vs* $\log_{10}a$ phase diagrams at the physical-chemical conditions of three selected vent fluids (Daiyon-Yonaguni Knoll hydrothermal field) using the Geochemist's Workbench 8.0 (GWB) software (based on the "thermo_minteq" database) (Bethke, 2008).

4.7. Investigations of filamentous structures

Raman spectra of selected sub-samples (light orange filamentous structures and surrounding dark red colloform mineral) from sample 2K1267 L1 were acquired using a Horiba LabRAM HR 800 Raman spectrometer (Department of Materials and Environmental Chemistry, Stockholm University), equipped with an air cooled double-frequency Nd:YAG laser operating at 532 nm. The selected sub-samples were exposed to a laser power of 5 mW through an objective lens with 50× magnification (NA 0.42). A diffraction grating with 600 grooves mm^{-1} was used to resolve the spectra. Acquisition time was set at 2 s, with 20 scans accumulated from 0 to 4000 cm^{-1} with a spectral resolution of 2 cm^{-1}.

The filamentous structures were further studied using a stereomicroscope (Olympus SZX2-ILLT) and an Olympus BX51 microscope with an X-cite Series 120 Q fluorescence light source. The filaments were stained by CalcoFlourwhite (BioTium), a dye that binds to chitin. Before staining, the samples were treated with sterile gloves and forceps to reduce the introduction of exotic fluorescent particles.

An XL30 environmental scanning electron microscope (ESEM) with a field emission gun (XL30 ESEM-FEG) was also used to analyze the filamentous structures. The ESEM was equipped with an Oxford x-act energy dispersive spectrometer (EDS), backscatter electron (BSE) detector and a secondary electron (SE) detector. The acceleration voltage was 20 kV. The

instrument was calibrated with a cobalt standard. Peak and element analyses were recorded using the accompanying AZTEC software.

5. Results

5.1. Mineralogy of hydrothermal deposits

The hand specimens of the studied deposits were porous, fragile, greyish-black (Fig. 2 A) to blackish-grey (Fig. 2 B, E, F) with orange to white stains (Fig. 2 B-F).

The XRD studies of bulk samples (active chimney and active chimney flange) showed that the major mineral that composes them is barite (Table 3). Only one sample of active chimney is composed of pyrite and isocubanite (Table 3). However, our stereomicroscope, optical polarizing microscope, SEM and EMP studies showed regular presence of two other minerals (stibnite and orpiment) and traces of several others (native sulfur, pyrite, gypsum, and clays). Obviously, these minerals are in quantities below the XRD detection limits: i.e., <4 wt.%. We will focus our attention on the stibnite and orpiment in the following description.

Long (0.3 mm), needle-like, black to grey with metallic lustre stibnite forms rosettes of radiating crystals, which fill cavities and cover the surface of greyish-white to white barite (Fig. 3 A). The optical microscope (thin polished sections) and SEM observations revealed that the studied samples were composed of bunches and stacks of prismatic and tabular transparent (in transmitted light) crystals of barite overgrown by long prismatic crystals of stibnite forming rosettes (Fig. 3 B, C). The average empirical formula of stibnite is $Sb_{1.93}As_{0.08}S_{3.00}$ (average of 10 point analyses; Table 4), which suggests that its chemistry is close to the stoichiometry with a little excess in cations. Mapping of the concentration distributions of the elements (in characteristic lines) present in the studied samples showed that Sb, As and S are homogenously distributed within the stibnite crystals (Fig. 4 A, B, D, E) and the stibnite always grows on barite (Fig. 4 A-D).

Orange filaments (Fig. 5 A) and dark red colloform aggregates (Fig. 5 B) of orpiment stain the surface of the samples and fill cracks in them. At places, yellow fine precipitates and yellow thin filaments of orpiment occur along with the orange orpiment filaments and overgrow

transparent to white barite crystals (Fig. 5 F). Orpiment mostly occurs as colloform masses (Fig. 5 D) composed of fine (<1 μm) crystals deposited on barite. Rarely, it occurs as stacks of branching filaments ~300 μm long and 20 μm wide (Fig. 5 C, E) with clear axis and two concentric zones in cross section (Fig. 5 E). Orpiment rarely contains traces of Sb and has an average empirical formula $As_{1.98}Sb_{0.01}S_{3.01}$ (average of 19 point analyses; Table 4). The chemistry of orpiment slightly deviates from the stoichiometry with a slight deficiency in cations and slight excess in S. Orpiment and barite show homogenous distribution of the major elements that compose them (As and S, and Ba and S, respectively; Fig. 6 A-E) and only the traces of Sb in the orpiment show slight enrichment in some zones (Fig. 6 B).

The most common morphology of barite in the studied samples is tabular (match box-like; Fig. 3 D), but radial barite crystals forming rosettes (dendritic barite) among the sulfides can rarely be observed (Fig. 3 E). The average empirical formula of barite $(Ba_{0.95}Ca_{0.03}Sr_{0.02})SO_4$ (average of 5 point analyses; Table 4) is close to the stoichiometry with traces of Ca and Sr as isomorphic replacements for Ba. Whitish-yellow to yellow native sulfur (as closely packed rhombic crystals; Fig. 3 F), fine-grained greenish-yellow pyrite, white gypsum, and flake-like alumino-silicates (presumably clays) filling the open space among the barite crystals are rare minerals.

5.2. Geochemistry of hydrothermal deposits

Logically, the chemistry of the stibnite and orpiment separates (expected to be monomineralic according to stereomicroscope observations) differ from that of the bulk samples (Table 5). Orpiment samples along with that of stibnite are rich in As, Ca, Mg, K, Al, Ti, Fe, Mn, Zn, Pb, Bi, Hf, Ta, U, and Au (Table 5). The bulk samples as well as the stibnite sample are rich in Sb, and P (Table 5). The stibnite separate is highly enriched in Tl (Table 5). The stibnite and orpiment separates are richer in REE than the bulk deposit samples (ΣREE; Table 6). The bulk samples exhibit well-pronounced negative Ce anomaly (Ce/Ce*<1) when normalized to chondrite REE concentrations whereas the stibnite and orpiment samples show either less-pronounced negative or weak positive Ce anomaly (Ce/Ce*>1) (Table 6; Fig. 7 A). Bulk deposit samples

show stronger both positive Eu anomaly (Eu/Eu*>1) and light REE enrichment relative to the heavy REE (La_{CN}/Lu_{CN}>1) than the stibnite and orpiment separates (Table 6; Fig. 7 A).

5.3. Geochemistry of vent fluids

Previous works investigated the major ion chemistry of the Daiyon-Yonaguni Knoll hydrothermal fluids (Suzuki et al., 2008) and in order to complete our knowledge on them, we focused our attention on the trace elements chemistry of these fluids (Table 7). Although the REE were studied in the Daiyon-Yonaguni Knoll fluids (Hongo et al., 2007), we extended this exploration with more detailed analysis of the Tiger vent fluids and analyzed for the first time the REE in the Abyss vent fluids (Table 8). In order to facilitate the interpretations of the vent fluid chemistry from the point of view of possible phase separation and to consider the potential vent fluid mixing with seawater, we also cite Cl and Mg concentrations in the same fluids from previous work (Suzuki et al., 2008) (Tables 7, 8). Chlorine and Mg concentrations in the seawater from the vicinity of the Tiger vent (Suzuki et al., 2008) are given as background values (Table 7). The chemistry of the Tiger vent end-member fluid was calculated by extrapolating the data points in Mg *vs.* Element diagrams to 0 mmol/kg Mg, considering that Mg is quantitatively removed from seawater during its interaction with hot magmatic rocks of the basement (Von Damm, 1990).

Vent fluid with the highest chlorinity (D762 W1 F, [Cl] = 606 mmol/kg) and lowest Mg concentration ([Mg] = 18.4 mmol/kg) has the highest concentrations of Fe, La, Ce, Pr, Nd, Sm, Eu, Tb, ΣREE, second high concentrations of Mn, Ni and Y, and the lowest concentrations of Sb (Tables 7, 8). Two other vent fluids with high chlorinity and low Mg content (D763 W2 F, D763 W4 F) have the highest concentrations of Zn, Pb, Cu and Cd, high contents of Fe, Mn, Ni and Sb, high Eu anomalies, low concentration of V, and the lowest content of U (along with sample D762 W1 F) (Tables 7, 8). The chemistry of the Tiger vent end-member fluid is close to that of the three vent fluids with the lowest Mg content and highest chlorinity (D762 W1 F, D763 W2 F, D763 W4 F). Iron, Mn, Y and REE concentrations of the Tiger end-member fluid are close to those of the vent fluid with the highest chlorinity (D762 W1 F), whereas the concentrations of Zn, Pb, Cu, Ni and Cd in the end-member fluid are similar to those in the other two high-

chlorinity and low-Mg vent fluids (D763 W2 F, D763 W4 F) (Tables 7, 8). The Tiger end-member fluid has very low Mo and V concentrations, and U content calculated to be negative (Table 7).

The fluid of the buoyant plume above the Tiger vent has the lowest concentrations of Fe, Mn, Ni, Y and REE, and the highest content of V (Tables 7, 8).

The low-temperature Abyss vent fluid (T = 80°C; Table 2) has a chlorinity ([Cl] = 547 mmol/kg) close to that of the local seawater ([Cl] = 544 mmol/kg), the highest Mn, Y, Dy, Ho, Er, Tm, Yb and Lu concentrations, the lowest Pb and Cd concentrations, among the lowest Zn, Mo, Sb and Co concentrations, and the lowest positive Eu anomaly (Tables 7, 8).

Chondrite-normalized REE distribution patterns of the Tiger venting and end-member fluids show weak negative Ce anomalies, weak to strong positive Eu anomalies and enrichment in the light relative to heavy REE (Fig. 7 B, Table 8). The REE distribution pattern of the Tiger end-member fluid closely resembles that of the venting fluid with the highest chlorinity (D762 W1 F; Fig. 7 B). Chondrite-normalized REE distribution pattern of the low-temperature Abyss vent fluid shows weak both negative Ce and positive Eu anomalies, and flat distribution of the heavy REE (Fig. 7 B, Table 8). Y/Ho ratio of all venting fluids and of the Tiger end-member fluid is between 50 and 100, and is lower than that of the previously published data for the Tiger hydrothermal fluids (Y/Ho > 100, Table 8; Hongo et al., 2007).

5.4. Sulfur isotope compositions of hydrothermal deposits and vent fluids

The S-isotope composition of the sulfides from the studied Daiyon-Yonaguni Knoll hydrothermal deposits varies in a narrow range ($\delta^{34}S_{sulfide}$ = 4.0 - 5.3‰; Table 5), falling within the range of the S-isotope composition of the Okinawa Trough hydrothermal deposits (Fig. 8).

The S-isotope composition of the Daiyon-Yonaguni Knoll vent fluid sulfate ($\delta^{34}S_{sulfate}$ = 20.3 - 21.6‰; Table 7) clusters around the average seawater value ($\delta^{34}S_{sulfate}$ = 20.97 ± 0.10‰; Paris et al., 2013) with some scattering to slightly lighter (2 samples) and slightly heavier (2 samples) isotope compositions relative to that of seawater (Table 7, Fig. 8).

5.5. Lead isotope composition of hydrothermal deposits

Lead isotope data for the analyzed hydrothermal deposits are presented in Table 9. The samples show relatively limited variations in $^{206}Pb/^{204}Pb$ (18.491 to 18.545), but wider spread in $^{207}Pb/^{204}Pb$ (15.575 to 15.652) and $^{208}Pb/^{204}Pb$ (38.564 to 38.951). As a result the data form a relatively steep linear trend in Pb isotope space (Fig. 9).

5.6. Stability phase diagrams modeling

In the modeling of Eh *vs* $\log_{10}a$ phase diagrams for the stability of the stibnite, orpiment, barite and the most possible Sb-, As- and Ba-ions at the conditions of Daiyon-Yonaguni Knoll hydrothermal system, we used the physical and chemical parameters of three vent fluids. We chose the vent fluids with: the highest temperature (sample D759 W1 F, Tiger vent), the lowest temperature (sample D762 B F, Abyss vent), and the highest both chlorinity and metal concentrations (sample D763 W2 F, Tiger vent) (Tables 2, 7). For the modeling we used our data for vent fluid temperature, pH, hydrostatic pressure (calculated from the depth of sampling), and trace element concentrations (Tables 2, 7). Major ion concentrations, which we used, were the unpublished vent fluid chemistry on the basis of which Suzuki et al. (2008) calculated the Daiyon-Yonaguni Knoll end-member hydrothermal fluid. They were as follows:

(1) sample D759 W1 F: [Cl] = 550 mmol/kg, [SO_4] = 28.8 mmol/kg, [NH_4] = 0.14 mmol/kg, [Na] = 450 mmol/kg, [K] = 9.9 mmol/kg, [Mg] = 49.2 mmol/kg, [Ca] = 9.4 mmol/kg, [B] = 0.40 mmol/kg, [SiO_2] = 0.18 mmol/kg, [Sr] = 81.6 µmol/kg;

(2) sample D763 W2 F: [Cl] = 600 mmol/kg, [SO_4] = 13.1 mmol/kg, [NH_4] = 4.96 mmol/kg, [Na] = 454 mmol/kg, [K] = 58.0 mmol/kg, [Mg] = 22.0 mmol/kg, [Ca] = 17.8 mmol/kg, [Li] = 2.53 mmol/kg, [B] = 2.49 mmol/kg, [SiO_2] = 7.33 mmol/kg, [Sr] = 98.8 µmol/kg;

(3) sample D762 B F: [Cl] = 547 mmol/kg, [SO_4] = 23.9 mmol/kg, [NH_4] = 1.04 mmol/kg, [Na] = 456 mmol/kg, [K] = 14.4 mmol/kg, [Mg] = 45.9 mmol/kg, [Ca] = 9.6 mmol/kg, [B] = 0.72 mmol/kg, [SiO_2] = 2.65 mmol/kg, [Sr] = 84. 1 µmol/kg.

5.7. Carbonaceous matter in the orpiment filaments

The Raman spectra of orpiment filaments (sample 2K1267 L1) are characterized by bands between 1000 and 1800 cm^{-1}, and between 2700 and 3000 cm^{-1}, denoted as first and second order regions, respectively (Fig. 10 B). These bands are typical of carbonaceous matter (Kouketsu et al., 2014; Qu et al., 2015) that suggests the orpiment filaments contain carbonaceous matter.

The two main bands occurring at approximately 1350 and 1600 cm^{-1} in the first order region are commonly identified as disordered carbon (D) and ordered graphite (G) bands, respectively. These bands have previously been attributed as ring breathing modes of disordered carbonaceous matter, and in-plane vibrations of sp^2 carbon atoms (Ferrari and Robertson, 2000). Moreover, the intensity ratio between the D and G bands (I(1350)/I(1600)) has previously been used to indicate the structure order of the carbonaceous matter (Kouketsu et al., 2014; Qu et al., 2015), and the calculated value of 0.765±0.08 was obtained for the analyzed filaments.

Additionally, a deconvolution of the region between 1000 and 1800 cm^{-1} was done. Using the FWHM-D1 value calculated, and applying the relationship determined by Kouketsu et al. (2014), the maximum temperature experienced by the filaments was calculated to be between 190-230°C.

The Raman spectra of both light orange filamentous (Fig. 10 B) and dark red colloform (Fig. 10 C) structures showed a weak band at 230 cm^{-1}, and a broad strong band at 339 cm^{-1}, which supported the electron microprobe analyses that both types of sub-samples are composed of an arsenic sulfide mineral phase. Previously, in analogous deposits from hydrothermal vents off Milos Island, similar Raman spectra were attributed to poorly to non-crystalline forms of orpiment (Godelitsas et al., 2015).

Staining with ChalcoFlourWhite under fluorescence microscopy turned out to be unsuccessful, thus suggesting that chitin is not present in the filaments.

The ESEM analyses (sample 2K1267 L1) are in support of the Raman data indicating a carbonaceous phase associated with the filaments. The carbonaceous matter occurs rather as a film coating the filaments than incorporated in them (Fig. 11).

6. Discussion

499 *6.1. Sequence of mineral precipitation at the Daiyon-Yonaguni Knoll hydrothermal field*
500
501 The chemistry of the major mineral in the studied deposits, barite (Table 3), is close to its
502 stoichiometry with negligible isomorphic replacement of Ca and Sr for Ba (Table 4). The
503 isomorphic replacements of As for Sb and of Sb for As in stibnite and orpiment, respectively, are
504 also insignificant and the chemistries of the studied stibnite and orpiment (Table 4) practically
505 match their stoichiometric empirical formulae. The textural relations between the major barite
506 and minor stibnite and orpiment (Figs 3 B, C; 4 A-E; 5 F; 6 A-E) suggest that the stibnite and
507 orpiment have precipitated after barite.
508 Barite is an abundant mineral in the back-arc basin hydrothermal deposits (Shikazono and
509 Kusakabe, 1999) and a number of studies have been focused on it (e.g., Shikazono, 1994;
510 Shikazono et al., 2012; Jamieson et al., 2016). These studies showed that tabular large-crystal
511 barite with smooth crystal faces precipitates from solutions with low degrees of supersaturation
512 (saturation index below ~100) and dominates the barite deposited at the back-arc basin
513 hydrothermal systems (Shikazono, 1994). Dendritic barite with rough crystal faces is rare (or
514 lacking) in these deposits and forms from solutions with high degrees of supersaturation
515 (Shikazono, 1994). It was found that dendritic barite at seafloor hydrothermal systems
516 precipitates from fluids composed of less than 40% hydrothermal end-member fluid (and more
517 than 60% seawater), whereas the tabular barite forms from fluids containing greater proportion of
518 hydrothermal end-member fluid (Jamieson et al., 2016). In general, the seafloor hydrothermal
519 barite precipitates from solutions with high flow rates (i.e., focused discharge) (Shikazono et al.,
520 2012) and at temperatures of between 100°C and 240°C (Tokunaga and Honma, 1974; Jamieson
521 et al., 2016).
522 Our studies of the Daiyon-Yonaguni Knoll hydrothermal deposits confirm the previous
523 observations that the tabular barite is the dominant barite morphology at the back-arc basin
524 hydrothermal systems (Shikazono, 1994). On the basis of the knowledge gained up to now we
525 may infer that the Daiyon-Yonaguni Knoll barite precipitated from focused-discharge fluids
526 composed of high proportion (>40%) of hydrothermal end-member fluid and at temperatures
527 100-240°C. The minor minerals, stibnite and orpiment, have precipitated after barite and seem to
528 be later lower temperature precipitates.

529

530 *6.2. Phase separation and trace element chemistry of the Daiyon-Yonaguni Knoll vent fluids*

531

532 The chlorinities of all studied fluids from the Tiger and Abyss vents vary and are higher
533 than that of the local ambient seawater (Table 7). The richest in chloride vent fluid (D762 W1 F)
534 has a chlorinity ~11% higher than that of the seawater. Deviations (positive and negative) from
535 seawater chlorinity have long been measured in seafloor hydrothermal fluids (Edmond et al.,
536 1979; Michard et al., 1984; Von Damm et al., 1985a; Von Damm and Bischoff, 1987; Bowers et
537 al., 1988; Butterfield et al., 1990; Von Damm, 1990; Butterfield et al., 1994; Von Damm et al.,
538 2005) and explained with sub-seafloor boiling and phase separation (Von Damm, 1990).
539 Analyzing the major ion chemistry of the Daiyon-Yonaguni Knoll vent fluids Suzuki et al. (2008)
540 also ascribed their enhanced chlorinity relative to the ambient seawater to sub-seafloor phase
541 separation.

542 Sub-seafloor boiling, phase separation and emission of brine-rich (chloride-rich) fluids
543 from the Daiyon-Yonaguni Knoll vents explain the enrichment in non-volatile elements (Fe, Mn,
544 Zn, Pb, Cu, Cd, Ni, Y, La, Ce, Pr, Nd, Sm, Eu and Tb) and depletion in volatile elements (Sb) of
545 the three Tiger vent fluids with the highest chlorinity and lowest Mg content as well as of the
546 Tiger vent end-member fluid (Tables 7, 8). The lowest concentrations of Mo, V and U in the
547 lowest-Mg (highest chlorinity) vent fluids and in the end-member fluid ([Mg] = 0 mmol/kg)
548 (Table 7) support the knowledge that these elements are nearly quantitatively removed from the
549 seawater during its interaction with the hot basement rocks (German and Von Damm, 2003) and
550 their contents in a vent fluid depend on the seawater proportion in it. The calculated negative U
551 concentration in the end-member fluid (Table 7) implies that U is not only 0 nmol/kg in this fluid,
552 but that the end-member fluid is a sink for U from the seawater and entrains it upon fluid-
553 seawater mixing.

554 The lowest concentrations of Fe, Mn, Ni, Y and REE, and the highest content of V in the
555 fluid of the buoyant plume above the Tiger vent (Tables 7, 8) are likely a result of removal of
556 dissolved Fe, Mn, Ni, Y and REE from the vent fluid to plume particles (Feely et al., 1990;
557 Ludford et al., 1996; Edmonds and German, 2004; Klevenz et al., 2011; Findlay et al., 2015) and
558 entrainment of seawater V (Trefry and Metz, 1989), respectively.

559 Although the chlorinity of the Abyss vent fluid is close to that of the ambient seawater it is
560 yet slightly higher than it (Table 7). This implies that the Abyss low-temperature vent fluid must
561 contain a proportion of high-temperature brine-rich vent fluid that has undergone phase
562 separation (Von Damm and Lilley, 2004). The low Pb, Cd, Zn and Sb concentrations in the
563 Abyss vent fluid (Table 7) are likely a result of sub-seafloor element-sulfide precipitation during
564 fluid cooling and dilution with seawater that are typical for low-temperature diffuse venting at the
565 seafloor (Koschinsky et al., 2002). As the most ubiquitous metal in the seafloor hydrothermal
566 fluids, Fe, preferentially precipitates relative to the other common metal Mn on cooling (Seyfried
567 and Ding, 1993) the low-temperature vent fluids usually appear to be enriched in Mn over Fe
568 (Thompson et al., 1985) and this explains the highest Mn concentration in the Abyss vent fluids
569 (Table 7).
570 The highest concentrations of La, Ce, Pr, Nd, Sm, Eu and Tb in the highest chlorinity (and
571 high-temperature) vent fluid (Tiger vent, D762 W1 F) and the highest concentrations of Y, Dy,
572 Ho, Er, Tm, Yb and Lu in the lowest chlorinity (and low-temperature) vent fluid (Abyss vent,
573 D762 B F) are directly related to the chlorinity and temperature control on the distribution of the
574 REE in the vent fluids (Table 8; Fig. 7 B). Previous studies revealed (1) that in a chloride-rich
575 hydrothermal fluid, the REE transport is facilitated by formation of chloride complexes at acidic
576 conditions and (2) that the light REE (La-Sm) are complexed more strongly by chloride, than the
577 heavy REE (Gd-Lu) (Haas et al., 1995). At elevated temperatures this relation (2) becomes more
578 pronounced. The REE speciation calculations (Douville et al., 1999a) confirmed that in the hot
579 acidic fluids of the seafloor hydrothermal systems the REE were mainly complexed by Cl^- ions.
580 Because the Cl complexing tends to be stronger for the light REE, an increased aqueous chloride
581 content will tend to favor these lighter elements. Therefore, the high-chlorinity high-temperature
582 Tiger vent fluids have the highest contents of La, Ce, Pr, Nd, Sm, Eu and Tb, whereas the low-
583 chlorinity low-temperature Abyss vent fluids have the highest contents of Y, Dy, Ho, Er, Tm, Yb
584 and Lu within the Daiyon-Yonaguni Knoll vent field.
585 Compared to the end-member hydrothermal fluids from three other sedimented seafloor
586 hydrothermal systems (Escanaba Trough, Guaymas Basin and Middle Valley), the Daiyon-
587 Yonaguni Knoll end-member hydrothermal fluid shows the highest Pb, La, Ce, Pr, Nd, Sm, Eu,
588 Tb, Dy, Ho and Er concentrations, and the lowest Mn concentration (Table 10). These differences

deserve particular scientific attention involving the chemistry of the source rocks (volcanic and sedimentary) that is beyond the scope of this work.

6.3. Yttrium and REE insights into fluid-rock equilibrium

In most seafloor hydrothermal fluids, Y is trivalent and behaves like Ho, and it is supposed that the Y/Ho molar ratio can give important clues for the origin of the hydrothermal fluids (Douville et al., 1999a). The Y/Ho molar ratio of the studied Daiyon-Yonaguni Knoll vent fluids (50.5 - 76.4; Table 8) is between that of the southern Okinawa Trough lavas [27.6 - 31.8, basalts, andesites, dacites and rhyolites; Shinjo et al. (1999), Shu et al. (2017), Guo et al. (2018)] and North Pacific deep water (101; Nozaki et al., 1999). It seems likely that the seawater-based hydrothermal fluids of the Daiyon-Yonaguni Knoll field have not completely lost their original high seawater Y/Ho molar ratio (Bau and Dulski, 1999; Nozaki et al., 1999). This suggests that the seawater has not completely reacted with the basement rocks and has not equilibrated with them.

The REE distribution pattern of the Daiyon-Yonaguni Knoll end-member fluid (Fig. 7 B) implies the same conclusion. It not only closely matches the REE distribution pattern of the highest chlorinity Tiger vent fluid (D762 W1 F) thus, suggesting that this fluid is close to the end-member, but still shows a weak negative Ce anomaly (Fig. 7 B). This supports the assumption that the mother fluid, seawater, has not completely reacted with the basement rocks and has not completely lost its original negative Ce anomaly.

The origin of the positive Eu anomaly and the enrichment of light REE over the heavy REE when the REE concentrations are normalized to those of chondrite are discussed elsewhere (Michard et al., 1983; Michard and Albarède, 1986; Michard, 1989; Klinkhammer et al., 1994; Bau and Dulski, 1999; Douville et al., 1999a) and we will not repeat this discussion here.

6.4. Trace elements in the Daiyon-Yonaguni Knoll hydrothermal deposits: hydrothermal – microbial – hydrogenetic interplay

618 The studied Daiyon-Yonaguni Knoll hydrothermal deposits (bulk samples and mineral
619 separates) are rich in Sb and As (Table 5). Previous works (Douville et al., 1999b; Breuer and
620 Pichler, 2013) found that these two volatile elements are particularly enriched in the
621 hydrothermal fluids discharged at back-arc and volcanic arc settings. Their high concentrations in
622 these fluids are inferred to be primarily controlled by phase separation processes and source rock
623 types: felsic volcanic rocks and sedimentary blanket. Thus, the fluid phase separation at the
624 Daiyon-Yonaguni Knoll vents (see *6.2*) and the source rock types, felsic volcanics [calc-alkaline
625 andesite to rhyolite; Shinjo et al. (1999)] and sediment cover (Sibuet et al., 1987) explain the high
626 Sb and As concentrations in the hydrothermal deposits. Antimony and As are highly volatile
627 elements and most probably separate in the vapor (low-chlorinity) during the boiling and phase
628 separation. As the chlorinities of all studied vent fluids are higher than that of the local ambient
629 seawater (Table 7), it seems reasonable to assume that Sb and As minerals in the Daiyon-
630 Yonaguni Knoll deposits had precipitated in the past when the vapor phase (rich in volatiles) had
631 dominated in the vent fluids.
632 Thallium is also a volatile element and its high concentration in the stibnite precipitates
633 (Table 5) may also be explained with vent fluid phase separation and source rock types.
634 Gold concentrations in the bulk Daiyon-Yonaguni Knoll hydrothermal deposits (0.50 - 1.00
635 ppm; Table 5) fall within the range of Au content in the Okinawa Trough hydrothermal deposits
636 (0.05 - 4.5 ppm; Fuchs et al., 2019) whereas the Daiyon-Yonaguni Knoll stibnite and orpiment
637 samples are richer in Au (1.00 - 11.0 ppm; Table 5) than the Okinawa Trough hydrothermal
638 deposits. However, the Au concentrations of the Daiyon-Yonaguni Knoll hydrothermal deposits
639 (0.50 - 11.0 ppm; Table 5) are within the lower end of the Au content range of the global seafloor
640 hydrothermal deposits (0.01 - 43.0 ppm; Fuchs et al., 2019). Almost linear correlation between
641 Au and As concentrations (diagram available on request) suggests that (1) Au (like As) is
642 hydrothermally derived in these deposits, (2) Au (like As) may also be contributed by direct
643 magmatic degassing (e.g., Fuchs et al., 2019), and (3) As plays an essential role in Au intake in
644 the As-containing sulfides (Pokrovski et al., 2021).
645 Higher concentrations of Fe, Mn, Zn, Pb and Bi in the orpiment samples than in the bulk
646 samples can be explained with high hydrothermal input.

In addition to the high Au concentrations, the stibnite and orpiment samples have also enhanced U concentrations relative to those of the bulk deposit samples (Table 5). This seems controversial because unlike Au, the U is quantitatively removed (~98%) from seawater during hydrothermal circulation through the oceanic crust (Michard and Albarede, 1985; Chen et al., 1986) and, as a result, the seafloor end-member hydrothermal fluids are depleted in U. Therefore, hydrothermal contribution of U to the Daiyon-Yonaguni Knoll hydrothermal deposits had likely been negligible and the low U concentrations of the bulk samples (0.03-0.07 ppm; Table 5) seem to show that. The enhanced U concentrations in the stibnite and orpiment samples (0.12-3.96 ppm; Table 5) relative to the bulk deposits suggest that a factor other than the hydrothermal fluid controlled U concentration in the stibnite and orpiment. Previous work (Lovley et al., 1991; Mills et al., 1994) suggested that U enrichment within the TAG seafloor hydrothermal deposits is microbially mediated. The presence of carbonaceous matter associated with the filamentous orpiment and inferred microbial activity (see *6.6*) imply that the elevated U content in this type of orpiment is a result of bacterial concentration of U from a seawater-dominated fluid. Thus, the enrichments of the stibnite and orpiment in two elements with different mechanisms of mobilization and fixation, Au and U, likely happened at different stages of the mineral deposition. Gold seems to have been deposited within stibnite and orpiment, and during their hydrothermal precipitation, while U has mostly likely been deposited within bacterial biofilms on stibnite and orpiment after their deposition.

Chondrite-normalized REE distribution patterns of the Daiyon-Yonaguni Knoll (bulk) deposits and one stibnite and one orpiment samples show negative Ce anomalies, positive Eu anomalies and enrichment of light relative to the heavy REE (Fig. 7 A; Table 6). These patterns resemble that of the Daiyon-Yonaguni Knoll end-member hydrothermal fluid, which slightly differs from those of the end-member fluids from other seafloor hydrothermal fields (Michard et al., 1983; Michard and Albarède, 1986; Michard, 1989; Klinkhammer et al., 1994; Bau and Dulski, 1999; Douville et al., 1999a) in possessing of a weak negative Ce anomaly (Fig. 7 B). We interpreted this feature as a result of incomplete reaction of seawater with the basement rocks and partial preservation of its original negative Ce anomaly (see *6.3*). Thus, the REE distribution patterns of the discussed deposits (bulk, one stibnite and one orpiment) seem to be inherited from the end-member hydrothermal fluid (mixed or not with ambient seawater). However, two of the

orpiment samples (2K1271 L1 flange, outer bottom, Op and 2K1267 L1, Op-1) have positive Ce anomalies, highest Nd concentrations, the smallest positive Eu anomalies, and the smallest fractionation between the light and heavy REE (La_{CN}/Lu_{CN}) (Table 6; Fig. 7 A). Previous studies showed that positive Ce anomalies and high Nd concentrations (>100 ppm) are typical for the seafloor hydrogenetic Fe-Mn deposits (Bau et al., 2014). The origin of the positive Ce anomaly in the seafloor Fe-Mn deposits is discussed elsewhere (Bau and Koschinsky, 2009). Although we are not aware of any particular study of the REE in the seafloor hydrothermal orpiment we may assume that the observed positive Ce anomalies, high Nd concentrations, little positive Eu anomalies, and little fractionation between the light and heavy REE in the two orpiment samples (Table 6) are results of hydrogenetic influence.

Hence, the trace element contents in the Daiyon-Yonaguni Knoll hydrothermal deposits suggest a complex interplay among hydrothermal (hydrothermal input), microbial (preferential concentration) and hydrogenetic (preferential scavenging from seawater) processes.

6.5. Origin of S in the sulfide precipitates and sulfate reduction in the vent fluids of the Daiyon-Yonaguni Knoll hydrothermal field

The S-isotope systematics in the seafloor hydrothermal systems at arc/back-arc settings show substantial variability in $\delta^{34}S$ (Fig. 8). The wide variation in $\delta^{34}S$ is a result of S-isotope fractionation due to three processes contributing to the S budget of the hydrothermal system: (1) basement rock sulfide supplied by interaction of hydrothermal fluid with basement rocks (Shanks and Seyfried, 1987; Shanks, 2001), (2) thermochemical reduction of sulfate supplied by seawater (Shanks and Seyfried, 1987; Shanks, 2001), (3) disproportionation of SO_2 supplied by magma vapors (Kusakabe et al., 2000; Peters et al., 2021).

Sulfide S of the Daiyon-Yonaguni Knoll hydrothermal deposits has isotope composition ($\delta^{34}S$) between those of the terrestrial mantle (basement rocks) sulfide and seawater sulfate, but being closer to the former (Table 5; Fig. 8). This suggests that the Daiyon-Yonaguni Knoll S bound in sulfides is a mixture of both basement rock and seawater S with a higher proportion of the basement rock S. The S-isotope composition of the Daiyon-Yonaguni Knoll sulfides supports the origin of sulfide S in the overall Okinawa Trough hydrothermal deposits being generally

dominated by basement rock S (Fig. 8). There are no clear indications for magmatic S supply to the Daiyon-Yonaguni Knoll hydrothermal deposits.

The slightly heavier S-isotope composition of sulfate in one Tiger vent and one Abyss vent fluids (21.2 and 21.6‰, respectively; Table 7) than that of the seawater ($\delta^{34}S_{sulfate}$ = 20.97 ± 0.10‰; Paris et al., 2013) is similar to the heavy S-isotope composition of sulfate of the CLAM hydrothermal fluids ($\delta^{34}S_{sulfate}$ > 21.0‰; Gamo et al., 1991) and deserves some consideration. We know that sulfate reduction in a closed system causes an increase of $\delta^{34}S$ of the residual sulfate (removal of the isotopically light sulfide during sulfate reduction) with decreasing sulfate concentration (Ohmoto and Rye, 1979; Shanks et al., 1981). Thus, the S-isotope composition of the sulfate from these two Daiyon-Yonaguni Knoll vent fluids can be interpreted as a result of sulfate reduction. Sulfate reduction or sulfide oxidation depends on the rate of mixing between the hydrothermal fluid and seawater (Peter and Shanks, 1992). Slow mixing of the hydrothermal fluid and seawater in the chimney walls or within a mound favors sulfate reduction. This sulfate reduction results in S isotope fractionation approaching equilibrium values and ^{34}S-enriched sulfate resulting from a reservoir effect, as ^{32}S is removed to the sulfide reservoir (Peter and Shanks, 1992). Overall, it appears that the hydrothermal fluid mixed slowly with seawater within the chimney walls of the Tiger and Abyss vents that favored reduction of the sulfate dissolved in the fluids and resulted in a heavy S-isotope composition of the vent fluids.

6.6. Sources of Pb to the Daiyon-Yonaguni Knoll hydrothermal deposits

The Pb isotope data for the Daiyon-Yonaguni Knoll hydrothermal deposits form a steep array indicating mixing of two Pb end-members (Fig. 9). At the low end of the array is sample 2K1271 L1 flange, outer bottom, Op. This sample plots below regional sedimentary and volcanic rocks, towards the NHRL indicating more primitive, mantle-like source of Pb. This in turn suggests presence of more depleted Pb isotopic source, possibly back-arc mafic volcanic rocks, in the area of Daiyon-Yonaguni Knoll. Three of the samples (2K1271 L1 flange, center upper; 2K1271 L1 flange, outer bottom, Stb; and 2K1271 L1, Op) plot close to the regional lavas. This suggests that Pb and other metals in these three hydrothermal samples can be derived from the local lavas. Alternatively, the Pb isotopic compositions of these three samples can be explained

by mixing between the more primitive source, responsible for the isotopic composition of 2K1271 L1 flange, outer bottom, Op and more enriched source reflected in the rest of the hydrothermal deposit samples. The enriched samples are very similar to laser ablation Pb isotope data for galena and anglesite from the Daiyon-Yonaguni Knoll (Zeng et al., 2022) and plot above the regional lavas indicating Pb derivation from more evolved source, potentially continental lithosphere and/or sedimentary rocks. This is consistent with Pb isotope studies of other hydrothermal deposits in the Okinawa Trough that also found evidence for significant involvement of sedimentary Pb in the hydrothermal systems (e.g., Ma et al., 2021; Zeng et al., 2022). However, it is interesting to note that the Pb isotope data for the closest hydrothermal fields [southern Okinawa Trough (SOT) sulfides] are very distinct from the Daiyon-Yonaguni Knoll hydrothermal deposits (Fig. 9). As can be seen on the Figure 9, the SOT sulfides are close to the regional sediment Pb data, thus providing direct evidence for a significant sedimentary component in the hydrothermal system (Ma et al., 2021). In contrast, the Daiyon-Yonaguni Knoll hydrothermal deposits are isotopically distinct from the SOT sulfides. Furthermore, the hydrothermal deposits are not close isotopically to any of the available sediment samples (Fig. 9). However, based on their position above the regional volcanic rocks it is most likely that another enriched source, either sediments or extended continental lithosphere, is present in the area of Daiyon-Yonaguni Knoll.

6.7. Filamentous orpiment: biogenic or abiogenic?

The morphology of the light orange filaments (Fig. 5 A, C, E) resembles microbial fossils (especially, fossilized fungi) previously described at the seafloor (Ivarsson et al., 2020). The longitudinal, branching filaments forming a network-like framework (Fig. 5 A, C) can be compared to fossilized fungal mycelium. The consistent and distinct center of the filaments (Fig. 5 C, E) corresponds size-wise to known sizes for fungal hyphae. The empty core (Fig. 5 E) can be the remains or cast of an initial microbial/fungal filament/hyphae. However, the concentric layering in cross sections of the filaments (Fig. 5 E) implies this morphology can be a result of repeated mineral deposition. Additionally, the overall features of the filaments with the rather straight appearance, the 90° branching and interconnections between filaments, the distinct

767 tapering and variation in diameter could be explained by abiotic biomorphs, or heavily encrusted
768 fungal hyphae. Based on morphology alone we can neither rule out nor support a biological or an
769 abiotic origin of the filaments at this point. The staining for chitin was unsuccessful, thus there is
770 no solid evidence for fungal (biogenic) origin of the filaments.
771 The Raman data, on the other hand, supports the presence of carbonaceous matter
772 associated with the orpiment filaments. Thus, even though a fungal origin of the orpiment
773 filaments cannot be unambiguously supported, the presence of microbial activity can be. The
774 filaments and their close proximity appear coated by a thin carbonaceous film that may represent
775 the remains of a biofilm. The I(1350)/I(1600) value indicates that the carbonaceous matter
776 associated with the filaments present medium structural order. The calculated maximum
777 temperature experienced by the filaments (209.1±37.1°C) falls within the temperature range of
778 the vent fluids (Table 2) and indicates that the carbonaceous matter reached low to medium-grade
779 thermal maturity. This excludes the possibility of recent contamination by carbonaceous matter
780 and supports the idea that the carbonaceous matter associated with the orpiment filaments is
781 indigenous to the primary hydrothermal environment.
782
783 *6.8. Stibnite, orpiment and barite hydrothermal precipitation: implications from stability phase*
784 *diagrams*
785
786 The maximum temperature, which the GWB can consider in the modeling is 300°C.
787 Therefore, we used this temperature when modeling the stability diagrams for vent fluid sample
788 D759 W1 F (T = 323°C) (Fig. 12 A, D, G).
789 In view of the chemistry of the Daiyon-Yonaguni Knoll vent fluids (Tables 7, 8; Suzuki et
790 al., 2008), it seems plausible to assume that the major Sb- and As-ions in these fluids will be
791 chloride and sulfide. We could not obtain any stability diagrams when using Sb-chloride and As-
792 chloride ions as major Sb- and As-ions, respectively, in the vent fluid. This may mean that the
793 incorporation of these species in the GWB data base may not be correct. Therefore, we used Sb-
794 sulfide ions as main Sb-ions in the vent fluids. Using the measured Sb concentrations in the
795 Daiyon-Yonaguni Knoll vent fluids (Table 7) in the modeling, we did not get any stability field
796 of stibnite. This suggests that stibnite does not precipitate from the current vent fluids: Sb content

is lower than that necessary for stibnite precipitation. Therefore, we put as a variable $\log_{10}a$ of the main Sb-ion suggested by the GWB, $Sb_2S_4^{2-}$, along one of the axes of the diagrams (Fig. 12 A, B, C).

On the basis of the vent fluid chemistry of the three vent fluids the GWB suggested only one As-sulfide ion, but it did not yield any diagram with stability field of orpiment. The main As-ion suggested by the GWB was $H_2AsO_4^-$ and we used it in the modeling. As we were not able to measure the As concentrations in the vent fluids (see sub-section *4.3*) we put as a variable $\log_{10}a$ of $H_2AsO_4^-$ along one of the axes of the diagrams and investigated a wide range of $\log_{10}a$: from -10 to +5 (Fig. 12 D, E, F).

We assumed that Ba^{2+} will be the major Ba ion in the studied vent fluids and therefore, we used Ba^{2+} in the modeling of barite stability (Fig. 12 G, H, I).

Modeling suggests that the stibnite has a limited area of stability within the physicochemical conditions of the selected vent fluids (Fig. 12 A, B, C). Its area of stability does not seem to depend on the vent fluid chlorinity: The area of stability of stibnite in the most chloride-rich fluid, D763 W2 F, does not differ substantially from those in the other fluids (Fig. 12 A, B, C). Obviously, the stability of stibnite increases with decreasing temperature of the vent fluid and results in precipitation at lower $\log_{10}a$ of $Sb_2S_4^{2-}$ (i.e., lower Sb concentrations) and less reduced environment (i.e., higher Eh, but still <0) (Fig. 12 A, B, C). In other words, the lowest temperature Daiyon-Yonaguni Knoll vent fluid (D762 B F; T = 80°C) is the most probable environment for stibnite precipitation.

Orpiment is stable (i.e., precipitates) in a wide range of $\log_{10}a$ of $H_2AsO_4^-$ (i.e., As concentrations) and in reducing conditions (Eh<0) (Fig. 12 D, E, F). With decreasing vent fluid temperature (from 300°C to 80°C), orpiment is stable (precipitates) at slightly less reduced conditions (higher Eh, but still <0) (Fig. 12 D, E, F). The differences in vent fluid chlorinity and vent fluid trace metal concentrations do not seem to affect the stability of orpiment (Fig. 12 D, E, F). Previous studies (Rytuba, 1984) add an additional constraint for orpiment precipitation. According to them, under conditions of constant temperature and pressure, the relative stability of As-sulfides is a function of S activity. Orpiment appears to be the stable As-sulfide at high S activity, which suggests high S activity during the orpiment precipitation at the Daiyon-Yonaguni Knoll hydrothermal site.

827 Modeling showed that in the high-temperature vent fluids D759 W1 F (T = 300°C) and
828 D763 W2 F (T = 210°C), the major Ba-ion is $BaCl^{+}$ (Fig. 12 G, H), whereas in the low-
829 temperature vent fluid D762 B F (T = 80°C) dissolved Ba appears as Ba^{2+} (Fig. 12 I). Barite is
830 stable in wide range of $\log_{10}a$ of Ba^{2+} (i.e., Ba concentrations) in all the three vent fluids and
831 precipitates from slightly reduced to slightly oxic conditions (Fig. 12 G, H, I). With decreasing
832 temperature of the vent fluid (from 300°C to 80°C), the stability field of barite slightly shifts to
833 less reduced (more oxic) conditions (Fig. 12 G, H, I). Modeling of barite precipitation from the
834 Daiyon-Yonaguni Knoll vent fluids shows large stability field of barite in wide temperature range
835 (80-300°C) and extends previous knowledge that hydrothermal barite precipitates at temperatures
836 100-240°C (see *6.1*).
837
838 **7. Summary**
839
840 The major mineral in the Daiyon-Yonaguni Knoll hydrothermal deposits is barite, which
841 likely precipitated from focused-discharge fluids composed of a high proportion (>40%) of
842 hydrothermal end-member fluid at T = 100-240°C. Stibnite and orpiment are minor minerals,
843 which seem to be later lower temperature precipitates.
844 The Daiyon-Yonaguni Knoll vent fluids were subjected to sub-seafloor boiling and phase
845 separation and are brine-rich (chloride-rich) enriched in non-volatile and depleted in volatile
846 elements. Sub-seafloor boiling and phase separation exerted major control on the REE
847 partitioning in the vent fluids, with the high-chlorinity high-temperature fluids enriched in light
848 REE and low-chlorinity low-temperature fluids enriched in heavy REE. The Y/Ho molar ratio
849 and Ce anomaly of the Daiyon-Yonaguni Knoll vent fluids suggest that the seawater had not
850 completely reacted with the basement rocks and had not equilibrated with them.
851 The trace element contents in the Daiyon-Yonaguni Knoll hydrothermal deposits suggest a
852 complex interplay among hydrothermal, microbial and hydrogenetic processes.
853 Sulfur isotope composition of the Daiyon-Yonaguni Knoll sulfides suggests that the sulfide
854 S is a mixture of both basement rock and seawater S, with a higher proportion of the basement
855 rock S. The hydrothermal fluid mixed slowly with seawater within the chimney walls of the Tiger

and Abyss vents which favored reduction of the sulfate dissolved in the fluids and resulted in a heavy S-isotope composition of the vent fluid sulfate.

The Pb isotope data for the Daiyon-Yonaguni Knoll hydrothermal deposits indicate involvement of two or even three sources of metals in the hydrothermal system. One of the sources can be local volcanic rocks, as three of the samples show Pb isotopes close to the latter. However, the Pb isotope data form a steep array that potentially can be explained by only two end-members, one enriched (continental lithosphere and/or sediments) and one depleted (possibly back-arc basalts). It is interesting to note that both of these end-members are discrete, not identifiable in the available Pb isotope data for southern Okinawa sedimentary and volcanic rocks.

The morphology details of the filamentous orpiment suggest that these filaments are either heavily mineralized fungal hyphae or pure abiogenic biomorphs. Although a fungal origin of the orpiment filaments cannot be unambiguously inferred, microbial activity (presence of carbonaceous matter) is detected at/around them. The filaments experienced temperature of 209.1±37.1°C which falls within the temperature range of the Daiyon-Yonaguni Knoll vent fluids and indicates that the carbonaceous matter on/within the filaments reached low to medium-grade thermal maturity.

Modeling of stability phase diagrams suggests that the stability of stibnite does not seem to depend on the vent fluid chlorinity, but rather on the vent fluid temperature: the area of stibnite stability increases with decreasing temperature of the vent fluid and results in stibnite precipitation at lower $\log_{10}a$ of $Sb_2S_4^{2-}$ and less reduced environment (i.e., high Eh, but still <0). Orpiment is stable in a wide range of $\log_{10}a$ of $H_2AsO_4^-$, in reduced conditions and at high S activity. The variations in vent fluid chlorinity and trace metal concentrations do not seem to affect the stability of orpiment. Barite is stable over a wide range of $\log_{10}a$ of Ba^{2+} and precipitates in slightly reduced to slightly oxic conditions.

Declaration of Competing Interest

The authors declare that they have no known competing financial interests or personal relationships that could have appeared to influence the work reported in this paper.

Acknowledgements

The successful completion of this work would not be possible without the valuable support of Dr. T. Tomiyama (JAMSTEC), who generously provided the hydrothermal deposit samples, Prof. Y. Takahashi (University of Tokyo), who gave us the possibility to perform the SEM studies in his lab, and Mrs. M. Otsuki (TUMSAT), who helped with the EMP analyses. We greatly appreciate their help. The suggestions and comments by two anonymous reviewers improved the paper significantly and are highly appreciated.

Supplementary data

Supplementary data to this article can be found online at Mendeley Data, V2, doi: 10.17632/r5twp9ftyy.2

References

Alibo, D.S., Nozaki, Y., 1999. Rare earth elements in seawater: particle association, shale-normalization, and Ce oxidation. Geochim. Cosmochim. Acta 63, 363-372.

Alt, J.C., Teagle, D.A.H., Brewer, T.S., Shanks, W.C. III, Halliday, A.N., 1998. Alteration and mineralization of an oceanic forearc and the ophiolite-ocean crust analogy. J. Geophys. Res. 103, 12,365-12,380.

Aries, S., Valladon, M., Polvé, M., Dupré, B., 2000. A routine method for oxide and hydroxide interference corrections in ICP-MS chemical analysis of environmental and geological samples. Geostand. Newsl. 24, 19-31.

Arnold, M., Sheppard, S.M.F., 1981. East Pacific Rise at latitude 21°N: isotopic composition and origin of the hydrothermal sulfur. Earth Planet. Sci. Lett. 56, 148-156.

Bau, M., Dulski, P., 1999. Comparing yttrium and rare earths in hydrothermal fluids from the Mid-Atlantic Ridge: Implications for Y and REE fractionation during near-vent mixing and for the Y/Ho ratio of Proterozoic seawater. Chem. Geol. 155, 77-90.

Bau, M., Koschinsky, A., 2009. Oxidative scavenging of cerium on hydrous Fe oxide: evidence from the distribution of rare earth elements and yttrium between Fe oxides and Mn oxides in hydrogenetic ferromanganese crusts. Geochem. J. 43, 37-47.

Bau, M., Schmidt, K., Koschinsky, A., Hein, J., Kuhn, T., Usui, A., 2014. Discriminating between different genetic types of marine ferro-manganese crusts and nodules based on rare earth elements and yttrium. Chem. Geol. 381, 1-9.

Bentahila, Y., Ben Othman, D., Luck, J.-M., 2008. Strontium, lead and zinc isotopes in marine cores as tracers of sedimentary provenance: A case study around Taiwan orogen. Chem. Geol. 248, 62-82.

Bethke, C.M., 2008. Geochemical and Biogeochemical Reaction Modeling. Cambridge University Press, New York, 547 p.

Bluth, G.J., Ohmoto, H., 1988. Sulfide-sulfate chimneys on the East Pacific Rise, 11° and 13°N latitudes. Part II: Sulfur isotopes. Can. Mineral. 26, 505-515.

Bowers, T.S., Campbell, A.C., Measures, C.I., Spivack, A.J., Khadem, M., Edmond, J., 1988. Chemical controls on the composition of vent fluids at 13°-11°N and 21°N, East Pacific Rise. J. Geophys. Res. 93, 4522-4536.

Breuer, C., Pichler, T., 2013. Arsenic in marine hydrothermal fluids. Chem. Geol. 348, 2-14.

Butler, I.B., Fallick, A.E., Nesbitt, R.W., 1998. Mineralogy, sulphur isotope geochemistry and the development of sulphide structures at the Broken Spur hydrothermal vent site, 29°10´N, Mid-Atlantic Ridge. J. Geol. Soc. London 155, 773-785.

Butterfield, D.A., Massoth, G.J., McDuff, R.E., Lupton, J.E., Lilley, M.D., 1990. Geochemistry of hydrothermal fluids from Axial Seamount Hydrothermal Emissions Study vent field, Juan de Fuca Ridge: Subseafloor boiling and subsequent fluid-rock interaction. J. Geophys. Res. 95, B8, 12895-12921.

Butterfield, D.A., McDuff, R.E., Franklin, J., Wheat, C.G., 1994. Geochemistry of hydrothermal vent fluids from Middle Valley, Juan de Fuca Ridge. In: Mottl, M.J., Davis, E.E., Fisher, A.T., and Slack, J.F. (Eds.), Proceedings of the Ocean Drilling Program, Scientific Results 139, 395-410.

Campbell, A.C., Bowers, T.S., Measures, C.I., Falkner, K.K., Khadem, M., Edmond, J.M., 1988. A time series of vent fluid compositions from 21°N East Pacific Rise (1979, 1981, 1985) and the Guaymas Basin, Gulf of California (1982, 1985). J. Geophys. Res. 93, 4537-4549.

Chen, J.H., Wasserburg, G.J., Von Damm, K.L., Edmond, J.M., 1986. The U-Th-Pb systematics in hot springs on the East Pacific Rise at 21°N and in the Guaymas Basin. Geochim. Cosmochim. Acta 50, 2467-2479.

Chen, Z., Zeng, Z., Yin, X., Wang, X., Zhang, Y., Chen, S., Shu, Y., Guo, K., Li, X., 2019. Petrogenesis of highly fractionated rhyolites in the southwestern Okinawa Trough: Constraints from whole-rock geochemistry data and Sr-Nd-Pb-O isotopes. Geol. J. 54, 316-332.

Corliss, J.B., Dymond, J., Gordon, L.I., Edmon, J.M., Von Herzen, R.P., Ballard, R.D., Green, K., Williams, D., Bainbridge, A., Crane, K., Van Andell, T.H., 1979. Submarine thermal springs on the Galapagos Rift. Science 203, 1073-1083.

Dekov, V.M., Savelli, C., 2004. Hydrothermal activity in the SE Tyrrhenian Sea: An overview of 30 years of research. Mar. Geol. 204, 161-185.

Dekov, V.M., Bindi, L., Burgaud, G., Petersen, S., Asael, D., Rédou, V., Fouquet, Y., Pracejus, B., 2013. Inorganic and biogenic As-sulfide precipitation at seafloor hydrothermal fields. Mar. Geol. 342, 28-38.

954 de Ronde, C.E.J., Hannington, M.D., Stoffers, P., Wright, I.C., Ditchburn, R.G., Reyes, A.G., Baker, E.T., Massoth,
955 G.J., Lupton, J.E., Walker, S.L., Greene, R.R., Soong, C.W.R., Ishibashi, J., Lebon, G.T., Bray, C.J., Resing,
956 J.A., 2005. Evolution of a submarine magmatic-hydrothermal system: Brothers volcano, southern Kermadec
957 Arc, New Zealand. Econ. Geol. 100, 1097-1133.
958 de Ronde, C.E.J., Massoth, G.J., Butterfield, D.A., Christenson, B.W., Ishibashi, J., Ditchburn, R.G., Hannington,
959 M.D., Brathwaite, R.L., Lupton, J.E., Kamenetsky, V.S., Graham, I.J., Zellmer, G.F., Dziak, R.P., Embley,
960 R.W., Dekov, V.M., Munnik, F., Lahr, J., Evans, L.J., Takai, K., 2011. Submarine hydrothermal activity and
961 gold-rich mineralization at Brothers Volcano, Kermadec Arc, New Zealand. Miner. Deposita 46, 541-584.
962 Douville, E., Bienvenu, P., Charlou, J.L., Donval, J.P., Fouquet, Y., Appriou, P., Gamo, T., 1999a. Yttrium and rare
963 earth elements in fluids from various deep-sea hydrothermal systems. Geochim. Cosmochim. Acta 63, 627-
964 643.
965 Douville, E., Charlou, J.L., Donval, J.P., Hureau, D., Appriou, P., 1999b. As and Sb behaviour in fluids from various
966 deep-sea hydrothermal systems. C. R. Acad. Sci. Paris, Sciences de la terre et des planètes 328, 97-104.
967 Duckworth, R.C., Knott, R., Fallick, A.E., Rickard, D., Murton, B.J., van Dover, C., 1995. Mineralogy and sulphur
968 isotope geochemistry of the Broken Spur sulphides, 29°N, Mid-Atlantic Ridge. In: Parson, L.M., Walker,
969 C.L., Dixon, D.R. (Eds.), Hydrothermal Vents and Processes. Geol. Soc. Spec. Publ. 87, 175-189.
970 Edmond, J.M., Measures, C.I., McDuff, R.E., Chan, L.H., Collier, R., Grant, B., Gordon, L.I., Corliss, J.B., 1979.
971 Ridge crest hydrothermal activity and the balance of the major and minor elements in the ocean: The
972 Galapagos data. Earth Planet. Sci. Lett. 46, 1-18.
973 Edmonds, H.N., German, C.R., 2004. Particle geochemistry in the Rainbow hydrothermal plume, Mid-Atlantic
974 Ridge. Geochim. Cosmochim. Acta 68, 759-772.
975 Feely, R.A., Geiselman, T.L., Baker, E.T., Massoth, G.J., Hammond, S.R., 1990. Distribution and composition of
976 hydrothermal plume particles from the ASHES Vent Field at Axial Volcano, Juan de Fuca Ridge. J. Geophys.
977 Res. Solid Earth 95, 12855-12873.
978 Ferrari, A.C., Robertson, J., 2000. Interpretation of Raman spectra of disordered and amorphous carbon. Phys. Rev.
979 B 61, 14095.
980 Findlay, A.J., Gartman, A., Shaw, T.J., Luther, G.W., 2015. Trace metal concentration and partitioning in the first
981 1.5 m of hydrothermal vent plumes along the Mid-Atlantic Ridge: TAG, Snakepit, and Rainbow. Chem. Geol.
982 412, 117-131.
983 Firstova, A., Stepanova, T., Cherkashov, G., Goncharov, A., Babaeva, S., 2016. Composition and formation of
984 gabbro-peridotite hosted seafloor massive sulfide deposits from the Ashadze-1 hydrothermal field, Mid-
985 Atlantic Ridge. Minerals 6, 19.
986 Fouquet, Y., Auclair, G., Cambon, P., Etoubleau, J., 1988. Geological setting, mineralogical, and geochemical
987 investigations on sulfide deposits near 13°N on the East Pacific Rise. Mar. Geol. 84, 145-178.
988 Fouquet, Y., Von Stackelberg, U., Charlou, J.-L., Erzinger, J., Herzig, P.M., Mühe, R., Wiedicke, M., 1993a.
989 Metallogenesis in back-arc environments: The Lau Basin example. Econ. Geol. 88, 2154-2181.

Fouquet, Y., Wafik, A., Cambon, P., Mevel, C., Meyer, G., Gente, P., 1993b. Tectonic setting and mineralogical and geochemical zonation in the Snake Pit sulfide deposit (Mid-Atlantic Ridge at 23° N). Econ. Geol. 88, 2018-2036.

Fouquet, Y., Knott, R., Cambon, P., Fallick, A., Rickard, D., Desbruyeres, D., 1996. Formation of large sulfide mineral deposits along fast spreading ridges. Example from off-axial deposits at 12°43´N on the East Pacific Rise. Earth Planet. Sci. Lett. 144, 147-162.

Fouquet, Y., Cambon, P., Etoubleau, J., Charlou, J.L., Ondréas, H., Barriga, F.J.A.S., Cherkashov, G., Semkova, T., Poroshina, I., Bohn, M., Donval, J.P., Henry, K., Murphy, P., Rouxel, O., 2010. Geodiversity of hydrothermal processes along the Mid-Atlantic Ridge and ultramafic-hosted mineralization: A new type of oceanic Cu-Zn-Co-Au volcanogenic massive sulfide deposit. In: Rona, P.A., Devey, C.W., Dyment, J., Murton, B.J. (Eds.), Diversity of Hydrothermal Systems on Slow Spreading Ocean Ridges. Geophysical Monograph 188, 321-367.

Fuchs, S., Hannington, M.D., Petersen, S., 2019. Divining gold in seafloor polymetallic massive sulfide systems. Miner. Deposita 54, 789-820.

Fujiwara, T., Toyoda, S., Uchida, A., Ishibashi, J., Nakai, S., Takamasa, A., 2015. ESR dating of barite in sea-floor hydrothermal sulfide deposits in the Okinawa Trough. In: Ishibashi, J., et al. (Eds), Subseafloor Biosphere Linked to Hydrothermal Systems: TAIGA Concept, pp. 369-386.

Gamo, T., Sakai, H., Kim, E-S., Shitashima, K., Ishibashi, J.-I., 1991. High alkalinity due to sulfate reduction in the CLAM hydrothermal field, Okinawa Trough. Earth Planet. Sci. Lett. 107, 328-338.

Gemmell, J.B., Sharpe, R., 1998. Detailed sulfur-isotope investigation of the TAG hydrothermal mound and stockwork zone, 26°N, Mid-Atlantic Ridge. In: Herzig, P.M., Humphris, S.E., Miller, D.J., Zierenberg, R.A. (Eds.), Proc. ODP, Sci. Results, College Station, TX, 158, pp. 71-84.

Gena, K., Chiba, H., Kase, K., 2005. Tin-bearing chalcopyrite and platinum-bearing bismuthinite in the active Tiger chimney, Yonaguni Knoll IV seafloor hydrothermal system, South Okinawa Trough, Japan. Earth Science Reports, Okayama University 12, 1-5.

German, C.R., Von Damm, K.L., 2003. Hydrothermal processes. In: Turekian, K.K., Holland, H.D. (Eds), *Treatise on Geochemistry*, Vol. 6 The Oceans and Marine Geochemistry, Elsevier, Oxford, pp. 181-222.

Glasby, G.P., Notsu, K., 2003. Submarine hydrothermal mineralization in the Okinawa Trough, SW of Japan: an overview. Ore Geol. Rev. 23, 299-339.

Godelitsas, A., Price, R.E., Pichler, T., Amend, J., Gamaletsos, P., Göttlicher, J., 2015. Amorphous As-sulfide precipitates from the shallow-water hydrothermal vents off Milos Island (Greece). Mar. Chem. 177, 687-696.

Guo, K., Zhai, S., Yu, Z., Wang, S., Zhang, X., Wang, X., 2018. Geochemical and Sr-Nd-Pb-Li isotopic characteristics of volcanic rocks from the Okinawa Trough: Implications for the influence of subduction components and the contamination of crustal materials. J. Mar. Syst. 180, 140-151.

Haas, J.R., Shock, E.L., Sassani, D.C., 1995. Rare earth elements in hydrothermal systems: Estimates of standard partial molal thermodynamic properties of aqueous complexes of the rare earth elements at high pressures and temperatures. Geochim. Cosmochim. Acta 59, 4329-4350.

Halbach, P., Pracejus, B., Märten, A., 1993. Geology and mineralogy of massive sulfide ores from the central Okinawa Trough, Japan. Econ. Geol. 88, 2210-2225.

Hannington, M.D., Scott, S.D., 1988. Mineralogy and geochemistry of an hydrothermal silica-sulfide-sulfate spire in the caldera of Axial-Seamount, Juan de Fuca Ridge. Can. Mineral. 26, 603-625.

Hannington, M., Herzig, P., Scott, S., Thompson, G., Rona, P., 1991. Comparative mineralogy and geochemistry of gold-bearing sulfide deposits on the mid-ocean ridges. Mar. Geol. 101, 217-248.

Hart, S.R., 1984. A large-scale isotope anomaly in the Southern Hemisphere mantle. Nature 309, 753-757.

Haymon, R.M., Kastner, M., 1981. Hot spring deposits on the East Pacific Rise at 21°N: Preliminary descriptions of mineralogy and genesis. Earth Planet. Sci. Lett. 53, 363-381.

Hekinian, R., Fevrier, H., Bischoff, J.L., Picot, P., Shanks, W.C., 1980. Sulfide deposits from the East Pacific Rise near 21°N. Science 207, 1433-1444.

Herzig, P.M., Hannington, M.D., 1995. Polymetallic massive sulfides at the modern seafloor: A review. Ore Geol. Rev. 10, 95-115.

Herzig, P.M., Petersen, S., Hannington, M.D., 1998. Geochemistry and sulfur-isotopic composition of the TAG hydrothermal mound, Mid-Atlantic Ridge, 26°N. In: Herzig, P.M., Humphris, S.E., Miller, D.J., Zierenberg, R.A. (Eds.), Proc. ODP, Sci. Results, College Station, TX, 158, pp. 47-70.

Herzig, P.M., Petersen, S., Kuhn, T., Hannington, M.D., Gemmell, J.B., Skinner, A.C., 2003. Shallow drilling of seafloor hydrothermal systems: The missing link. In: Eliopoulos, D., et al. (Eds), Mineral Exploration and Sustainable Development, Millpress, Rotterdam. pp. 103-105.

Hirata, N., Kinoshita, H., Katao, H., Baba, H., Kaiho, Y., Koresawa, S., Ono, Y., Hayashi, K., 1991. Report on DELP 1988 cruises in the Okinawa Trough part 3. Crustal structure of the southern Okinawa Trough. Bull. ERI Univ. Tokyo 66, 37-70.

Hongo, Y., Obata, H., Gamo, T., Nakaseama, M., Ishibashi, J., Konno, U., Saegusa, S., Ohkubo, S., Tsunogai, U., 2007. Rare earth elements in the hydrothermall system at Okinawa Trough back-arc basin. Geochem. J. 41, 1-15.

Hsu, S.-C., Lin, F.-J., Jeng, W.-L., Chung, Y.-C., Shaw, L.-M., 2003. Hydrothermal signatures in the southern Okinawa Trough detected by the sequential extraction of settling particles. Mar. Chem. 84, 49-66.

Iizasa, K., Fiske, R.S., Ishizuka, O., Yuasa, M., Hashimoto, J., Ishibashi, J., Naka, J., Horii, Y., Fujiwara, Y., Imai, A., Koyama, S., 1999. A Kuroko-type polymetallic sulfide deposit in a submarine silicic caldera. Science 283, 975-977.

Imai, N., Terashima, S., Itoh, S., Ando, A., 1995. 1994 compilation of analytical data for minor and trace elements in seventeen GSJ geochemical reference samples, "igneous rock series". Geostandard Newslett. 19, 135-213.

Ishibashi, J., Ikegami, F., Tsuji, T., Urabe, T., 2015. Hydrothermal activity in the Okinawa Trough Back-Arc Basin: geological background and hydrothermal mineralization. In: Ishibashi, J. (Ed.), Subseafloor Biosphere Linked to Hydrothermal Systems: TAIGA Concept. Springer, New York, pp. 337-359.

Jamieson, J.W., Hannington, M.D., Tivey, M.K., Hansteen, T., Williamson, N.M.-B., Stewart, M., Fietzke, J., Butterfield, D., Frische, M., Allen, L., Cousens, B., Langer, J., 2016. Precipitation and growth of barite within

hydrothermal vent deposits from the Endeavour Segment, Juan de Fuca Ridge. Geochim. Cosmochim. Acta 173, 64-85.

Kamenov, G.D., Mueller, P., Perfit, M., 2004. Optimization of mixed Pb-Tl solutions for high precision isotopic analyses by MC-ICP-MS. J. Anal. At. Spectrom 19, 1262-1267.

Kase, K., Yamamoto, M., Shibata, T., 1990. Copper-rich sulfide deposit near 23°N, Mid-Atlantic Ridge: chemical composition, mineral chemistry, and sulfur isotopes. In: Detrick, R., Honnorez, J., Bryan, W.B., Juteau, T., et al. (Eds.), Proc. ODP, Sci. Results, College Station, TX, 106/109, pp. 163-177.

Kato, Y., Ohta, I., Tsunematsu, T., Watanabe, Y., Isozaki, Y., Maruyama, S., Imai, N., 1998. Rare earth element variations in mid-Archean banded iron formations: Implications for the chemistry of ocean and continent and plate tectonics. Geochim. Cosmochim. Acta 62, 3475-3497.

Kato, Y., Nakao, K., Isozaki, Y., 2002. Geochemistry of Late Permian to Early Triassic pelagic cherts from southwest Japan: implications for an oceanic redox change. Chem. Geol. 182, 15-34.

Kato, Y., Fujinaga, K., Suzuki, K., 2005. Major and trace element geochemistry and Os isotopic composition of metalliferous umbers from the Late Cretaceous Japanese accretionary complex. Geochem. Geophys. Geosyst. 6, Q07004.

Kawasumi, S., Chiba, H., Ishibashi, J., 2016. Sulfur systematics in the Izena Hole seafloor hydrothermal systems, Okinawa Trough: Stable isotope, mineralogy and redox equilibria. Japan Geoscience Union meeting 2016, May 22-26, Makuhari Messe.

Kerridge, J.F., Haymon, R.M., Kastner, M., 1983. Sulfur isotope systematics at the 21°N site, East Pacific Rise. Earth Planet. Sci. Lett. 66, 91-100.

Kim, J., Lee, I., Lee, K.-Y., 2004. S, Sr, and Pb isotopic systematic of hydrothermal chimney precipitates from the Eastern Manus Basin, western Pacific: Evaluation of magmatic contribution to hydrothermal system. J. Geophys. Res. 109, B12210, doi:10.1029/2003JB002912.

Kim, J., Lee, K.-Y., Kim, J.-H., 2011. Metal-bearing molten sulfur collected from a submarine volcano: Implications for vapor transport of metals in seafloor hydrothermal systems. Geology 39, 351-354.

Kimura, M., Kaneoka, I., Kato, Y., Yamamoto, S., Kushiro, I., Tokuyama, H., Kinoshita, H., Isezaki, N., Masaki, H., Ishida, A., Uyeda, S., Hilde, T.W.C., 1986. Report on DELP 1984 Cruise in the Middle Okinawa Trough-5: topography and geology of the central grabens and their vicinity. Bull. Earth. Res. Inst. Univ. Tokyo 61, 269-310.

Klevenz, V., Bach, W., Schmidt, K., Hentscher, M., Koschinsky, A., Petersen, S., 2011. Geochemistry of vent fluid particles formed during initial hydrothermal fluid–seawater mixing along the Mid-Atlantic Ridge. Geochem. Geophys. Geosyst. 12, Q0AE05.

Klingelhoefer, F., Lee, C.-S., Lin, J.-Y., Sibuet, J.-C., 2009. Structure of the southernmost Okinawa Trough from reflection and wide-angle seismic data. Tectonophysics 446, 281-288.

Klinkhammer, G.P., Elderfield, H., Edmond, J.M., Mitra, A., 1994. Geochemical implications of rare earth element patterns in hydrothermal fluids from mid-ocean ridges. Geochim. Cosmochim. Acta 58, 5105-5113.

Knott, R., Fallick, A.E., Rickard, D., Bäcker, H., 1995. Mineralogy and sulphur isotope characteristics of a massive sulphide boulder, Galapagos Rift, 85°55´W. In: Parson, L.M., Walker, C.L., Dixon, D.R. (Eds.), Hydrothermal Vents and Processes. Geol. Soc. Spec. Pub. 87, 207-222.

Konno, U., Tsunogai, U., Nakagawa, F., Nakaseama, M., Ishibashi, J.-I., Nunoura, T., Nakamura, K., 2006. Liquid CO_2 venting on the seafloor: Yonaguni Knoll IV hydrothermal system, Okinawa Trough. Geophys. Res. Lett. 33, L16607.

Koschinsky, A., Seifert, R., Halbach, P., Bau, M., Brasse, S., de Carvalho, L.M., Fonseca, N.M., 2002. Geochemistry of diffuse low-temperature hydrothermal fluids in the North Fiji basin. Geochim. Cosmochim. Acta 66, 1409-1427.

Koski, R.A., Clague, D.A., Oudin, Ë., 1984. Mineralogy and chemistry of massive sulfide deposits from the Juan de Fuca Ridge. Geol. Soc. Am. Bull. 95, 930-945.

Koski, R.A., Shanks, W.C. III, Bohrson, W.A., Oscarson, R.L., 1988. The composition of massive sulfide deposits from the sediment-covered floor of Escanaba Trough, Gorda Ridge: Implications for depositional processes. Can. Mineral. 26, 655-674.

Kouketsu, Y., Mizukami, T., Mori, H., Endo, S., Aoya, M., Hara, H., Nakamura, D., Wallis, S., 2014. A new approach to develop the Raman carbonaceous material geothermometer for low-grade metamorphism using peak width. Island Arc 23, 33-50.

Kusakabe, M., Mayeda, S., Nakamura, E., 1990. S, O and Sr isotope systematics of active vent materials from the Mariana backarc basin spreading axis at 18°N. Earth Planet. Sci. Lett. 100, 275-282.

Kusakabe, M., Komoda, Y., Takano, B., Abiko, T., 2000. Sulfur isotopic effects in the disproportionation reaction of sulfur dioxide in hydrothermal fluids: implications for the $\delta^{34}S$ variations of dissolved bisulfate and elemental sulfur from active crater lakes. J. Volcanol. Geotherm. Res. 97, 287-307.

Labidi, J., Cartigny, P., Birck, J.L., Assayag, N., Bourrand, J.J., 2012. Determination of multiple sulfur isotopes in glasses: A reappraisal of the MORB $\delta^{34}S$. Chem. Geol. 334, 189-198.

Lovley, D.R., Phillips, E.J.P., Gorby, Y.A., Landa, E.R., 1991. Microbial reduction of uranium. Nature 350, 413-416.

Lu, Y., Makishima, A., Nakamura, E., 2007. Coprecipitation of Ti, Mo, Sn and Sb with fluorides and application to determination of B, Ti, Zr, Nb, Mo, Sn, Sb, Hf and Ta by ICP-MS. Chem. Geol. 236, 13-26.

Lüders, V., Pracejus, B., Halbach, P., 2001. Fluid inclusion and sulfur isotope studies in probable modern analogue Kuroko-type ores from the JADE hydrothermal field (Central Okinawa Trough, Japan). Chem. Geol. 173, 45-58.

Ludford, E.M., Palmer, M.R., German, C.R., Klinkhammer, G.P., 1996. The geochemistry of Atlantic hydrothermal particles. Geophys. Res. Lett. 23, 3503-3506.

Ma, L., Xi, S., Zhang, X., Luan, Z., Du, Z., Li, L., Yan, J., 2021. Influence of vapor-phase fluids on the geochemical characterization of hydrothermal sulfides in the shimmering waters of the southern Okinawa Trough. Ore Geol. Rev. 139, 104496.

Makishima, A., Nakamura, E., 2006. Determination of major/minor and trace elements in silicate samples by ICP-QMS and ICP-SFMS applying isotope dilution-internal standardization (ID-IS) and multi-stage internal standardisation. Geostand. Geoanalytical Res. 30, 245-271.

Marchig, V., Puchelt, H., Rösch, H., Blum, N., 1990. Massive sulfides from ultra-fast spreading ridge, East Pacific Rise at 18-21°S: A geochemical stock report. Mar. Mining 9, 459-493.

Marumo, K., Urabe, T., Goto, A., Takano, Y., Nakaseama, M., 2008. Mineralogy and isotope geochemistry of active submarine hydrothermal field at Suiyo Seamount, Izu-Bonin Arc, West Pacific Ocean. Resource Geology 58, 220-248.

Matsumoto, T., Kinoshita, M., Nakamura, M., Sibuet, J.-C., Lee, C.-S., Hsu, S.-K., Oomori, T., Shinjo, R., Hashimoto, Y., Hosoya, S., Imamura, M., Ito, M., Tukuda, K., Yagi, H., Tatekawa, K., Kagaya, I., Hokakubo, S., Okada, T., Kimura, M., 2001. Volcanic and hydrothermal activities and possible "segmentation" of the axial rifting in the westernmost part of the Okinawa Trough – preliminary results from the YOKOSUKA/SHINKAI 6500 Lequios Cruise, JAMSTEC Journal of Deep-Sea Research 19, 95-107. (in Japanese with English abstract).

McDonough, W.F., Sun, S.-s., 1995. The composition of the Earth. Chem. Geol. 120, 223-253.

Melekestseva, I.Yu., 2010. Sulfur isotopic composition of massive sulfides from the Semenov hydrothermal cluster, 13°31´N, MAR. Minerals of the Ocean-5 and Deep-Sea Minerals and Mining-2 Joint International Conference, St. Petersburg, Russia, 28 June – 01 July 2010, Abstract Volume, pp. 70-73.

Michard, A., 1989. Rare earth element systematics in hydrothermal fluids. Geochim. Cosmochim. Acta 53, 745-750.

Michard, A., Albarède, F., 1985. Hydrothermal uranium uptake at ridge crests. Nature 317, 244-246.

Michard, A., Albarède, F., 1986. The REE content of some hydrothermal fluids. Chem. Geol. 55, 51-60.

Michard, G., Albarède, F., Michard, A., Minster, J.F., Charlou, J.L., 1983. Rare-earth elements and uranium in high-temperature solutions from East Pacific Rise hydrothermal vent field (13 °N). Nature 303, 795-797.

Michard, G., Albarède, F., Michard, A., Minster, J.-F., Charlou, J.-L., Tan, N., 1984. Chemistry of solutions from the 13°N East Pacific Rise hydrothermal site. Earth Planet. Sci. Lett. 67, 297-307.

Mills, R.A., Thomson, J., Elderfield, H., Hinton, R.W., Hyslop, E., 1994. Uranium enrichment in metalliferous sediments from the Mid-Atlantic Ridge. Earth Planet. Sci. Lett. 124, 35-47.

Minami, T., Konagaya, W., Zheng, L., Takano, S., Sasaki, M., Murata, R., Nakaguchi, Y., Sohrin, Y., 2015. An off-line automated preconcentration system with ethylenediaminetriacetate chelating resin for the determination of trace metals in seawater by high-resolution inductively coupled plasma mass spectrometry. Anal. Chim. Acta 854, 183-190.

Nagumo, S., Kinoshita, H., Kasahara, J., Ouchi, T., Tokuyama, H., Asanuma, T., Koresawa, S., Akiyoshi, H., 1986. Report on DELP 1984 cruises in the middle Okinawa Trough part 2: seismic structural studies. Bull. ERI Univ. Tokyo 61, 167-202.

Nakashima, K., Sakai, H., Yoshida, H., Chiba, H., Tanaka, Y., Gamo, T., Ishibashi, J.-I., Tsunogai, U., 1995. Hydrothermal mineralization in the Mid-Okinawa Trough. In: Sakai, H., Nozaki, Y. (Eds), Biogeochemical Processes and Ocean Flux in the Western Pacific. Terra Scientific Publishing Company, Tokyo, pp. 487-508.

1172 Nedachi, M., Ueno, H., Oki, K., Shiga, Y., Hayasaka, S., Ossaka, J., Nogami, K., Ito, N., Hashimoto, J., 1991.
1173 Sulfide veinlets and the surrounding marine sediments in the fumarole area in the Wakamiko Caldera,
1174 northern Kagoshima Bay. JAMSTEC Journal of Deep-Sea Research 7, 235-243.
1175 Nishio, R., Chiba, H., 2012. Mineralogical and sulfur stable isotopic study of mineralization at the No.4 Yonaguni
1176 Knoll seafloor hydrothermal system, Okinawa Trough. Annual Meeting of the Geochemical Society of Japan,
1177 Abstracts, Geochemical Society of Japan, 59.
1178 Nozaki, Y., Alibo, D.S., Amakawa, H., Gamo, T., Hasumoto, H., 1999. Dissolved rare earth elements and
1179 hydrography in the Sulu Sea. Geochim. Cosmochim. Acta 63, 2171-2181.
1180 Nozaki, T., Ishibashi, J.-I., Shimada, K., Nagase, T., Takaya, Y., Kato, Y., Kawagucci, S., Watsuji, T., Shibuya, T.,
1181 Yamada, R., Saruhashi, T., Kyo, M., Takai, K., 2016. Rapid growth of mineral deposits at artificial seafloor
1182 hydrothermal vents. Scientific Reports 6, 22163.
1183 Ohmoto, H., Rye, R.O., 1979. Isotopes of sulfur and carbon. In: Barnes, H.L. (Ed.), Geochemistry of Hydrothermal
1184 Ore Deposits, Wiley, New York, pp. 509-567.
1185 Okamoto, K., Ishibashi, J.-I., Motomura, Y., Yamanaka, T., Fujikura, K., 2002. Mineralogical studies of
1186 hydrothermal deposits collected from the Daiyon-Yonaguni Knoll and the Hatoma Knoll in the Okinawa
1187 Trough. JAMSTEC Journal of Deep-Sea Research 21, 75-81. (in Japanese with English abstract).
1188 Ono, S., Shanks III, W.C., Rouxel, O.J., Rumble, D., 2007. S-33 constraints on the seawater sulfate contribution in
1189 modern seafloor hydrothermal vent sulfides. Geochim. Cosmochim. Acta 71, 1170-1182.
1190 Oshida, A., Tamaki, K., Kimura, M., 1992. Origin of the magnetic anomalies in the southern Okinawa Trough. J.
1191 Geomagn. Geoelectr. 44, 345-359.
1192 Oudin, Ë., 1983. Hydrothermal sulfide deposits of the East Pacific Rise (21° N). Part I: Descriptive mineralogy. Mar.
1193 Mining 4, 39-72.
1194 Paris, G., Sessions, A.L., Subhas, A.V., Adkins, J.F., 2013. MC-ICP-MS measurement of $\delta^{34}S$ and $\Delta^{33}S$ in small
1195 amounts of dissolved sulfate. Chem. Geol. 345, 50-61.
1196 Peter, J.M., Shanks, W.C. III, 1992. Sulfur, carbon, and oxygen isotope variations in submarine hydrothermal
1197 deposits of Guaymas Basin, Gulf of California, USA. Geochim. Cosmochim. Acta 56, 2025-2040.
1198 Peters, C., Strauss, H., Haase, K., Bach, W., de Ronde, C.E.J., Kleint, C., Stucker, V., Diehl, A., 2021. SO_2
1199 disproportionation impacting hydrothermal sulfur cycling: Insights from multiple sulfur isotopes for
1200 hydrothermal fluids from the Tonga-Kermadec intraoceanic arc and the NE Lau Basin. Chem. Geol. 586,
1201 120586.
1202 Peters, M., Strauss, H., Farquhar, J., Ockert, C., Eickmann, B., Jost, C.L., 2010. Sulfur cycling at the Mid-Atlantic
1203 Ridge: A multiple sulfur isotope approach. Chem. Geol. 269, 180-196.
1204 Peters, M., Strauss, H., Petersen, S., Kummer, N.-A., Thomazo, C., 2011. Hydrothermalism in the Tyrrhenian Sea:
1205 Inorganic and microbial sulfur cycling as revealed by geochemical and multiple sulfur isotope data. Chem.
1206 Geol. 280, 217-231.
1207 Petersen, S., 1992. Mineralogie und Geochemie goldführender Massivsulfide des Lau Back-Arc (Südwest-Pazifik).
1208 M.Sc. thesis, Aachen University of Technology, Aachen, Germany, 92 pp.

Petersen, S., Herzig, P.M., Hannington, M.D., Jonasson, I.R., Arribas, JR. A., 2002. Submarine gold mineralization near Lihir Island, New Ireland fore-arc, Papua New Guinea. Econ. Geol. 97, 1795-1813.

Petersen, S., Monecke, T., Westhues, A., Hannington, M.D., Gemmell, J.B., Sharpe, R., Peters, M., Strauss, H., Lackschewitz, K., Augustin, N., Gibson, H., Kleeberg, R., 2014. Drilling shallow-water massive sulfides at the Palinuro Volcanic Complex, Aeolian Island Arc, Italy. Econ. Geol. 109, 2129-2158.

Pokrovski, G.S., Escoda, C., Blanchard, M., Testemale, D., Hazemann, J.-L., Gouy, S., Kokh, M.A., Boiron, M.-C., de Parseval, F., Aigouy, T., Menjot, L., de Parseval, P., Proux, O., Rovezzi, M., Béziat, D., Salvi, S., Kouzmanov, K., Bartsch, T., Pöttgen, R., Doert, T., 2021. An arsenic-driven pump for invisible gold in hydrothermal systems. Geochem. Persp. Let. 17, 39-44.

Price, R.E., Planer-Friedrich, B., Savov, I.P., Pichler, T., 2009. Elevated concentrations of arsenic, predominance of thioarsenates, and orpiment precipitation on the seafloor at the marine shallow-water hydrothermal system off Milos Island, Greece. American Geophysical Union, Fall Meeting, abstract #B23E-0416.

Qu, Y., Engdahl, A., Zhu, S., Vajda, V., McLoughlin, N., 2015. Ultrastructural heterogeneity of carbonaceous material in ancient cherts: Investigating biosignature origin and preservation. Astrobiology 15, 825-842.

Rouxel, O., Fouquet, Y., Ludden, J.N., 2004. Copper isotope systematics of the Lucky Strike, Rainbow, and Logatchev sea-floor hydrothermal fields on the Mid-Atlantic Ridge. Econ. Geol. 99, 585-600.

Rytuba, J.J., 1984. Arsenic minerals as indicators of conditions of gold deposition in Carlin-type gold deposits. J. Geochem. Explor. 25, 237-238.

Seyfried, W.E., Ding, K., 1993. The effect of redox on the relative solubilities of copper and iron in Cl-bearing aqueous fluids at elevated temperatures and pressures: An experimental study with application to subseafloor hydrothermal systems. Geochim. Cosmochim. Acta 57, 1905-1917.

Shanks, W.C., 2001. Stable isotopes in seafloor hydrothermal systems: Vent fluids, hydrothermal deposits, hydrothermal alteration, and microbial processes. In: Valley, J.W., Cole, D.R. (Eds), Stable Isotope Geochemistry. Rev. Mineral. Geochem. 43, pp. 469-525.

Shanks, W.C. III, Bischoff, J.L., Rosenbauer, R.J., 1981. Seawater sulfate reduction and sulfur isotope fractionation in basaltic systems: Interaction of seawater with fayalite and magnetite at 200-350°C. Geochim. Cosmochim. Acta 45, 1977-1995.

Shanks, W.C. III, Koski, R.A., Woodruff, L.G., 1984. Mineralogy and stable isotope systematics of sulfide deposits from the Juan de Fuca Ridge. EOS 65, 1113.

Shanks, W.C. III, Seyfried, W.E. Jr., 1987. Stable isotope studies of vent fluids and chimney minerals, southern Juan de Fuca Ridge. Sodium metasomatism and seawater sulfate reduction. J. Geophys. Res. 92, 11387-11399.

Shikazono, N., 1994. Precipitation mechanisms of barite in sulfate-sulfide deposits in back-arc basins. Geochim. Cosmochim. Acta 58, 2203-2213.

Shikazono, N., Kusakabe, M., 1999. Mineralogical characteristics and formation mechanism of sulfate-sulfide chimneys from Kuroko area, Mariana Trough and mid-ocean ridges. Resour. Geol., Spec. Issue, 20, 1-12.

Shikazono, N., Kawabe, H., Ogawa, Y., 2012. Interpretation of mineral zoning in submarine hydrothermal ore deposits in terms of coupled fluid flow-precipitation kinetics model. Resour. Geol. 62, 352-368.

1246 Shinjo, R., Chung, S.-L., Kato, Y., Kimura, M., 1999. Geochemical and Sr-Nd isotopic characteristics of volcanic
1247 rocks from the Okinawa Trough and Ryukyu Arc: Implications for the evolution of a young intracontinental
1248 back arc basin. J. Geophys. Res. 104, 10591-10608.
1249 Shu, Y., Nielsen, S.G., Zeng, Z., Shinjo, R., Blusztajn, J., Wang, X., Chen, S., 2017. Tracing subducted sediment
1250 inputs to the Ryukyu arc-Okinawa Trough system: Evidence from thallium isotopes. Geochim. Cosmochim.
1251 Acta 217, 462-491.
1252 Sibuet, J.-C., Letouzey, J., Barbier, F., Charvet, J., Foucher, J.-P., Hilde, T., Kimura, M., Ling-Yun, C., Marsset, B.,
1253 Muller, C., Stephan, J.-F., 1987. Back arc extension in the Okinawa Trough. J. Geophys. Res. 92, 14041-
1254 14063.
1255 Skirrow, R., Coleman, M.L., 1982. Origin of sulfur and geothermometry of hydrothermal sulfides from the
1256 Galapagos Rift, 86°N. Nature 299, 142-144.
1257 Sohrin, Y., Urushihara, S., Nakatsuka, S., Kono, T., Higo, E., Minami, T., Norisuye, K., Umetani, S., 2008.
1258 Multielemental determination of GEOTRACES key trace metals in seawater by ICPMS after
1259 preconcentration using an ethylenediaminetriacetic acid chelating resin. Anal. Chem. 80, 6267-6273.
1260 Spiess, F.N., Macdonald, K.C., Atwater, T., Ballard, R., Carranza, A., Cordoba, D., Cox, C., Diaz Garcia, V.M.,
1261 Francheteau, J., Guerrero, J., Hawkins, J., Haymon, R., Hessler, R., Juteau, T., Kastner, M., Larson, R.,
1262 Luyendyk, B., Macdougall, J.D., Miller, S., Normark, W., Orcutt, J., Rangin, C., 1980. East Pacific Rise: hot
1263 springs and geophysical experiments. Science 207, 1421-1433.
1264 Stuart, F.M., Turner, G., Duckworth, R.C., Fallick, A.E., 1994. Helium isotopes as tracers of trapped hydrothermal
1265 fluids in ocean-floor sulfides. Geology 22, 823-826.
1266 Stuart, F.M., Harrop, P.J., Knott, R., Fallick, A.E., Turner, G., Fouquet, Y., Rickard, D., 1995. Noble gas isotopes in
1267 25 000 years of hydrothermal fluids from 13°N on the East Pacific Rise. In: Parson, L.M., Walker, C.L.,
1268 Dixon, D.R. (Eds.), Hydrothermal Vents and Processes. Geol. Soc. Spec. Publ. 87, 133-143.
1269 Styrt, M.M., Brackmann, A.J., Holland, H.D., Clark, B.C., Pisutha-Arnold, V., Eldridge, C.S., Ohmoto, H., 1981.
1270 The mineralogy and the isotopic composition of sulfur in hydrothermal sulfide/sulfate deposits on the East
1271 Pacific Rise, 21°N latitude. Earth Planet. Sci. Lett. 53, 382-390.
1272 Suzuki, R., Chiba, H., Ishibashi, J., Gena, K., 2005. Mineralogy and geochemistry of submarine hydrothermal
1273 deposits at the Dai-yon Yonaguni Knoll. Society of Resource Geology, 55th Annual Conference, Abstract
1274 with Program, P26.
1275 Suzuki, R., Ishibashi, J., Nakaseama, M., Konno, U., Tsunogai, U., Gena, K., Chiba, H., 2008. Diverse range of
1276 mineralization induced by phase separation of hydrothermal fluid: Case study of the Yonaguni Knoll IV
1277 hydrothermal field in the Okinawa Trough back-arc basin. Resour. Geol. 58, 267-288.
1278 Takaya, Y., Hiraide, T., Fujinaga, K., Nakamura, K., Kato, Y., 2014. A study on the recovery method of rare-earth
1279 elements from REY-rich mud toward the development and the utilization of REY-rich mud. J. MMIJ 130,
1280 104-114 (in Japanese with English abstract).
1281 Thompson, G., Mottl, M.J., Rona, P.A., 1985. Morphology, mineralogy and chemistry of hydrothermal deposits from
1282 the TAG area, 26°N Mid-Atlantic Ridge. Chem. Geol. 49, 243-257.

Tokunaga, M., Honma, H., 1974. Fluid inclusions in the minerals from some Kuroko deposits. Soc. Mining Geol. Jpn., Spec. Issue, 6, 385-388.

Trefry, J.H., Metz, S., 1989. Role of hydrothermal precipitates in the geochemical cycling of vanadium. Nature 342, 531-533.

Tsunogai, U., Toki, T., Nakayama, N., Gamo, T., Kato, H., Kaneko, S., 2003. WHATS: a new multi-bottle gas-tight sampler for seafloor vent fluids. Chikyukagaku (Geochemistry) 37, 101-109 (in Japanese).

Ueno, H., Hamasaki, H., Murakawa, Y., Kitazono, S., Takeda, T., 2003. Ore and gangue minerals of sulfide chimneys from the North Knoll, Iheya Ridge, Okinawa Trough, Japan. JAMSTEC J. Deep Sea Res. 22, 49-62.

Von Damm, K.L., 1990. Seafloor hydrothermal activity: Black smoker chemistry and chimneys. Annu. Rev. Earth Planet. Sci. 18, 173-204.

Von Damm, K.L., Bischoff, J.L., 1987. Chemistry of hydrothermal solutions from the Southern Juan de Fuca Ridge. J. Geophys. Res. 92, 11334-11346.

Von Damm, K.L., Lilley, M.D., 2004. Diffuse flow hydrothermal fluids from 9°50'N East Pacific Rise: Origin, evolution and biogeochemical controls. In: Wilcock, W.S.D., DeLong, E.F., Kelley, D.S., Baross, J.A., Cary, S.C. (Eds), The Subseafloor Biosphere at Mid-Ocean Ridges. Geophysical Monograph Series 144, American Geophysical Union, Washington, DC. pp. 245-268.

Von Damm, K.L., Edmond, J.M., Grant, B., Measures, C.I., Walden, B., Weiss, R.F., 1985a. Chemistry of submarine hydrothermal solutions at 21°N, East Pacific Rise. Geochim. Cosmochim. Acta 49, 2197-2220.

Von Damm, K.L., Edmond, J.M., Measures, C.I., Grant, B., 1985b. Chemistry of submarine hydrothermal solutions at Guaymas Basin, Gulf of California. Geochim. Cosmochim. Acta 49, 2221-2237.

Von Damm, K.L., Parker, C.M., Zierenberg, R.A., Lilley, M.D., Olson, E.J., Clague, D.A., McClain, J.S., 2005. The Escanaba Trough, Gorda Ridge hydrothermal system: Temporal stability and subseafloor complexity. Geochim. Cosmochim. Acta 69, 21, 4971-4984.

Webber, A.P., Roberts, S., Murton, B.J., Hodgkinson, M.R.S., 2015. Geology, sulfide geochemistry and supercritical venting at the Beebe Hydrothermal Vent Field, Cayman Trough. Geochem. Geophys. Geosyst. 16, 2661-2678.

Woodruff, L.G., Shanks, W.C., III., 1988. Sulfur isotope study of chimney minerals and vent fluids from 21°N, East Pacific Rise: Hydrothermal sulfur sources and disequilibrium sulfate reduction. J. Geophys. Res. 93, 4562-4572.

Yamanaka, T., Maeto, K., Akashi, H., Ishibashi, J.-I., Miyoshi, Y., Okamura, K., Noguchi, T., Kuwahara, Y., Toki, T., Tsunogai, U., Ura, T., Nakatani, T., Maki, T., Kubokawa, K., Chiba, H., 2013. Shallow submarine hydrothermal activity with significant contribution of magmatic water producing talc chimneys in the Wakamiko Crater of Kagoshima Bay, southern Kyushu, Japan. J. Volcanol. Geotherm. Res. 258, 74-84.

Yang, B., Liu, J., Shi, X., Zhang, H., Wang, X., Wu, Y., Fang, X., 2020. Mineralogy and sulfur isotope characteristics of metalliferous sediments from the Tangyin hydrothermal field in the southern Okinawa Trough. Ore Geol. Rev. 120, 103464.

Yasukawa, K., Liu, H., Fujinaga, K., Machida, S., Haraguchi, S., Ishii, T., Nakamura, K., Kato, Y., 2014. Geochemistry and mineralogy of REY-rich mud in the eastern Indian Ocean. J. Asian Earth Sci. 93, 25-36.

Yasukawa, K., Kino, S., Azami, K., Tanaka, E., Mimura, K., Ohta, J., Fujinaga, K., Nakamura, K., Kato, Y., 2020. Geochemical features of Fe-Mn micronodules in deep-sea sediments of the western North Pacific Ocean: Potential for co-product metal extraction from REY-rich mud. Ore Geol. Rev. 127, 103805.

Zeng, Z., Chen, Z., Qi, H., 2022. Two processes of anglesite formation and a model of secondary supergene enrichment of Bi and Ag in seafloor hydrothermal sulfide deposits. J. Mar. Sci. Eng. 10, 35.

Zierenberg, R.A., Shanks, W.C., III., Bischoff, J.L., 1984. Massive sulfide deposits at 21°N, East Pacific Rise: chemical composition, stable isotopes, and phase equilibria. Geol. Soc. Am. Bull. 95, 922-929.

Figure captions

Fig. 1. (A) Map of Ryukyu Trench-Arc system and Okinawa Trough with location of Daiyon-Yonaguni Knoll hydrothermal field (red solid square); (B) Detail map of the Daiyon-Yonaguni Knoll hydrothermal field with location of sample site (red solid dot).

Fig. 2. Studied samples from the Daiyon-Yonaguni Knoll hydrothermal field: (A) active hydrothermal chimney, sample 2K1271 L1 lower outer; (B) active hydrothermal chimney flange, sample 2K1271 L1 flange, outer top; (C) active hydrothermal chimney flange, sample 2K1271 L1 flange, center upper; (D) active hydrothermal chimney flange, sample 2K1271 L1 flange, outer bottom; (E) massive sulfide, sample 2K1267 L1; (F) massive sulfide, sample 2K1267 L2.

Fig. 3. Photomicrographs of stibnite, barite, and native sulfur from the Daiyon-Yonaguni Knoll hydrothermal deposits: (A) needle-like crystals of stibnite (Stb) (stereomicroscope, sample 2K1271 L1 flange, center upper); (B) thin, needle-like, radial crystals of stibnite (Stb) over prismatic, transparent crystals of barite (Bt) (thin polished section, optical microscope, transmitted plain polarized light, sample 2K1271 L1 flange, outer top); (C) rosettes of stibnite (Stb) radial crystals (SEM, SEI, sample 2K1271 L1 flange, outer top); (D) match box-like crystals of barite (Bt) (SEM, SEI, sample 2K1267 L1); (E) radial barite (Bt) crystals (dendritic barite) among coated by amorphous silica pyrite (Py) (SEM, SEI, sample 2K1267 L2); (F) rhombic crystals of native sulfur (SEM, SEI, sample 2K1267 L1).

Fig. 4. X-ray maps and BSE image of stibnite (Stb) within barite (Bt) matrix in the Daiyon-Yonaguni Knoll hydrothermal deposit (sample 2K1271 L1 flange, outer top): (A) X-ray scan in Sb *L*α; (B) X-ray scan in As *L*α; (C) X-ray scan in Ba *L*α; (D) X-ray scan in S *K*α; (E) BSE image. Color scales (right-hand side), elemental concentrations.

Fig. 5. Photomicrographs of orpiment from the Daiyon-Yonaguni Knoll hydrothermal deposits: (A) fillaments of orpiment (orange) (stereomicroscope, sample 2K1271 L1 flange, outer top); (B) colloform orpiment (red) (stereomicroscope, sample 2K1267 L1); (C) fillaments of orpiment among thin tabular crystals of barite (Bt) (SEM, SEI, sample 2K1267 L1); (D) colloform orpiment (SEM, SEI, sample 2K1267 L1); (E) cross-section of the filament-like orpiment shown at (C), note the concentric internal structure of the filaments (SEM, SEI, sample 2K1267 L1); (F) bunches of reddish-white barite (Bt) crystals partly covered by fine yellow orpiment (Op) crystals (thin polished section, optical microscope, reflected plain polarized light, sample 2K1271 L1 flange, outer top).

Fig. 6. X-ray maps and BSE image of orpiment (Op) over barite (Bt) crystals in the Daiyon-Yonaguni Knoll hydrothermal deposit (sample 2K1271 L1 flange, outer top): (A) X-ray scan in As *L*α; (B) X-ray scan in Sb *L*α; (C) X-ray scan in Ba *L*α; (D) X-ray scan in S *K*α; (E) BSE image. Color scales (right-hand side), elemental concentrations.

Fig. 7. CI chondrite-normalized (McDonough and Sun, 1995) REE distribution patterns of the studied hydrothermal deposits (A) and vent fluids (B) from the Daiyon-Yonaguni Knoll hydrothermal field (Okinawa Trough). NPDW = North Pacific Deep Water (Alibo and Nozaki, 1999).

Fig. 8. Sulfur-isotope composition (range) of selected hydrothermal deposits from mid-ocean ridges [unsedimented (mafic- and ultramafic-hosted) and sedimented], volcanic arcs and back-arc basins compared to those of studied stibnite-orpiment-containing deposits and vent fluids (sulfate S) from the Daiyon-Yonaguni Knoll hydrothermal field, Okinawa Trough. References: terrestrial

mantle (Labidi et al., 2012), seawater (Paris et al., 2013), Galapagos Rift (Skirrow and Coleman, 1982; Knott et al., 1995), 21°N EPR (Hekinian et al., 1980; Arnold and Sheppard, 1981; Styrt et al., 1981; Kerridge et al., 1983; Zierenberg et al., 1984; Woodruff and Shanks, 1988; Stuart et al., 1994), 11-13°N EPR (Bluth and Ohmoto, 1988; Stuart et al., 1995; Fouquet et al., 1996; Ono et al., 2007), 9-10°N EPR (Ono et al., 2007), 18-21°S EPR (Marchig et al., 1990; Ono et al., 2007), Lucky Strike (Rouxel et al., 2004; Ono et al., 2007), Broken Spur (Duckworth et al., 1995; Butler et al., 1998), TAG (Stuart et al., 1994; Gemmell and Sharpe, 1998; Herzig et al., 1998; Shanks, 2001), Snakepit (Kase et al., 1990; Stuart et al., 1994), Southern MAR (Peters et al., 2010), Rainbow (Rouxel et al., 2004), Logatchev (Rouxel et al., 2004; Peters et al., 2010), Semenov (Melekestseva, 2010), Red Sea (Shanks, 2001), Juan de Fuca (Shanks et al., 1984; Shanks and Seyfried, 1987; Hannington and Scott, 1988; Stuart et al., 1994), Escanaba Trough (Shanks, 2001), Guaymas Basin (Shanks, 2001), Okinawa Trough (Lüders et al., 2001; Ueno et al., 2003; Nishio and Chiba, 2012; Kawasumi et al., 2016; Yang et al., 2020), Izu-Bonin Arc (Alt et al., 1998), Mariana Trough (Kusakabe et al., 1990), Manus Basin (Kim et al., 2004), Lau Basin (Kim et al., 2011), Kermadec Arc (de Ronde et al., 2005; 2011), Aeolian Arc (Peters et al., 2011; Petersen et al., 2014).

Fig. 9. Pb isotope data for the studied Daiyon-Yonaguni Knoll (DYK) hydrothermal (hydroT) deposits compared to DYK hydrothermal Pb minerals (galena and anglesite) (Zeng et al., 2022), southern Okinawa Trough (SOT) sulfides (Ma et al., 2021), and southern (S) Okinawa and Ryukyu sediments and lavas (Bentahila et al., 2008; Shu et al., 2017; Chen et al., 2019). Dotted line is the Northern Hemisphere Reference Line (NHRL), after Hart (1984). Note that the studied DYK hydrothermal deposits form a trend from the DYK Pb hydrothermal minerals to the regional lavas and one sample extending to much lower $^{207}Pb/^{204}Pb$ and $^{208}Pb/^{204}Pb$ toward the NHRL, for more discussion see the text.

Fig. 10. (A) Photomicrograph (stereomicroscope) of orpiment from the Daiyon-Yonaguni Knoll hydrothermal deposits (sample 2K1267 L1) with positions (B, C) of the sub-samples analyzed by Raman spectroscopy (see Raman spectra at panels B and C); (B) Raman spectrum of light orange filamentous orpiment containing carbonaceous matter with characteristic D and G bands in the

first-order region, and bands in the second-order region; (C) Raman spectrum of dark red colloform orpiment surrounding the filamentous orpiment. Raman intensity in arbitrary units (a.u.).

Fig. 11. ESEM image (A) and EDS spectra (B: spectrum 136) and (C: spectrum 137) showing the distribution of carbon as indicative of carbonaceous matter associated with the orpiment filaments (note, the major elements are As and S).

Fig. 12. Stability phase diagrams for the chemical species (dissolved and solid) in the three selected vent fluids from the Daiyon-Yonaguni Knoll hydrothermal field: (A), (B) and (C) - Eh-$\log_{10}$a diagrams calculated for $Sb_2S_4^{2-}$; (D), (E) and (F) - Eh-$\log_{10}$a diagrams calculated for $H_2AsO_4^-$; (G), (H) and (I) - Eh-$\log_{10}$a diagrams calculated for Ba^{2+}.

Figure 1

Click here to access/download;Figure;stibnite-Fig. 1.tif

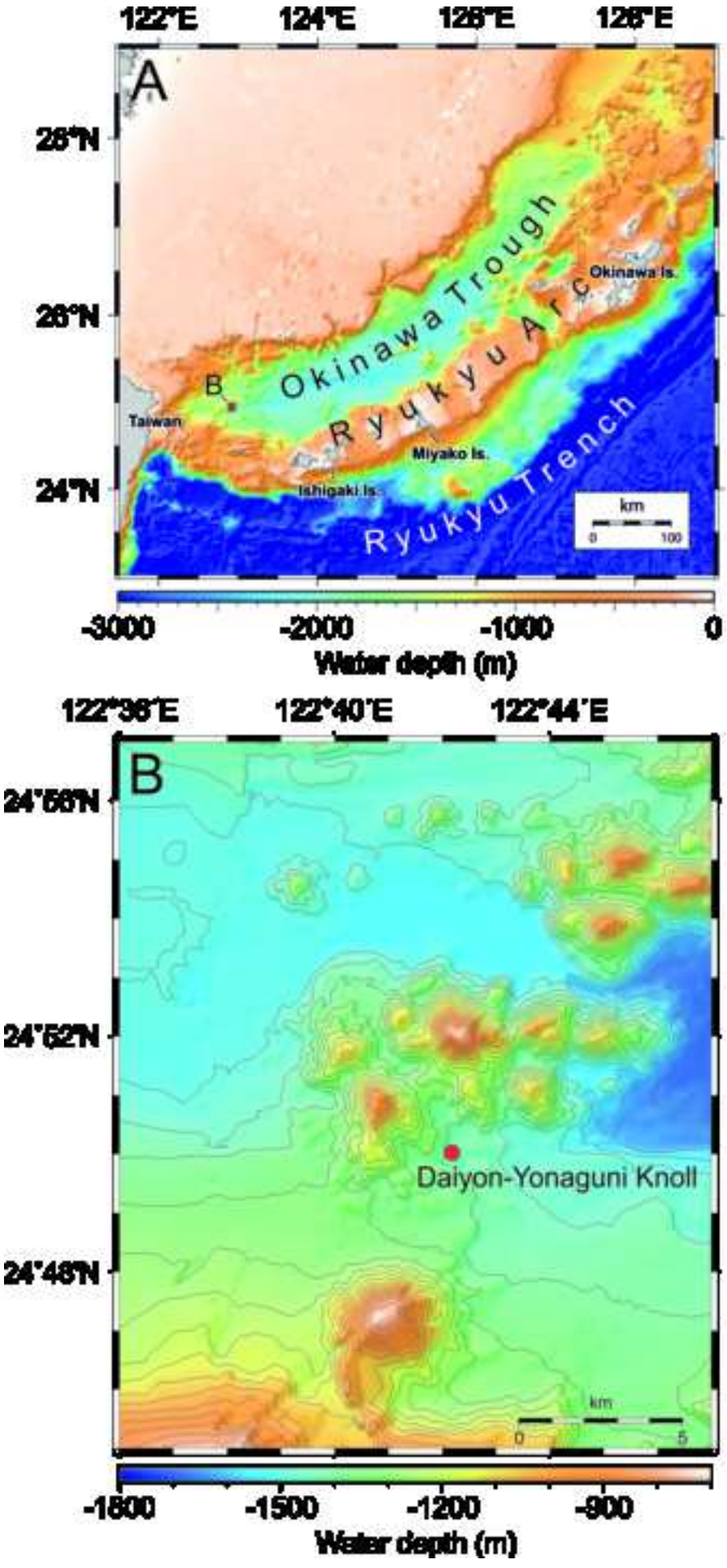

Figure 2

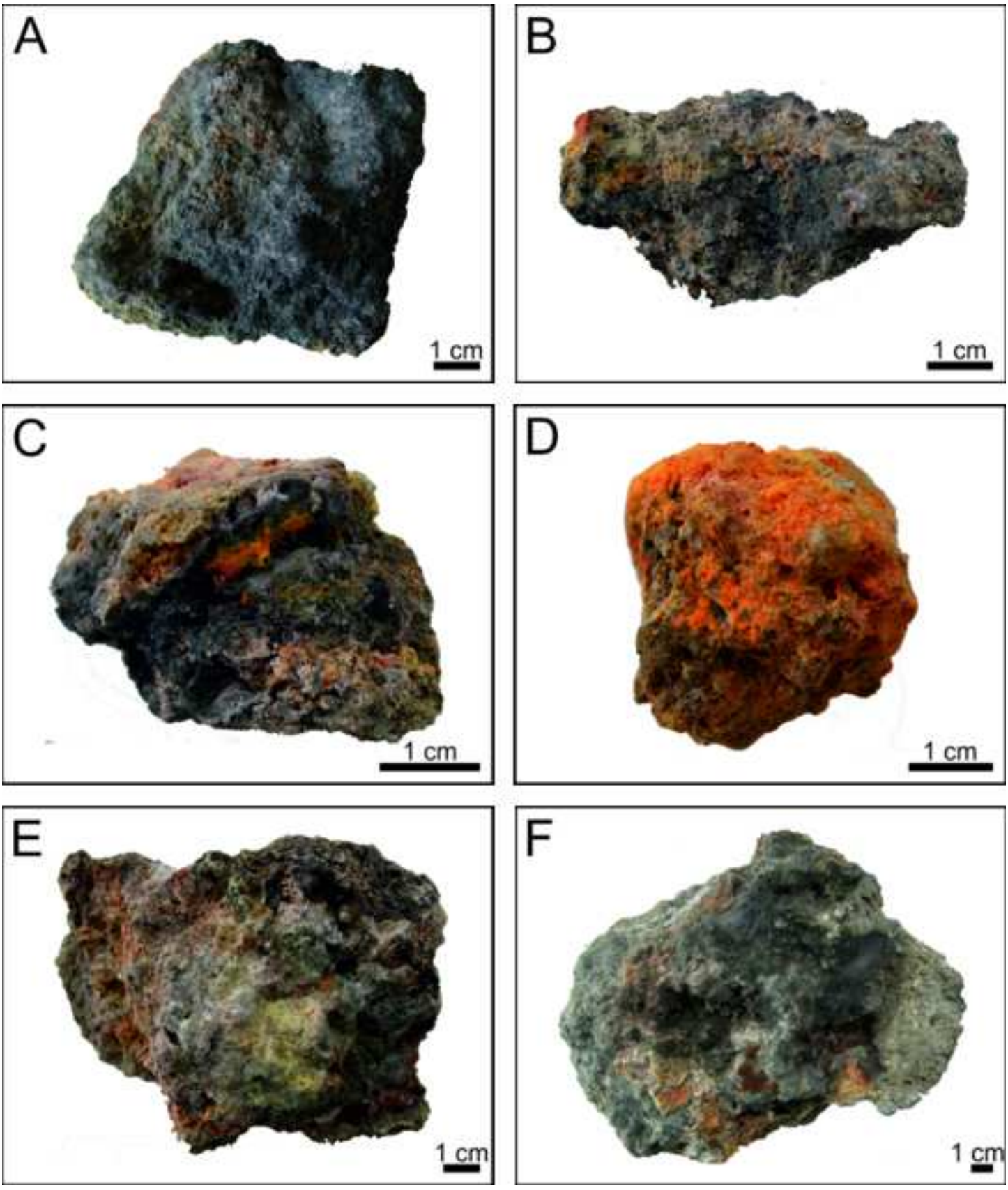

Figure 3

Click here to access/download;Figure;stibnite-Fig. 3.tif

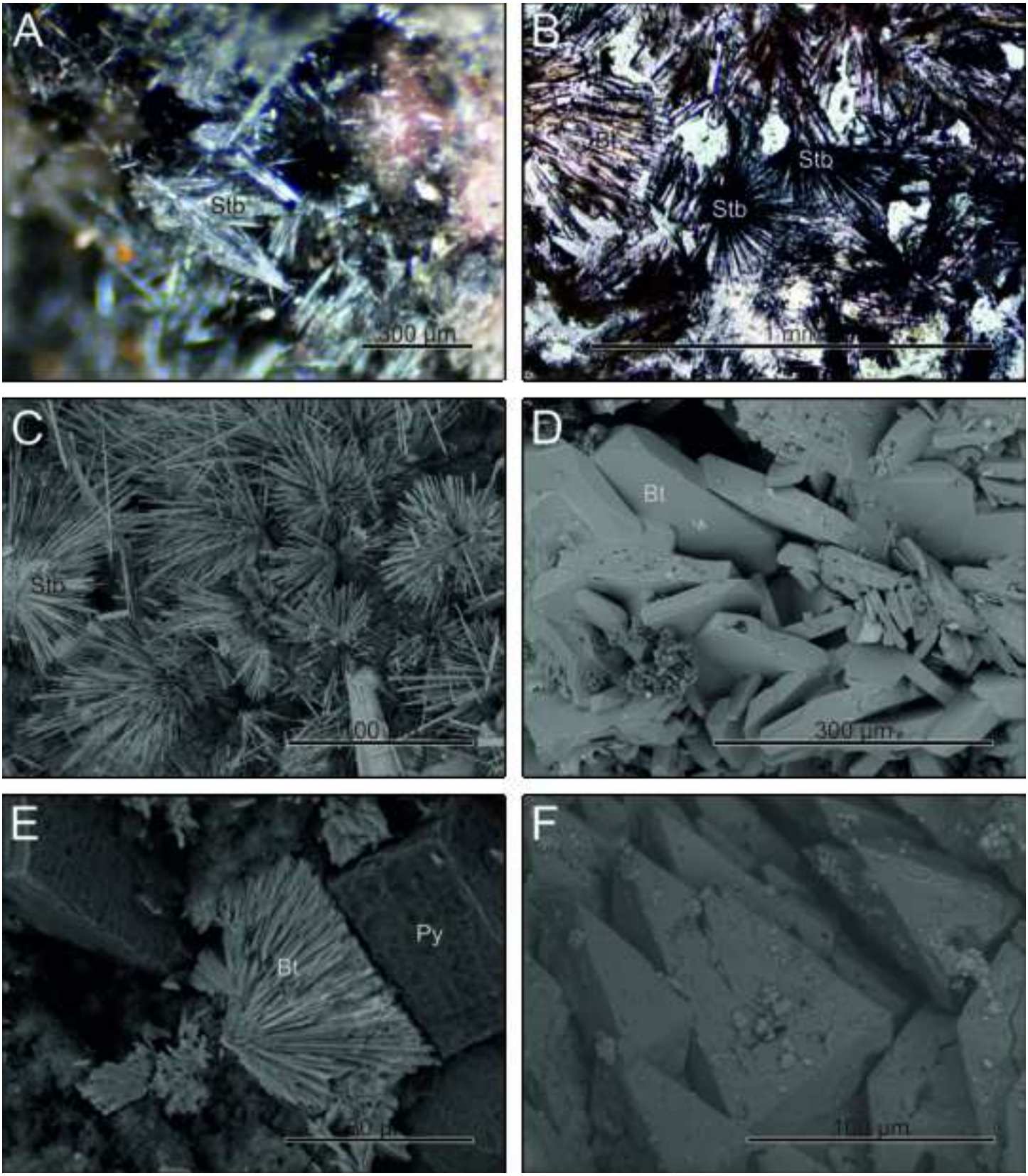

Figure 4

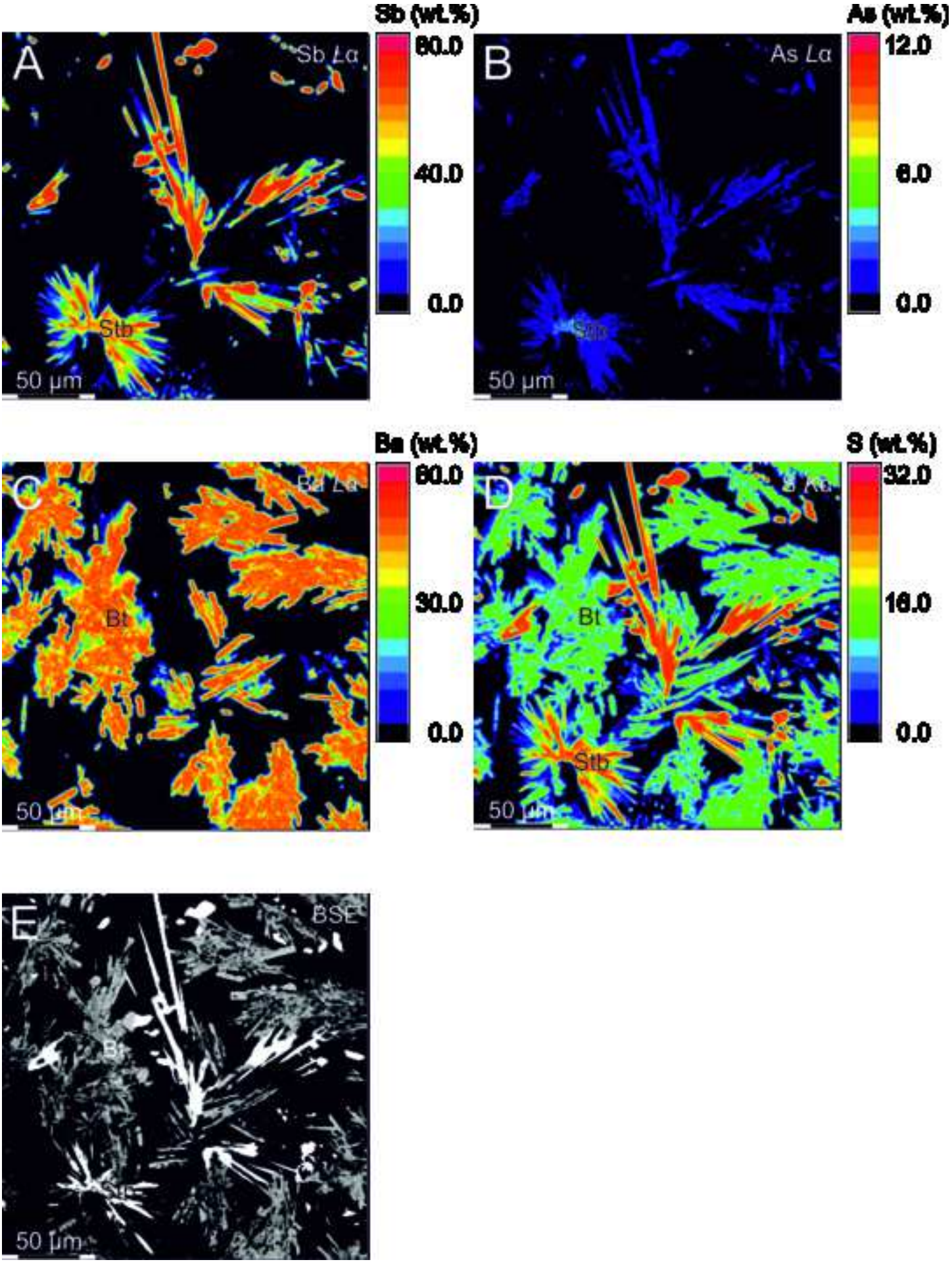

Figure 5

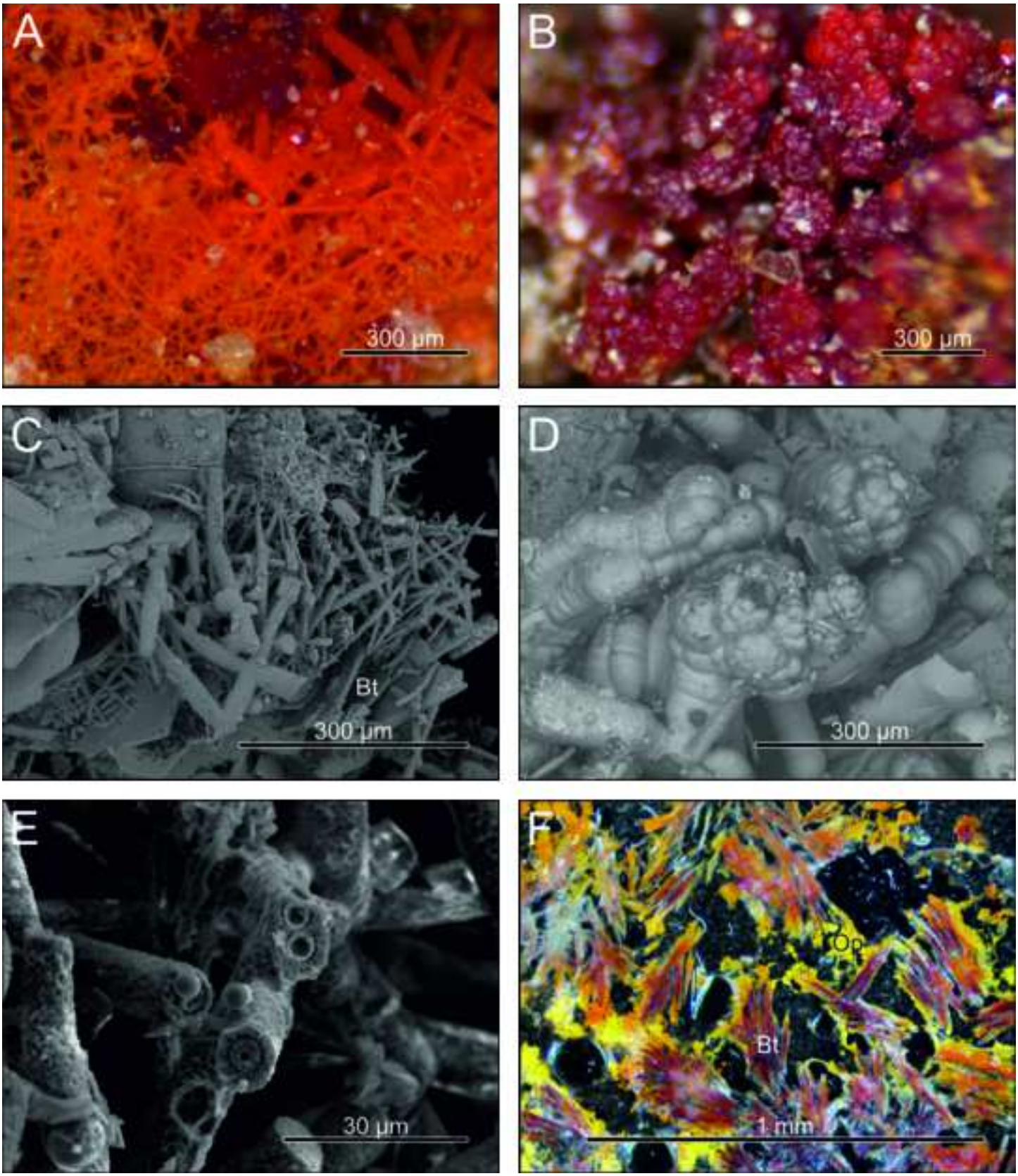

Figure 6

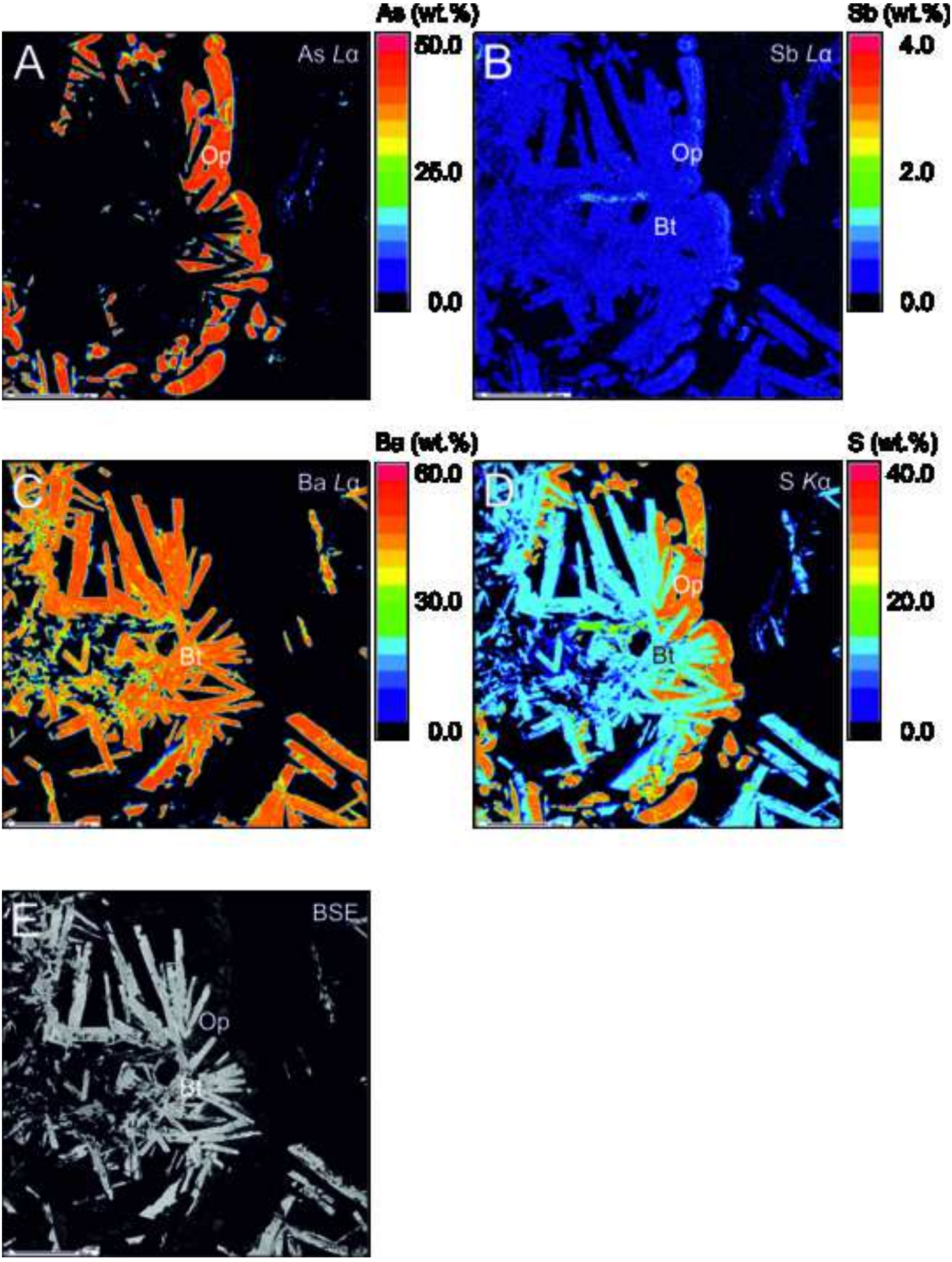

Figure 7

Click here to access/download;Figure;stibnite-Fig. 7.tif

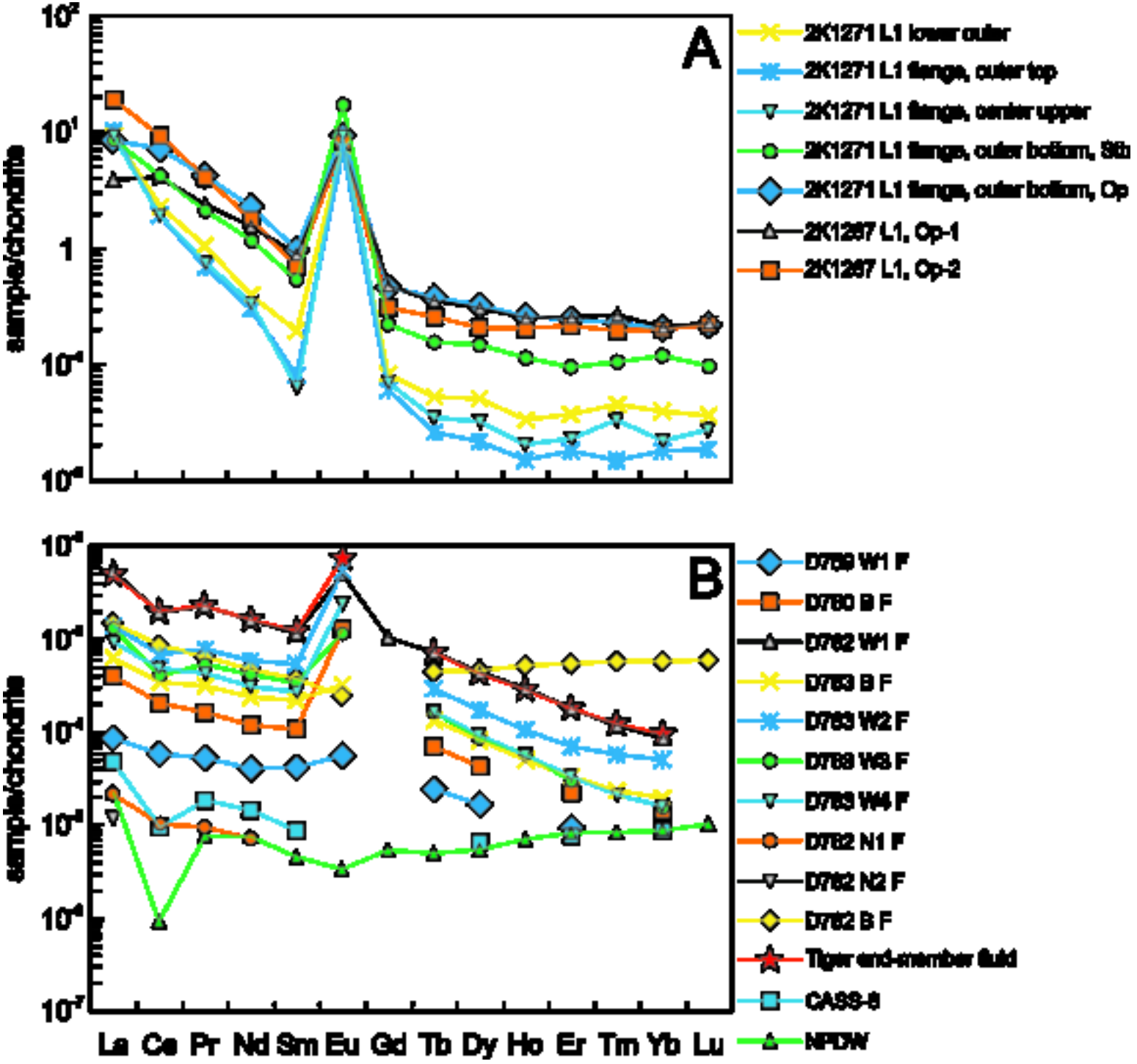

Figure 8

Click here to access/download;Figure;stibnite-Fig. 8.tif

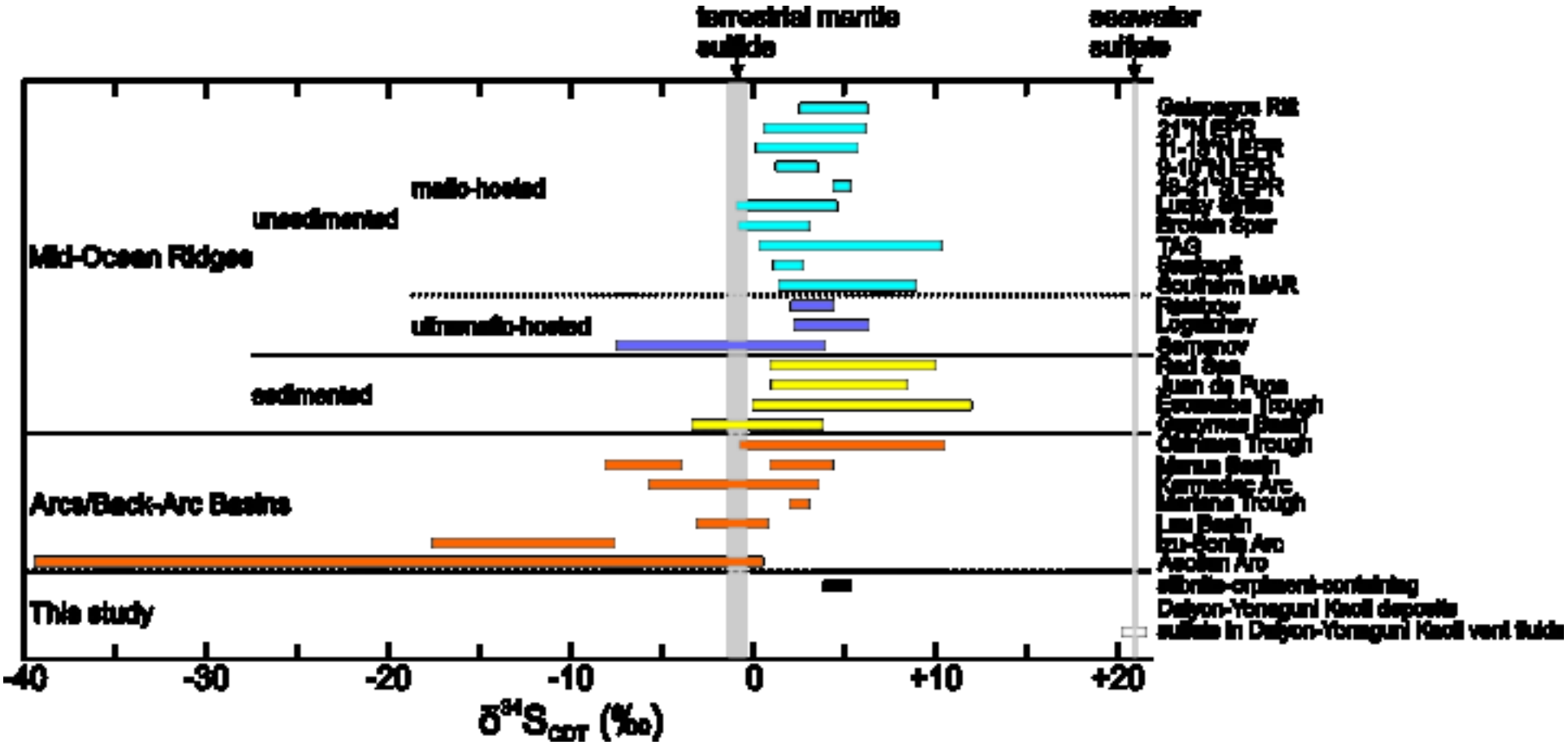

Figure 9

Click here to access/download;Figure;stibnite-Fig. 9.tif

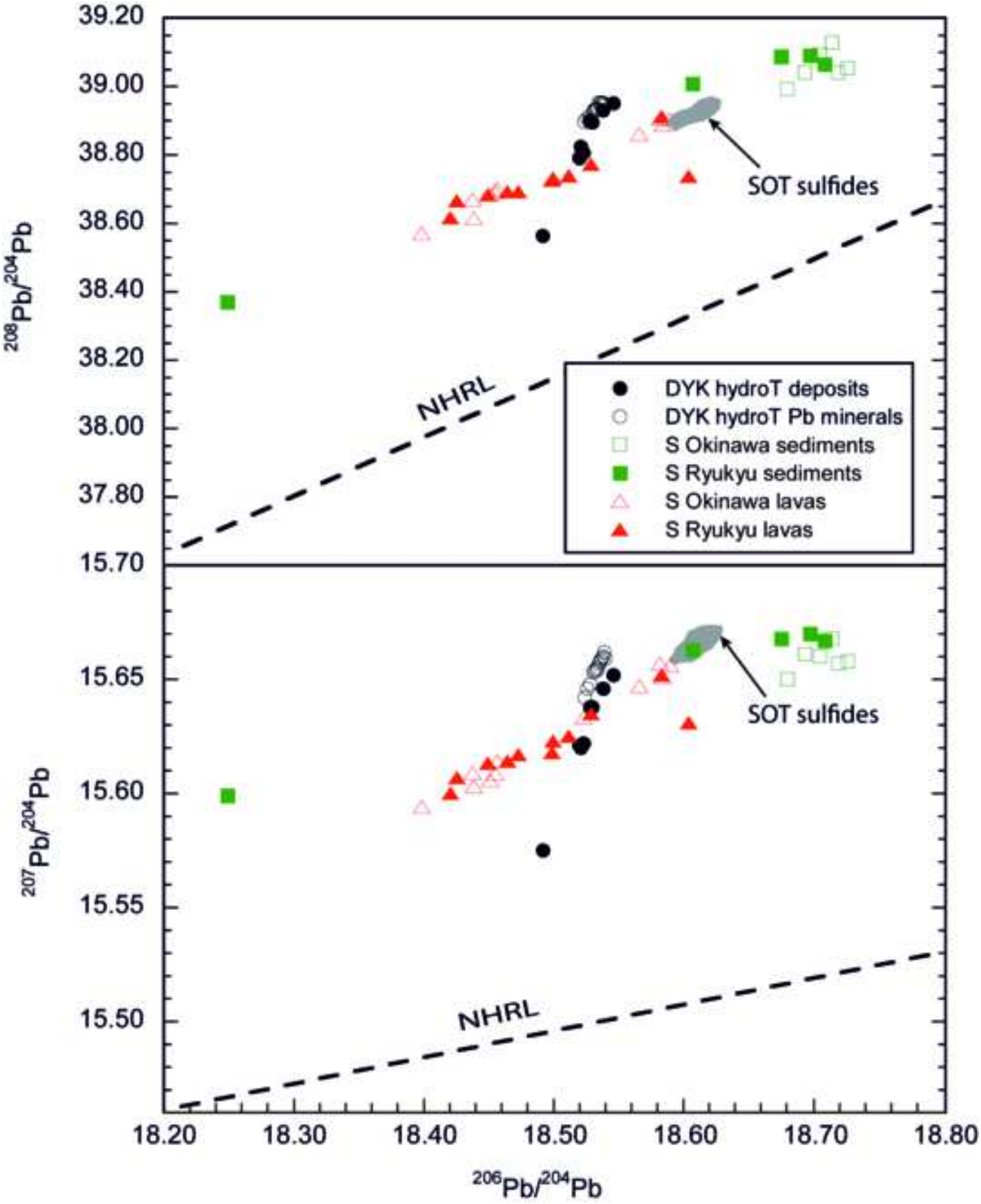

Figure 10

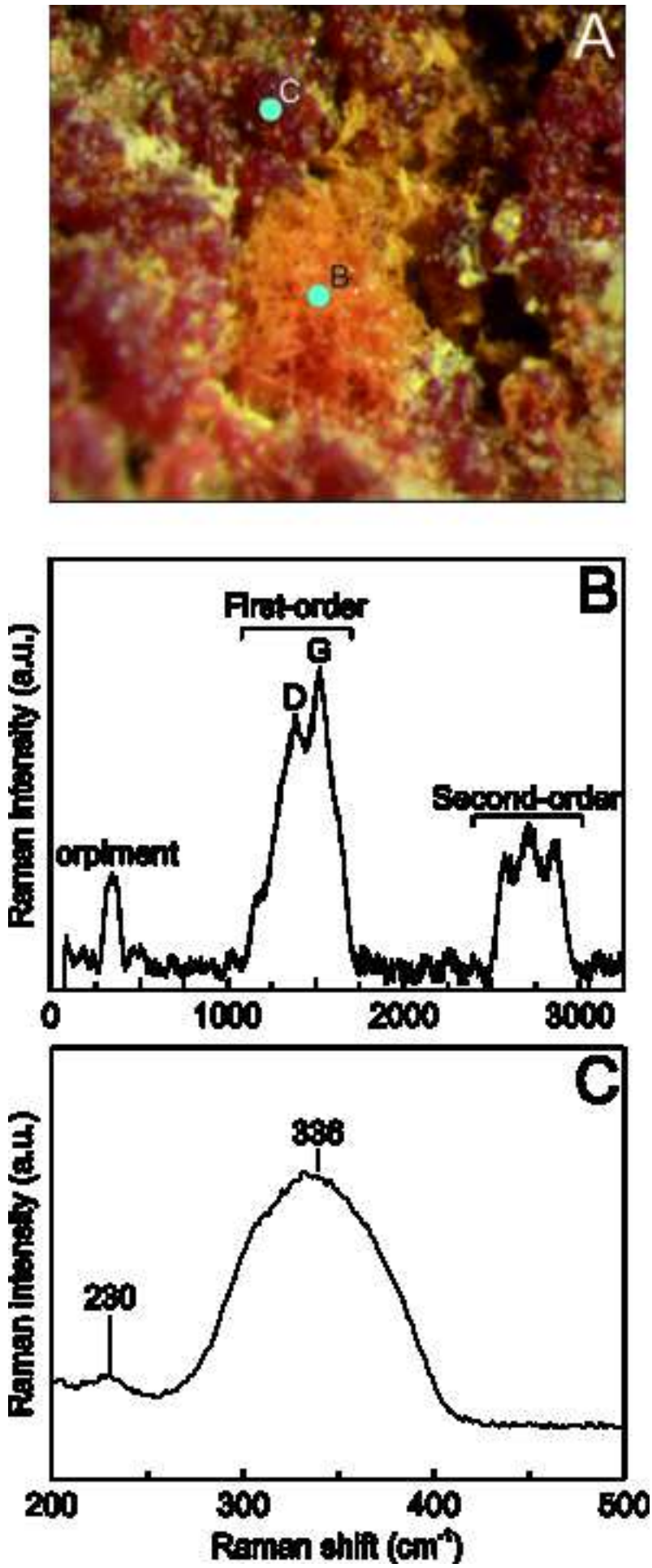

Figure 11

Click here to access/download;Figure;stibnite-Fig. 11.tif

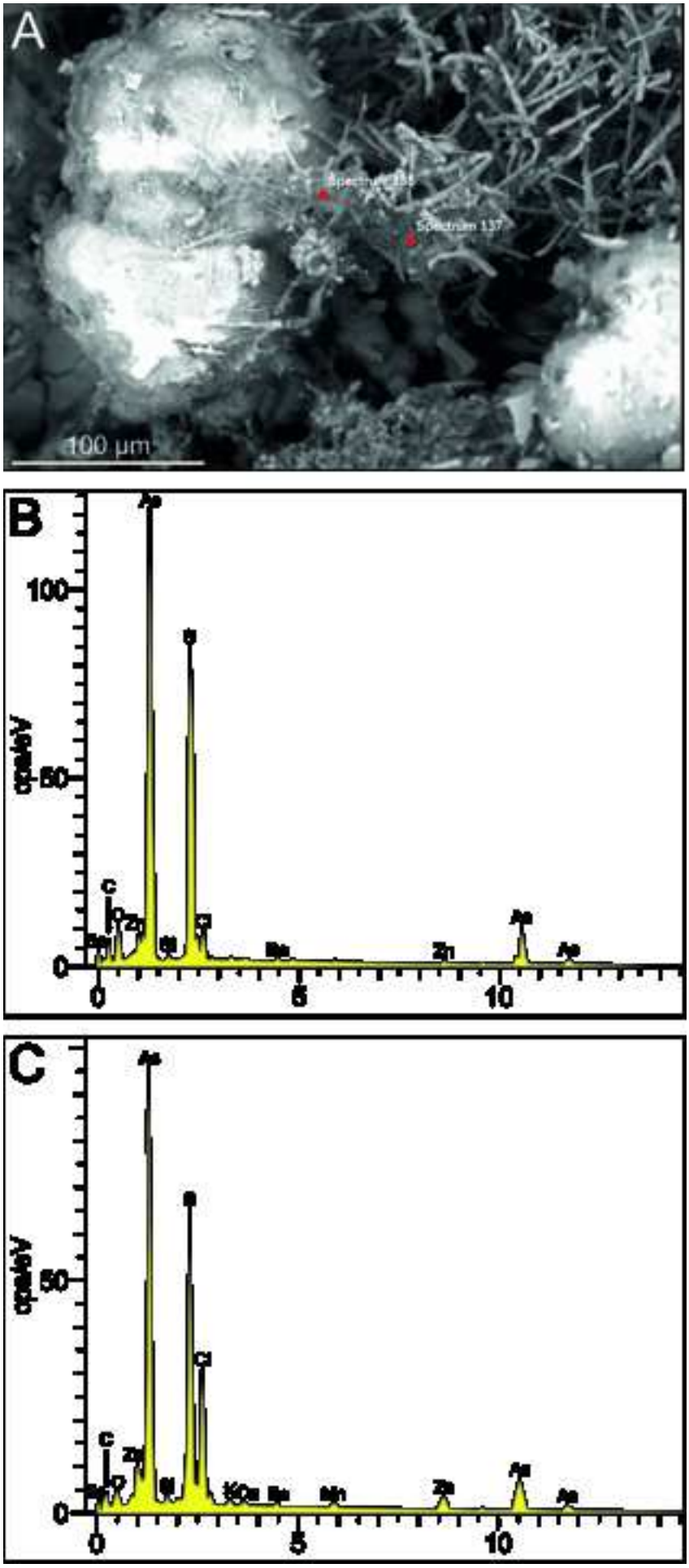

Figure 12

Click here to access/download;Figure;stibnite-Fig. 12.tif

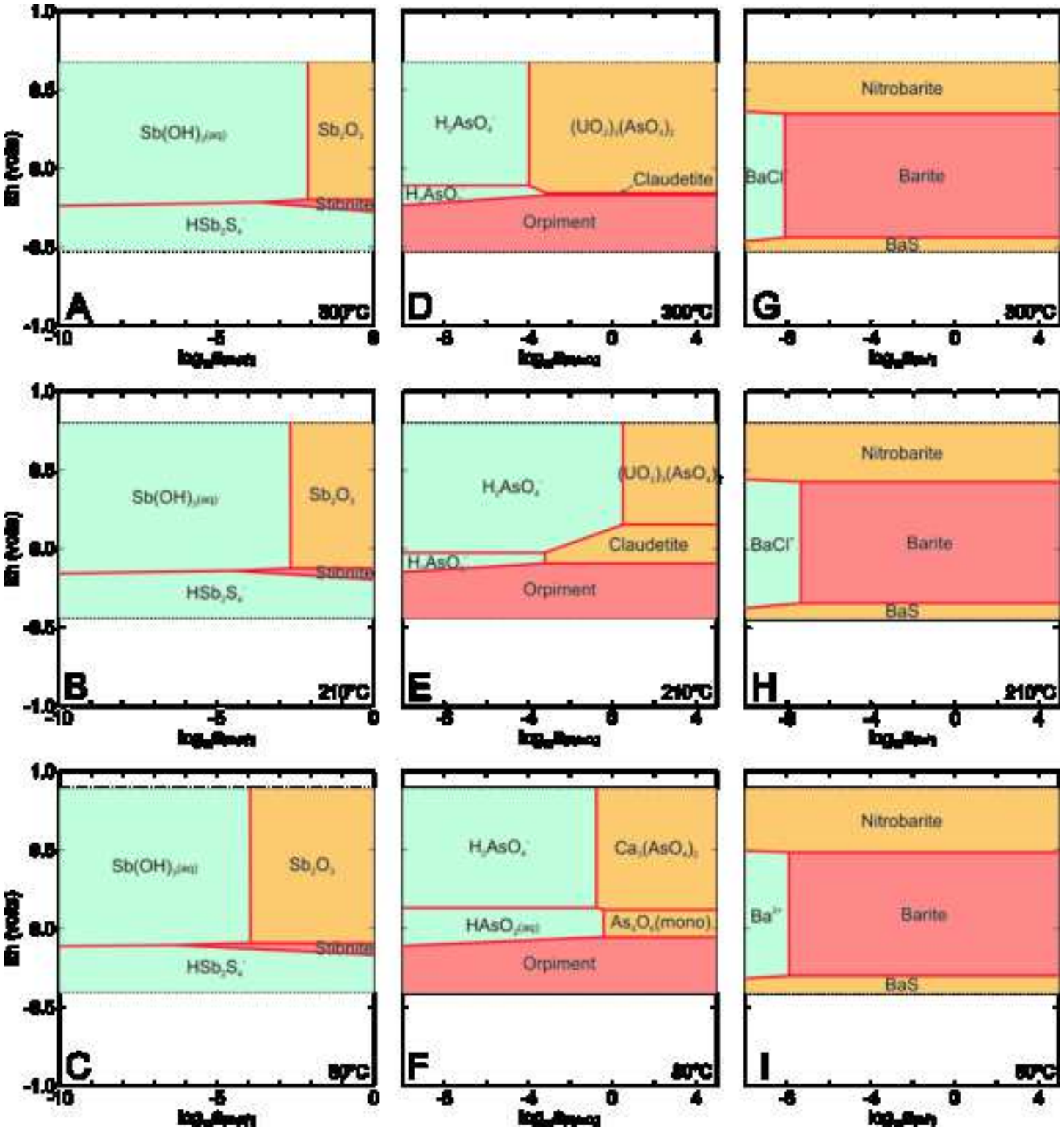

Table 1

Studied hydrothermal deposit samples from the Daiyon-Yonaguni Knoll hydrothermal field (Okinawa Trough).

Sample ID	Vent name	Sample type	Latitude (°N)	Longitude (°E)	Depth (m)	Sampling device
2K1271 L1 lower outer	Tiger	active chimney	24.8497	122.6992	1364	submersible, *Shinkai 2000*
2K1271 L1 flange, outer top	Tiger	active chimney flange	24.8497	122.6992	1364	submersible, *Shinkai 2000*
2K1271 L1 flange, center upper	Tiger	active chimney flange	24.8497	122.6992	1364	submersible, *Shinkai 2000*
2K1271 L1 flange, outer bottom	Tiger	active chimney flange	24.8497	122.6992	1364	submersible, *Shinkai 2000*
2K1267 L1	Tiger	active chimney	24.8489	122.7002	1366	submersible, *Shinkai 2000*
2K1267 L2	Tiger	active chimney	24.8489	122.7002	1366	submersible, *Shinkai 2000*

Table 2

Studied vent fluid samples from the Daiyon-Yonaguni Knoll hydrothermal field (Okinawa Trough).

Sample ID[a]	Vent name	Type of venting fluid	Latitude (°N)	Longitude (°E)	Depth (m)	Temperature (°C)	pH	Sampling device
D759 W1 F	Tiger	grey smoky	24.8	122.7	1366	323	5.292	WHATS
D760 B F	Tiger	clear	24.8	122.7	1362	-[b]	5.051	bag sampler
D762 W1 F	Tiger	grey smoky	24.8	122.7	1365	-	-	WHATS
D763 B F	Tiger	grey smoky	24.8	122.7	1365	210	-	bag sampler
D763 F F	Tiger	grey smoky	24.8	122.7	1365	210	-	-
D763 W2 F	Tiger	grey smoky	24.8	122.7	1365	210	4.906	WHATS
D763 W3 F	Tiger	grey smoky	24.8	122.7	1365	210	4.743	WHATS
D763 W4 F	Tiger	grey smoky	24.8	122.7	1365	210	4.842	WHATS
D762 N1 F	buoyant plume above Tiger	grey smoky	24.8	122.7	1359	-	6.550	Niskin sampler
D762 N2 F	buoyant plume above Tiger	grey smoky	24.8	122.7	1359	-	6.951	Niskin sampler
D762 B F	Abyss	clear	24.8	122.7	1380	80	5.297	bag sampler

[a] Abbreviations in the sample IDs: W = WHATS sampler; B = bag sampler with pump; N = Niskin sampler; F = filtered.

[b] No data.

Table 3
Bulk mineralogy (XRD) of the studied hydrothermal deposits from the Daiyon-Yonaguni Knoll hydrothermal field (Okinawa Trough).

Sample ID	Mineralogy
2K1271 L1 outer lower	barite
2K1271 L1 flange, outer top	barite
2K1271 L1 flange, center upper	barite
2K1271 L1 flange, outer bottom	barite
2K1267 L1	barite
2K1267 L2	pyrite, isocubanite

Table 4
Mineral chemistry (EMP data) and empirical formulae of stibnite, orpiment, and barite from the studied hydrothermal deposits from the Daiyon-Yonaguni Knoll hydrothermal field (Okinawa Trough).

Sample ID	#[a]	Mineral	Sb (wt.%)	S	As	BaO[b]	SrO	SO_3	CaO	Total	Empirical formulae
2K1271 L1 flange, outer bottom	10	stibnite	69.68	28.56	1.72	b.d.l.[c]	b.d.l.	b.d.l.	b.d.l.	99.95	$Sb_{1.93}As_{0.08}S_{3.00}$
2K1271 L1 flange, center upper	5	barite	b.d.l.	b.d.l.	b.d.l.	64.88	1.03	35.77	0.83	102.50	$(Ba_{0.95}Ca_{0.03}Sr_{0.02})SO_4$
2K1267 L1	19	orpiment	0.22	39.49	60.49	b.d.l.	b.d.l.	b.d.l.	b.d.l.	100.20	$As_{1.98}Sb_{0.01}S_{3.01}$

[a] Number of EMP analyses.
[b] Concentrations of Ba, Sr, S, and Ca are given in oxide form as they were measured in barite.
[c] b.d.l. = below detection limits.

Table 5
Chemical (ICP-MS) and S isotope compositions of the studied hydrothermal deposits from the Daiyon-Yonaguni Knoll hydrothermal field (Okinawa Trough).

Sample ID	Sb (wt.%)	As	Ca	Mg	Na	K	Al	Ti	P	Fe	Mn	($\delta^{34}S_{sulfide}$)[a] (‰)
2K1271 L1 lower outer	4.49	0.52	0.13	0.01	n.m.[b]	0.05	0.05	0.0002	0.047	0.04	0.002	4.0
2K1271 L1 flange, outer top	6.29	0.45	0.09	0.01	n.m.	0.04	0.06	0.0003	0.004	0.03	0.003	5.1
2K1271 L1 flange, center upper	4.87	0.07	0.53	0.01	n.m.	0.01	0.03	0.0003	0.087	0.02	0.003	n.m.
2K1271 L1 flange, outer bottom, Stb[c]	1.96	1.95	0.82	0.01	n.m.	0.12	0.07	0.0038	0.032	0.04	0.017	n.m.
2K1271 L1 flange, outer bottom, Op[d]	0.35	5.33	0.80	0.06	0.58	0.15	0.27	0.0125	b.d.l.[e]	0.17	0.039	n.m.
2K1267 L1, Op-1	0.90	3.47	0.64	0.07	0.58	0.16	0.24	0.0078	b.d.l.	0.10	0.011	5.3[f]
2K1267 L1, Op-2	0.13	4.17	0.75	0.04	0.20	0.05	0.10	0.0049	b.d.l.	0.05	0.087	n.m.
Standards												
JB-2 (measured)	0.00002	0.00026	6.84	2.69	1.43	0.32	7.41	0.77	0.038	9.69	0.168	
JB-2 (reference)	0.00002	0.00029	6.68	2.74	1.49	0.35	7.62	0.70	0.039	9.58	0.162	
JB-3 (measured)	0.00001	0.00015	7.17	3.12	2.12	0.61	8.75	1.01	0.125	7.94	0.134	
JB-3 (reference)	0.00001	0.00018	6.93	3.13	2.03	0.66	9.26	0.82	0.128	8.39	0.143	
JMS-2 (measured)	0.00045	0.00378	3.47	1.77	4.08	2.04	6.98	0.86	0.54	7.26	1.62	
JMS-2 (reference)	0.00040	0.00356	3.43	2.02	4.37	2.28	7.66	0.84	0.58	7.65	1.78	
Detection limits in rock (ppb)	15	45	75	3140	3140	29120	26235	1365	28570	35	1445	

[a] Averages of two duplicate measurements.
[b] n.m. = not measured.
[c] Stb = stibnite separate.
[d] Op = orpiment separate.
[e] b.d.l. = below detection limits.
[f] Measured on bulk sample 2K1267 L1.

Sample ID	Cu (ppm)	Zn	Pb	Tl	Bi	Ba	Sr	Hf	Ta	Th	U	Au
2K1271 L1 lower outer	736	108	54.2	301	0.09	585	1204	0.006	0.005	0.06	0.05	0.79
2K1271 L1 flange, outer top	880	321	69.4	278	0.20	567	968	0.004	0.002	0.02	0.07	0.74
2K1271 L1 flange, center upper	659	n.m.	43.0	427	0.09	328	1040	0.006	0.002	0.02	0.03	0.50
2K1271 L1 flange, outer bottom, Stb[c]	301	n.m.	15.7	1769	0.13	377	2140	0.011	0.010	0.10	0.12	1.66
2K1271 L1 flange, outer bottom, Op[d]	733	1681	236	n.m.	1.77	156	1187	0.024	0.017	0.07	3.96	7.75
2K1267 L1, Op-1	276	591	27.2	n.m.	0.32	182	1162	0.023	0.018	0.07	1.02	4.25
2K1267 L1, Op-2	907	1200	532	n.m.	0.91	128	1280	0.012	0.005	0.03	0.78	11.0
Standards												
JB-2 (measured)	220	101	4.53	0.011	0.025	202	164	1.47	0.03	0.26	0.15	0.01452
JB-2 (reference)	219	107	4.88	0.034	0.028	215	177	1.45	0.03	0.26	0.16	0.00564
JB-3 (measured)	192	93.1	4.65	0.02	0.01	223	369	2.58	0.10	1.24	0.44	0.01088
JB-3 (reference)	179	114	4.85	0.046	0.015	239	414	2.65	0.11	1.30	0.48	0.00199
JMS-2 (measured)	430	139	81.4	2.68	1.27	1745	405	4.95	1.31	13.8	2.62	0.07265
JMS-2 (reference)	472	167	77.5	2.79	1.38	1799	435	4.88	1.42	14.2	2.77	-
Detection limits in rock (ppb)	975	105	2.5	0.45	2.5	4	0.35	0.05		0.25	0.25	0.45

Table 6

REE concentrations (ICP-MS) in the studied hydrothermal deposits from the Daiyon-Yonaguni Knoll hydrothermal field (Okinawa Trough).

Sample ID[a]	La (ppb)	Ce	Pr	Nd	Sm	Eu	Gd	Tb	Dy	Ho	Er	Tm	Yb	Lu	ΣREE	(Ce/Ce*)[b]	(Eu/Eu*)[c]	La_{CN}/Lu_{CN}
2K1271 L1 lower outer	2235	1404	98.9	181	28.8	414	16.4	1.91	12.5	1.83	6.04	1.13	6.34	0.90	4409	0.44	53.1	258
2K1271 L1 flange, outer top	2460	1195	64.5	140	11.8	399	12.0	0.95	5.37	0.83	2.89	0.37	2.96	0.46	4296	0.35	101	553
2K1271 L1 flange, center upper	2252	1218	70.4	155	9.51	531	13.9	1.26	8.02	1.13	3.75	0.84	3.57	0.69	4269	0.39	141	339
2K1271 L1 flange, outer bottom, Stb	2040	2611	198	546	80.1	974	45.0	5.63	36.5	6.27	15.3	2.63	19.2	2.40	6582	0.79	45.1	88.4
2K1271 L1 flange, outer bottom, Op	1986	4419	397	1056	144	544	91.5	13.8	79.3	14.1	39.2	5.73	32.4	5.63	8827	1.14	13.5	36.6
2K1267 L1, Op-1	918	2510	218	713	132	443	94.6	12.8	75.3	13.7	40.6	6.61	33.5	5.62	5217	1.32	11.5	16.9
2K1267 L1, Op-2	4568	5758	376	831	103	461	62.3	9.41	51.7	11.0	34.4	4.90	32.3	5.40	12308	0.81	16.3	87.8
Standards																		
JB-2 (measured)	2132	6689	1079	6171	2126	776	3099	551	3858	824	2468	367	2443	364	32946	-[d]	-	-
JB-2 (reference)	2140	6390	1100	6320	2190	818	3200	579	4010	868	2580	376	2490	386	33447	-	-	-
JB-3 (measured)	8437	21714	3176	15952	4151	1264	4606	713	4561	926	2646	385	2461	373	71364	-	-	-
JB-3 (reference)	8120	20900	3140	15900	4170	1310	4770	741	4660	949	2690	380	2500	377	70607	-	-	-
JMS-3 (measured)	136276	164512	35906	152814	34515	8604	38855	5789	37337	7673	22405	3091	19616	2913	670306	-	-	-
JMS-3 (reference)	135261	159305	37381	150059	35927	9003	40093	6120	38561	8065	23274	3223	20301	3151	669725	-	-	-
Detection limits in rock (ppb)	0.83	4.58	2.46	9.27	1.23	0.34	0.78	0.27	0.00	0.00	0.46	0.11	0.00	0.30				

[a] Abbreviations Stb and Op see in Table 5.

[b] $Ce/Ce^* = 2Ce_{CN}/(La_{CN}+Pr_{CN})$.

[c] $Eu/Eu^* = 2Eu_{CN}/(Sm_{CN}+Gd_{CN})$.

[d] Ce/Ce*, Eu/Eu*, and La_{CN}/Lu_{CN} not presented for the standards.

Table 7
Chemical (ICP-MS) and S isotope compositions of the vent fluids from the Daiyon-Yonaguni Knoll hydrothermal field (Okinawa Trough).

Sample ID	Vent name	Cl[a] (mmol/kg)	Mg[a]	Fe (nmol/kg)	Mn	Zn	Pb	Cu	Ni	Mo	Sb	V	Co	Cd	U	Y	($\delta^{34}S_{sulfate}$)[b] (‰)
D759 W1 F	Tiger	550	49.2	825	1937	200	3.28	24.7	509	169	18.3	25.9	5.81	1.69	11.6	0.27	n.m.[c]
D760 B F	Tiger	525	40.7	2161	6121	311	3.40	62.9	47.1	115	18.8	34.3	0.59	0.35	4.25	0.72	20.5
D762 W1 F	Tiger	606	18.4	46031	20086	148	4.81	7.97	840	130	2.25	26.4	4.67	1.35	2.01	7.57	n.m.
D763 B F	Tiger	583	49.4	839	1931	254	7.02	13.9	11.6	138	119	34.5	0.44	0.71	13.6	1.17	21.0
D763 F F	Tiger	-	-	129	1407	36.6	0.95	5.89	556	181	565	6.61	20.6	0.34	12.0	0.03	21.2
D763 W2 F	Tiger	600	22.0	18921	9691	26774	2698	1310	63.0	60.2	150	8.72	1.06	49.1	2.35	1.79	n.m.
D763 W3 F	Tiger	589	32.1	6143	12980	188	11.7	14.2	49.4	189	11.4	21.3	0.35	1.00	2.71	1.01	20.3
D763 W4 F	Tiger	583	30.7	15392	9088	25788	2151	1366	1196	136	135	1.94	3.09	52.0	1.19	1.21	n.m.
D762 N1 F	buoyant plume above Tiger	563	48.0	b.d.l.[d]	1411	414	13.8	13.4	13.9	142	15.3	33.7	2.40	1.43	2.46	0.07	21.0
D762 N2 F	buoyant plume above Tiger	553	49.0	108	255	285	24.6	11.5	11.3	141	13.2	34.9	0.99	1.12	9.17	0.08	21.0
D762 B F	Abyss	547	45.9	2921	53286	59.8	0.95	70.3	29.9	63.2	10.5	21.8	0.49	0.32	4.56	13.3	21.6
	Tiger end-member fluid	-	0	51907	24944	17646	2067	1202	822	84.3	78.2	3.17	2.59	46.0	-6.79	6.81	-
seawater[e]		544	48	-	-	-	-	-	-	-	-	-	-	-	-	-	-
CASS-6 (measured)	-	-	-	36.1	47.4	21.3	0.12	8.93	8.14	b.d.l.	-	6.42	0.43	0.24	6.97	0.22	-
CASS-6 (reference)	-	-	-	27.4	39.7	19.0	0.05	8.18	6.99	93.4	-	9.62	1.12	0.19	12.0	-	-

[a] Vent fluid data used for calculation of the chemistry of the end-member hydrothermal fluid of the Daiyon-Yonaguni Knoll hydrothermal field (Suzuki et al., 2008).
[b] Averages of two duplicate measurements.
[c] n.m. = not measured because of insufficient sample volume.
[d] b.d.l. = below detection limits.
[e] Averages of two seawater samples collected in the vicinity of the Tiger vent (Suzuki et al., 2008).

Table 8

REE concentrations (ICP-MS) in the vent fluids from the Daiyon-Yonaguni Knoll hydrothermal field (Okinawa Trough).

Sample ID	Vent name	Cl[a] (mmol/kg)	La (nmol/kg)	Ce	Pr	Nd	Sm	Eu	Gd	Tb	Dy	Ho	Er	Tm	Yb	Lu	Y/Ho	ΣREE (ppb)	(Ce/Ce*)[b]	(Eu/Eu*)[c]	La_{CN}/Lu_{CN}
D759 W1 F	Tiger	550	0.147	0.257	0.035	0.129	0.041	0.021	b.d.l.[d]	0.006	0.025	b.d.l.	0.009	b.d.l.	b.d.l.	b.d.l.	-	0.096	0.85	2.66	-
D760 B F	Tiger	525	0.705	0.914	0.111	0.384	0.107	0.474	b.d.l.	0.016	0.065	b.d.l.	0.022	0.003	0.013	b.d.l.	-	0.404	0.72	23.5	-
D762 W1 F	Tiger	606	9.132	8.644	1.509	5.153	1.141	1.849	1.327	0.166	0.664	0.099	0.175	0.018	0.081	b.d.l.	76.4	4.295	0.52	4.52	-
D763 B F	Tiger	583	1.111	1.523	0.207	0.758	0.217	0.121	b.d.l.	0.031	0.125	0.017	0.032	0.003	0.018	b.d.l.	69.1	0.595	0.72	2.95	-
D763 F F	Tiger	-	b.d.l.	b.d.l.	b.d.l.	b.d.l.	b.d.l.	b.d.l.	b.d.l.	b.d.l.	b.d.l.	b.d.l.	0.001	b.d.l.	b.d.l.	b.d.l.	-	0.001	-	-	-
D763 W2 F	Tiger	600	2.369	3.039	0.514	1.838	0.529	2.031	b.d.l.	0.068	0.265	0.036	0.069	0.009	0.047	b.d.l.	50.5	1.562	0.64	20.4	-
D763 W3 F	Tiger	589	2.251	1.790	0.363	1.353	0.345	0.438	b.d.l.	0.038	0.130	0.020	0.029	0.002	0.014	b.d.l.	52.0	0.966	0.44	6.76	-
D763 W4 F	Tiger	583	1.630	2.154	0.288	0.993	0.272	0.926	b.d.l.	0.038	0.142	0.019	0.033	0.003	0.015	b.d.l.	64.0	0.935	0.71	18.1	-
D762 N1 F	buoyant plume above Tiger	563	0.037	0.045	0.006	0.023	b.d.l.	b.d.l.	b.d.l.	b.d.l.	b.d.l.	b.d.l.	0.002	b.d.l.	b.d.l.	b.d.l.	-	0.016	0.67	-	-
D762 N2 F	buoyant plume above Tiger	553	0.021	b.d.l.	b.d.l.	b.d.l.	b.d.l.	b.d.l.	b.d.l.	b.d.l.	b.d.l.	b.d.l.	0.002	b.d.l.	b.d.l.	b.d.l.	-	0.003	-	-	-
D762 B F	Abyss	547	2.613	3.839	0.432	1.507	0.377	0.093	b.d.l.	0.104	0.702	0.177	0.532	0.086	0.549	0.085	75.4	1.623	0.80	1.31	2.52
	Tiger end-member fluid	-	8.855	8.708	1.530	5.278	1.242	2.947	-	0.172	0.675	0.099	0.170	0.019	0.090	b.d.l.	69.0	4.263	0.53	12.6	-
CASS-6 (measured)		-	0.084	0.042	0.012	0.046	0.009	0.002	b.d.l.	0.002	0.010	b.d.l.	0.007	0.001	0.008	b.d.l.	-	0.032	0.28	0.00	-
CASS-6 (reference)		-	-	-	-	-	-	-	-	-	-	-	-	-	-	-	-	-	-	-	-
D816-WT1[e]	Tiger	-	7.161	9.708	1.070	3.992	0.983	4.401	1.171	0.165	0.907	0.190	0.564	0.070	0.366	0.057	121		0.76		
D816-WT2[e]	Tiger	-	8.402	11.545	1.285	4.846	1.222	4.893	1.402	0.191	1.035	0.219	0.659	0.083	0.418	0.063	116		0.76		
D821-WT1[e]	Tiger	-	5.643	7.023	0.837	3.200	0.742	3.214	0.878	0.135	0.816	0.195	0.580	0.067	0.315	0.045	125		0.70		

[a] Vent fluid data used for calculation of the chemistry of the end-member hydrothermal fluid of the Daiyon-Yonaguni Knoll hydrothermal field (Suzuki et al., 2008).

[b] $Ce/Ce^* = 2Ce_{CN}/(La_{CN}+Pr_{CN})$

[c] $Eu/Eu^* = 2Eu_{CN}/(Sm_{CN}+Gd_{CN})$

[d] b.d.l. = below detection limits

[e] Data from Hongo et al. (2007).

Table 9
Pb isotope composition of the studied hydrothermal deposits from the Daiyon-Yonaguni Knoll hydrothermal field (Okinawa Trough).

Sample ID[a]	$^{206}Pb/^{204}Pb$	$^{207}Pb/^{204}Pb$	$^{208}Pb/^{204}Pb$
2K1271 L1 lower outer	18.545	15.652	38.951
2K1271 L1 flange, outer top	18.537	15.646	38.931
2K1271 L1 flange, center upper	18.522	15.622	38.807
2K1271 L1 flange, outer bottom, Stb	18.519	15.621	38.791
2K1271 L1 flange, outer bottom, Op	18.491	15.575	38.564
2K1271 L1, Op	18.520	15.620	38.824
2K1267 L1	18.529	15.638	38.896
2K1267 L1, Op-1	18.527	15.638	38.900
2K1267 L1, Op-2	18.527	15.638	38.898

[a] Abbreviations Stb and Op see in Table 5.

Table 10
Trace and rare earth elements chemistry of the end-member hydrothermal fluids from sedimented seafloor hydrothermal systems.

Hydrothermal field	Vent name	Fe (nmol/kg)	Mn	Zn	Pb	Cu	Co	Cd	U
Daiyon-Yonaguni Knoll	Tiger	51907	24944	17646	2067	1202	2.59	46.0	-6.79
Escanaba Trough[a]	6X, 0	40800-58100	25000-31100	11300	1560	3200	115	115	-0.2 – 2.0
Guaymas Basin[b]	South Field, East Hill	8000-180000	128000-236000	100-40000	<20-652	<20-1100	<5	<10-46	-
Middle Valley[c]	Bent Hill, Dead Dog	10000-20000	63000-78000	700-1700	50-125	300-1300	-	-	-

[a] Von Damm et al. (2005).
[b] Von Damm et al. (1985b), Campbell et al. (1988).
[c] Butterfield et al. (1994).

Hydrothermal field	Vent name	La (nmol/kg)	Ce	Pr	Nd	Sm	Eu	Gd	Tb	Dy	Ho	Er	Tm	Yb	Lu
Daiyon-Yonaguni Knoll	Tiger	8.855	8.708	1.530	5.278	1.242	2.947	-	0.172	0.675	0.099	0.170	0.019	0.090	b.d.l.[d]
Escanaba Trough[e]	6X, 0	0.870	1.020	0.122	0.490	0.112	0.165	0.093	0.013	0.080	0.026	0.036	-	-	-
Guaymas Basin[e]	South Field, East Hill	0.670-1.470	0.620-1.590	0.063-0.143	0.216-0.390	0.029-0.053	0.228-1.530	0.017-0.030	0.003-0.005	0.015-0.017	0.003-0.004	0.005-0.011	-	-	-
Middle Valley	Bent Hill, Dead Dog	-	-	-	-	-	-	-	-	-	-	-	-	-	-

[d] b.d.l. = below detection limits
[e] Klinkhammer et al. (1994).

Research Data

Click here to access/download

Background dataset for online publication only

stibnite-Research Data.xlsx

Declaration of interests

☒The authors declare that they have no known competing financial interests or personal relationships that could have appeared to influence the work reported in this paper.

☐The authors declare the following financial interests/personal relationships which may be considered as potential competing interests: